11-1-2016

Hydrogeochemical Evaluation of the Uinta Formation and Green River Formation, Piceance Creek Basin, Northwestern Colorado, USA

Megan E. Masterson
Portland State University

Hydrogeochemical Evaluation of the Uinta Formation and Green River Formation, Piceance Creek Basin, Northwestern Colorado, USA

by

Megan E. Masterson

A thesis submitted in partial fulfillment of the
requirements for the degree of

Master of Science
in
Geology

Thesis Committee:
Robert B. Perkins, Chair
Carl Palmer
John Bershaw
Maxwell Rudolph

Portland State University
2016

ABSTRACT

The Piceance Creek Basin in northwestern Colorado contains extensive oil shale deposits that produce natural gas and which could potentially yield ~1.5 trillion barrels of shale oil. However, much of the oil shale lies at depths too great for traditional mining practices and various innovative approaches for *in situ* conversion of kerogen to oil have been proposed. A firm understanding of the existing hydrogeochemistry is needed as resulting mineralogical changes or rock-fluid reactions may affect rock porosity and permeability. Using an existing database complied by the USGS, the water chemistry of 267 surface and groundwater samples in the Piceance Creek primary drainage basin have been evaluated by mapping major ion concentrations and mineral saturation indicies with respect to hydrostratigraphic units and geologic structures. Controlling processes have been further assessed using statistical correlation and factor analysis.

Results indicate that shallow waters in recharge zones are dominated by mixed cations (Na, Ca, Mg) and bicarbonate anions but with increased depth, groundwater transition to nearly 100% sodium bicarbonate type water. The chemistry of lower aquifer waters are principally controlled by nahcolite dissolution, but evidence of sulfate reduction and cation exchange aid in maintaining a sodium-bicarbonate water type. Ion evolution in surface and upper aquifer waters are influenced by an increase in sulfate concentration which is necessary to evolve water to an intermediate stage with sulfate-dominant anions.

The source of sulfate is speculative, but likely due in part to the oxidation of sulfide-enriched groundwater and possible dissolution of sulfate-bearing carbonates. Surface and upper aquifer water chemistry in the northern portion of the basin is the result of discharge of deeper groundwater which is controlled to some degree by preferential pathways created by faults. Lower aquifer water migrates upward and mixes with the less-concentrated near-surface water, resulting in sodium bicarbonate type water in all hydrologic units.

ACKNOWLEDGEMENTS

I would like to thank my advisor, Ben Perkins, for his support, guidance, and patience over the duration of this process. Thanks to my committee members, Carl Palmer, John Bershaw, and Max Rudolph for their thoughtful comments and insights. I would also like to thank my family and friends who have been endlessly patient and supportive during this process. I could not have done this without them. Funding for this research was provided by the Geological Society of America and the American Association of Petroleum Geologists.

Table of Contents

List of Tables

List of Figures

CHAPTER 1 - INTRODUCTION & BACKGROUND

INTRODUCTION

The Piceance Creek Basin in northwestern Colorado is of great interest due to its vast economic potential. In addition to its large quantities of natural gas, the basin contains the world's thickest and richest oil shale deposit, which has an estimated in-place reserve of ~1.5 trillion barrels of shale oil (Johnson et al., 2010). However, much of the shale resides at depths greater than 200 meters, far too deep for traditional mining practices. Thus, innovative methods involving *in situ* conversion of kerogen to oil have been considered.

Prior research has generally focused on characterization, origin, and richness of the oil shale units (e.g. Desborough, 1978; Eugster and Surdam, 1973; Johnson et al., 2010; Smith et al., 2008; Tanavsuu-Milkeviciene and Sarg, 2012), with little attention paid to the hydrogeochemistry of the basin. A firm understanding of the existing basin hydrogeochemistry is needed to predict the impacts of energy resource development on aquifer hydraulic properties and water quality. Mineralogical changes or rock-fluid reactions are likely to result from proposed development methods, including introduction of foreign fluids and *in situ* heating involving temperatures up to 300˚C. Such perturbations may affect formation porosity and permeability, as well as the composition of groundwaters (Palmer et al., 2009; 2010; Perkins et al., 2008).

The objective of this study is to understand the aqueous chemistry in the Green River and Uinta Formation in terms of major geochemistry distributions, mineralogical controls (saturation indicies) and residence times (sample depths and position along presumed flow paths). To accomplish this goal, a dataset published by the U.S. Geological Survey (USGS, 2009) was obtained and includes water chemistry data for different wells and depths across the basin. The database was queried for applicable information. The hydrochemical data was evaluated in Chapters 2 and 3 for the objective of understanding the hydrogeochemistry of the Piceance Basin.

Chapter 1 of the study focuses on previous research on the geology, history, stratigraphy, mineralogy, and hydrology of the Piceance Basin. In Chapter 2, the dominant groundwater flow paths in the different hydrologic units are defined and the dissolved constituent concentrations are analyzed by geographic location, flow path and aquifer to determine major geochemistry distributions and source. Chapter 3 focuses on mineralogic controls in the groundwater and residence times. The final chapter, Chapter 4, summarizes the conclusions of the study. The results of the research will expand the current knowledge of the Piceance Basin and can be applied to evaluations of environmental impacts of energy development within the basin.

BACKGROUND

Geology

The Piceance Creek Basin is located in northwestern Colorado (Figure 1). It is one of four continental basins that formed to the east of the Cordilleran fold in the central Rocky Mountain region, along with the Uinta Basin in Utah and the Green River Basin and Washakie Basin in Wyoming (Smith et al., 2008). The Uinta and Piceance Basin were occupied by ancient Lake Uinta, and the Green River and Washakie Basin were occupied by ancient Lake Gosiute (Tuttle, 1973). The basins were originally conjoined but were separated during the Laramide Orogeny by regional tectonics; the Uinta and Piceance Creek Basins were divided by the Douglas Creek Arch, a north-south trending faulted anticline, while the Piceance Creek and the Green River and Washakie Basin were divided by the Axial Basin uplift. For most of their history, these lake basins developed separately, but were occasionally hydrologically connected (Smith et al., 2008).

There are three formations present in the Piceance Basin. From oldest to youngest, these are the Wasatch Formation, the Green River Formation (which consists of five members), and the Uinta Formation (Figure 2). The Wasatch Formation, comprised of clay, shale, lenticular sandstone and conglomerate, was deposited prior to ancient Lake Uinta development in the Piceance Creek Basin.

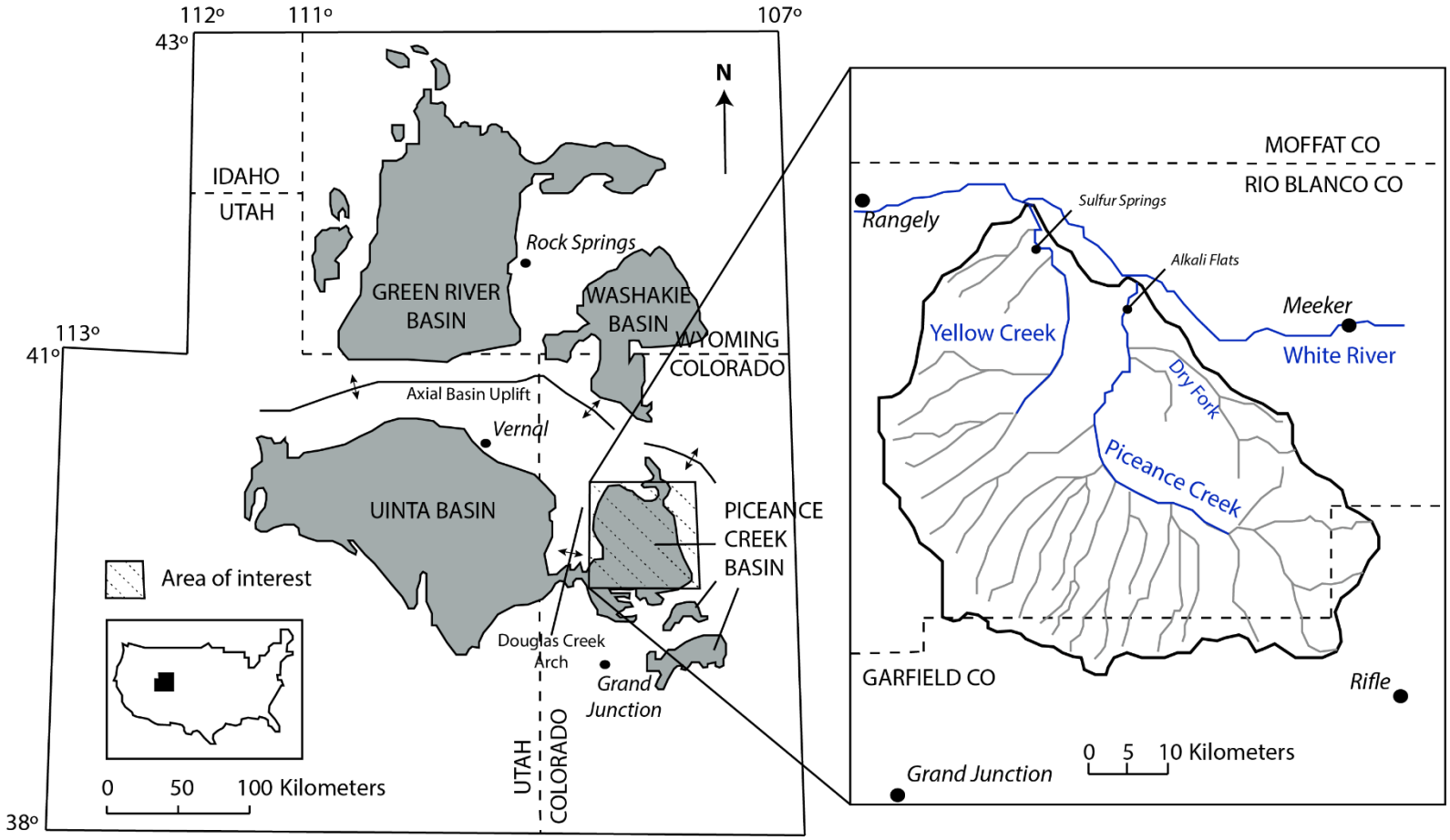

Figure 1. Location map for the Piceance Creek Basin in northwestern Colorado (left) and a closer image of the thesis area (right). The gray shaded regions are the four basins (Green River, Uinta, Washakie, and Piceance Creek Basin). The blue lines (right) represent major creeks and rivers in the region. Town names are labeled for reference along with the location of two springs – Sulfur Springs and Alkali Flats. Figure modified from Dyni (2005) and Weeks et al. (1974).

Lake development in the Piceance Basin began during the early Eocene and lacustrine sediments deposited *ca.* 53-48 Ma are assigned to the Green River Formation. Five members have been formally identified in the Green River Formation; they are, from oldest to youngest, the Cow Ridge, Garden Gulch, Douglas Creek, Anvil Point, and Parachute Creek Members. The Cow Ridge Member is comprised of a sandstone, shale, and limestone mixture. Continuous lacustrine sediment accumulation is marked by the Long Point bed, an ostracod, mollusc-rich bed, which also marks the overall transgression of the lake basin (Tanavsuu-Milkeviciene and Sarg, 2012). The Cow Ridge Member is overlain by basin margin limestones, sandstones, and mudstones of the Douglas Creek Member to the south and west, marginal sandstones of the Anvil Point Member to the north and east, and by clay-rich oil shale deposits of the Garden Gulch Member in the basin center (Tanavsuu-Milkeviciene and Sarg, 2012). The Parachute Creek Member is the largest unit, ranging between 325-400 meters thick (Cole and Picard, 1989). This unit consists of dolomitic oil shales interbedded with siltstone and sandstone layers. There is a particularly kerogen-rich oil shale layer near the top of the member referred to as the Mahogany Zone, which is the richest, most laterally extensive oil shale layer in the Green River Formation (Taylor, 1987). Tongues of the overlying Uinta Formation form the upper boundary of the Parachute Creek Member.

The Uinta Formation ranges from 180-250 meters thick (Cole and Picard, 1989) and consists of alluvial, turbidite, and deltaic deposits. The deposits are primarily sandstones, fallout tuffs, and volcaniclastics from previously active

volcanic provinces, including the Absaroka Volcanic Province, Challis volcanic field, and other minor fields in the region (Smith et al., 2008; Tanavsuu-Milkevicene and Sarg, 2012).

Structural overview

The Piceance Creek Basin is part of a large syncline, modified by numerous smaller structures (Donnell, 1961). Dominant faults in the basin trend northwest and secondary joints trend northeast. The faults are high-angle normal faults with small displacements of less than 15 meters (Donnel, 1961). This is evident when comparing mapped faults on the surface with mapped faults on the top of the Mahogany Zone (Figure 3). The green lines in Figure 3 represent faults mapped at the surface from the U.S. Geological Survey, The National Map (2015), and the red lines represent mapped faults on the top of the Mahogany Zone from a USGS digital data series accompanying a publication by Johnson et al. (2010).

Lake Evolution

The mineral distribution in the Green River Formation is crucial to understanding the Piceance Basin's evolution. Discontinuous evaporite beds of halite and nahcolite are found at depth in the central, northcentral region, referred to as the saline zone (Figure 4 and Figure 5; Cole and Picard, 1978; Weeks et

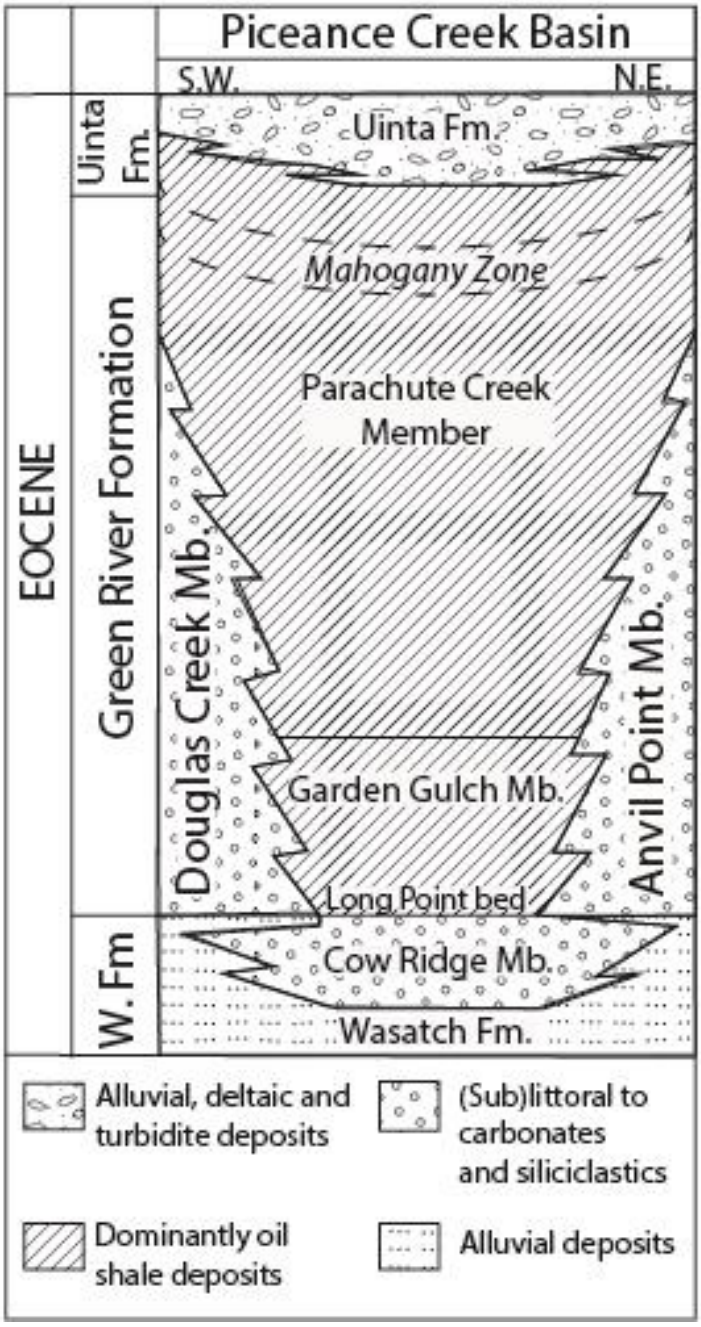

Figure 2. Stratigraphic column of the Piceance Creek Basin (modified from Tanavsuu-Milkeviciene and Sarg, 2012). Fm stands for formation, Mb stands for member, and W stands for Wasatch.

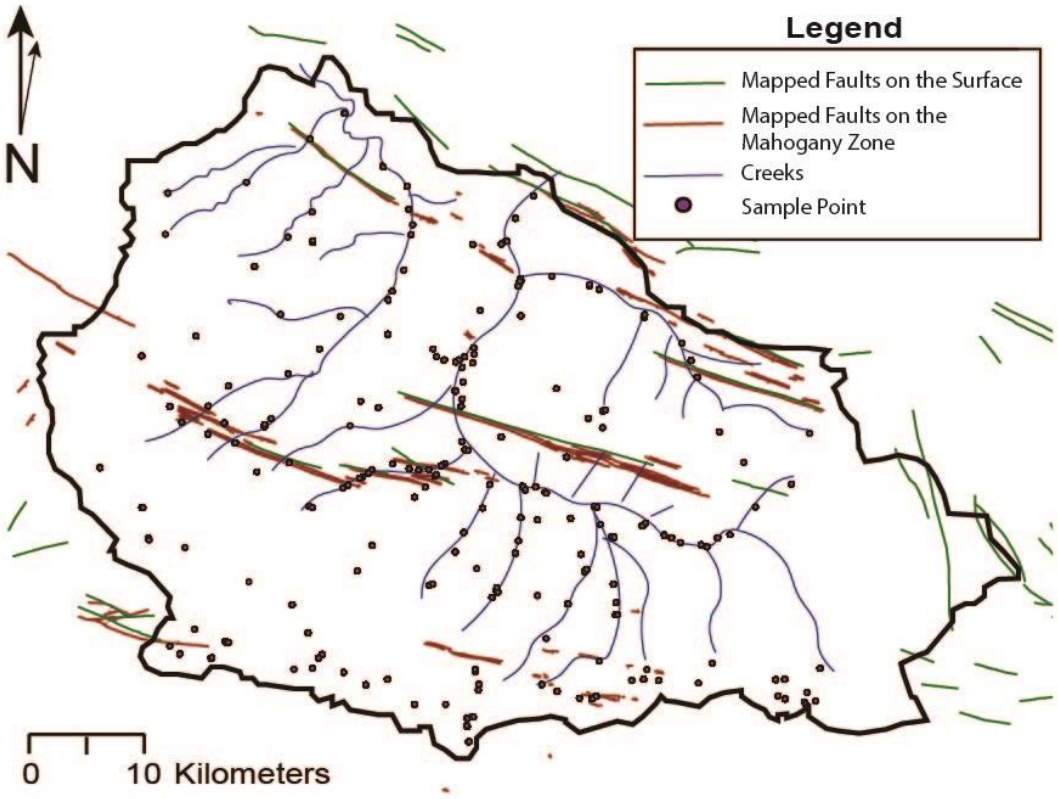

Figure 3. Mapped structures on the ground surface (green) and on top of the Mahogany Zone (red) (USGS, 2015; Johnson et al., 2010).

al., 1974; Taylor, 1987). Calcite is distributed throughout the basin, but the dominant carbonate unit is dolomite, which requires a magnesium to calcium ratio of 5-10 to precipitate in hypersaline environments (Desborough, 1978; Müller et al., 1972; Folk and Land, 1975). To explain these observations, the basin has been described as a stratified lake (Bradley and Eugster, 1969), a playa lake (Eugster and Surdam, 1973), and a biogenic-chemical stratified lake (Desborough, 1978).

The stratified lake and playa lake models were deemed deficient as neither properly accounted for the mineral compositions or spatial distribution of minerals and organics. Desborough's (1978) biogenic-chemical stratified lake model addresses both. In this model, the basin is divided into two zones based on density differences: a lower zone, which is highly reduced and saline and a less saline, oxidized, upper zone. Primary production in the upper zone generated organic matter and biogenic calcite, which would sink to the bottom. During times of extreme salinity, nahcolite and halite would precipitate in the lower zone, which accounts for the evaporites in the center of the basin. According to Desborough (1978), magnesium is preferentially concentrated in blue-green algae, which, on settling out of the water column, release the magnesium to bottom sediments. When the Mg:Ca ratio is great enough, protodolomite precipitates.

The lacustrine lake closed around 48 Ma as the climate cooled after the Early Eocene Climate Optimum (EECO) and precipitation increased (Tanavasuu-Milkeviciene and Sarg, 2012). At the same time, active volcanism produced new sediment from the Absaroka Volcanic Province (northwest Wyoming and southwest Montana), Challis volcanic field (Idaho) or other nearby fields (Smith et al., 2008). Fluvial processes transported the new sediments to the basin until the lake filled up and disappeared. These volcaniclastic and deltaic deposits continued to cover the region, creating the Uinta Formation.

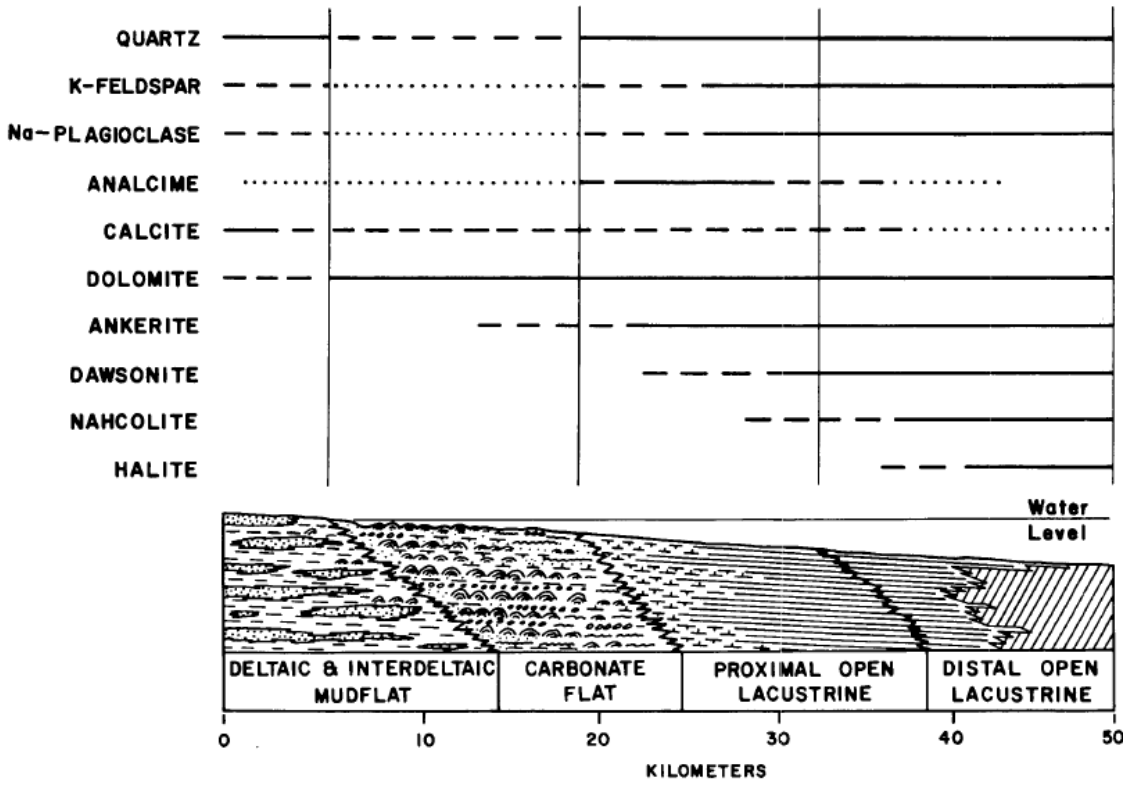

Figure 4. Schematic diagram of mineral variations in the Green River Formation of the Piceance Creek Basin. Solid lines indicate the mineral is relatively abundant; dashed lines indicate the mineral is common; dotted lines indicate the mineral is rare; no lines indicate the mineral is absent (Cole and Picard, 1978). Note the narrow presence of saline minerals, nahcolite and halite, in the basin center.

Mineralogy

The sedimentary rocks of the Piceance Basin fall into three primary categories: carbonates, evaporites, and clastics. The principle carbonate minerals in the Green River and Uinta Formation include calcite ($CaCO_3$), dolomite ($(CaMg)(CO_3)_2$), and ankerite ($Ca(Mg,Fe)(CO_3)_2$). Halite (NaCl), nahcolite ($Na(HCO_3)$), and dawsonite ($(NaAl(CO_3)_2(OH)_2$) are the common evaporite minerals in the basin and volcaniclastics and siliciclastic sediments,

primarily found in the Uinta Formation, are high in quartz (SiO_2), albite ($NaAlSi_3O_8$), and secondary analcime ($NaAlSi_2O_3$) which formed from the alteration of detrital clays during evaporation on the marginal mudflats of Lake Uinta (Birdwell et al., 2013).

Cole and Picard (1978) analyzed the relative distribution of minerals in the Parachute Creek Member and determined four zones based on spatial relationships to the lakeshore: The deltaic and interdeltaic mudflat, carbonate flat, proximal open lacustrine, and distal open lacustrine zone. Their results indicated that dolomite is the dominant carbonate mineral in the basin and evaporites of nahcolite and halite are found only in a narrow region in the distal open lacustrine zone (Figure 4). Poole (2014) analyzed 117 core samples in the basin and confirmed similar results to Cole and Picard (1978); The center basin is enriched in saline minerals dawsonite, nahcolite, and halite, and the margins are enriched in the zeolite analcime. Poole reported a large proportion of carbonates in the Green River Formation with dolomite or ferroan dolomite being the dominant carbonate mineral.

Groundwater Characterization and Flow Paths

Coffin et al. (1971) identified two aquifers in the Piceance Basin: the upper and lower aquifer. The upper aquifer extends from the water table down to the top of the Mahogany Zone and the lower aquifer, from the Mahogany Zone to the boundaries of the Parachute Creek Member of the Green River Formation. The

Mahogany Zone is an oil shale layer approximately 20-70 meters thick and serves as a laterally extensive leaky aquitard preventing mixing of water types from the upper and lower formations, except through slow permeation, and major faults and joints (Figure 5). The Douglas Creek and Garden Gulch members, along with the saline zone are considered impermeable and bound the hydrologic unit. Robson and Saulnier (1981) estimate the saturated thickness of the aquifers in the northeast part of the basin to be 610 meters and estimate the hydraulic conductivity to range from 3.5 to 60 cm/day laterally, and $2x10^{-2}$ to 30.5 cm/day vertically.

Weeks et al. (1974) developed a groundwater flow model in which water enters the basin as recharge from precipitation along the western, southern, and eastern margins and flows towards the center, exiting the subsurface through the groundwater-fed Piceance Creek (Figure 6). This suggests that the residence times in the Piceance Creek Basin depends on the flow path taken, with the longest transit infiltrating the lower sediments and the shortest transit existing as shallow groundwater flow.

Robson and Saulnier (1981) refined the groundwater model by contouring the potentiometric surface of the upper and lower aquifer. Ground water levels range from approximately 1750m near the discharge point of Piceance and Yellow Creeks in the north, to approximately 2250m along the southern margin in both aquifers (Figure 7 - Figure 8). This indicates a general groundwater movement from the recharge areas to the northern discharge region of the creeks. Groundwater gradients in the upper aquifer range from 3.5 to 22.5 m/km

and 3.5 to 25 m/km in the lower aquifer (Robson and Saulnier, 1981). Differences in the potentiometric surface between two adjacent wells screened in the two aquifers can be up to 70m and are displayed in Figure 9 (Robson and Saulnier, 1981). The differences between potentiometric levels in the aquifers indicates a potential for downward flow of groundwater along the western, southern, and eastern margins, along the drainage divide between Piceance and Yellow Creek, and the divide between Piceance Creek and Dry Fork. Potential for upward movement of water is along Piceance Creek and the downstream reaches of its tributaries (Robson and Saulnier, 1981).

Using carbon isotopes, Kimball (1984) concluded that groundwater ranges from approximately 750 years, for wells near recharge areas (defined as regions along the western, southern, and eastern margin), to over 20,000 years for wells farther down the hydrologic gradient. The longer the flow path, the more time the water has to equilibrate with the surrounding bedrock. Thus, waters at depth will likely have achieved equilibrium with a larger quantity of minerals, owing to both the longer residence times and increased rates of reaction due to the geothermal gradient.

Groundwater Chemistry in the Piceance Basin

This study focuses on the geochemistry of groundwater in the Piceance Basin, a topic that has been largely ignored in literature. Thomas and McMahon (2012) evaluated the groundwater-quality for an area encompassing, but much

larger than, the study area. Thomas and McMahon evaluated the concentrations of major and minor ions and compared them to drinking water standards. Additionally, Robson and Saulnier (1981), who evaluated previously published water chemistry data (included in this study), observed the following changes occurring towards the basin center and with increasing depth: a change in water type from mixed cation bicarbonate water to a sodium bicarbonate water, oxidation and reduction of sulfur species, and relatively large increases in certain trace elements, such as strontium and fluoride. They suggest the high sodium values are the result of ion exchange and nahcolite and halite dissolution.

Reduced sulfur in the basin is evident from the presence of pyrite (FeS_2), and the occurrence of hydrogen sulfide gas (Kimball, 1984; Robson et al., 1981). The abundant organic material helps to maintain reduced conditions which stabilizes the reduced sulfur species and likely contributes significant sulfur itself (Robson et al., 1981; Thomas and McMahon, 2009). However, the source for oxidized sulfur is speculative. Robson et al. (1981), Hansen et al. (2010), and Thomas and McMahon (2009), offer two suggestions: 1) gypsum dissolution; 2) the upward movement and oxidation of water enriched in sulfides along faults and fractures. The mention of gypsum in literature for the study area is inconsistent. Although some research articles note the presence or theoretical presence of gypsum (Thomas and McMahon, 2009; Sanborn, 1977), these articles generally characterize the Uinta Basin (Utah) and the Piceance Basin together, and/or include a much larger area of the Piceance Basin than is considered in this study without much spatial differentiation. Papers that focus on

the particular area of this study generally note halite, nahcolite, and dawsonite as the evaporative minerals present in the basin with no mention of gypsum or anhydrite (Cole and Picard, 1978; Tanavasuu-Milkeviciene and Sarg, 2012; Hansen et al., 2010). Robson et al. (1981) note that gypsum has been found in discharge areas of the Uinta Formation but not in recharge areas or near the water table.

USGS Database

In this study of the groundwater chemistry of the Piceance Basin, a database published in 2009 by the U.S. Geological Survey (USGS, 2009) was used. This database is a compilation of data from over 22 agencies, spanning the period 1947 to 2009. The database was complied with the goal of creating a publicly-accessible repository of water quality data to aid in the “planning, monitoring, conservation, and management of water resources in the face of large-scale energy development” (USGS, 2009). Contributors to the collective database came from industry, local, State, Federal, and other sources.

The data subset used for this research included the following parameters: water temperature, pH, total dissolved solids, specific conductivity, sample depth, geographic locations (decimal degrees) and dissolved concentrations (generally in ppm or ppb) of major ions.

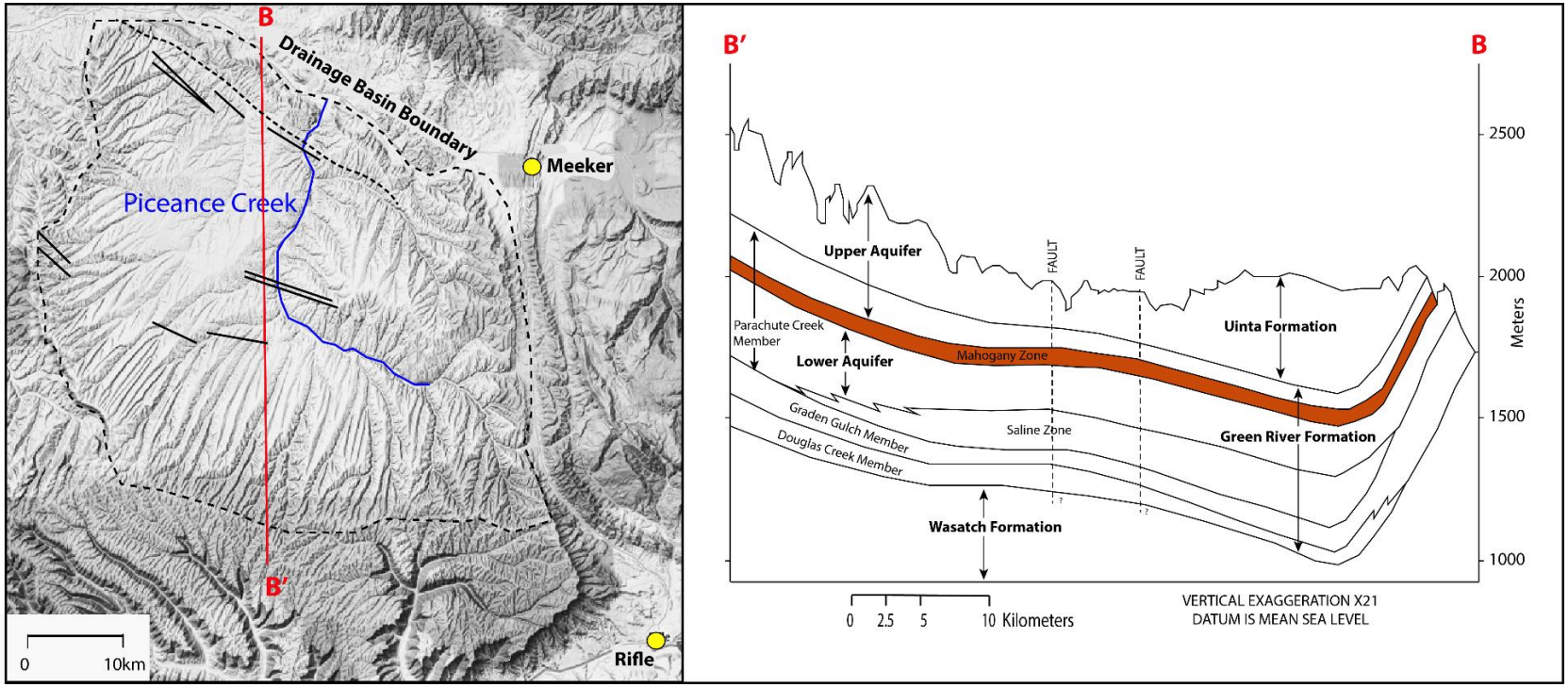

Figure 5. Plan view map (left: modified from Robson and Saulnier, 1981) and north-south cross section (right: modified from Weeks et al., 1974) of the Piceance Creek Basin. The black lines on the map view depict major faults. The main formations and members are labeled along with the bounds of the upper and lower aquifer. The red-colored layer is the Mahogany Zone which acts as an aquitard between the two aquifers.

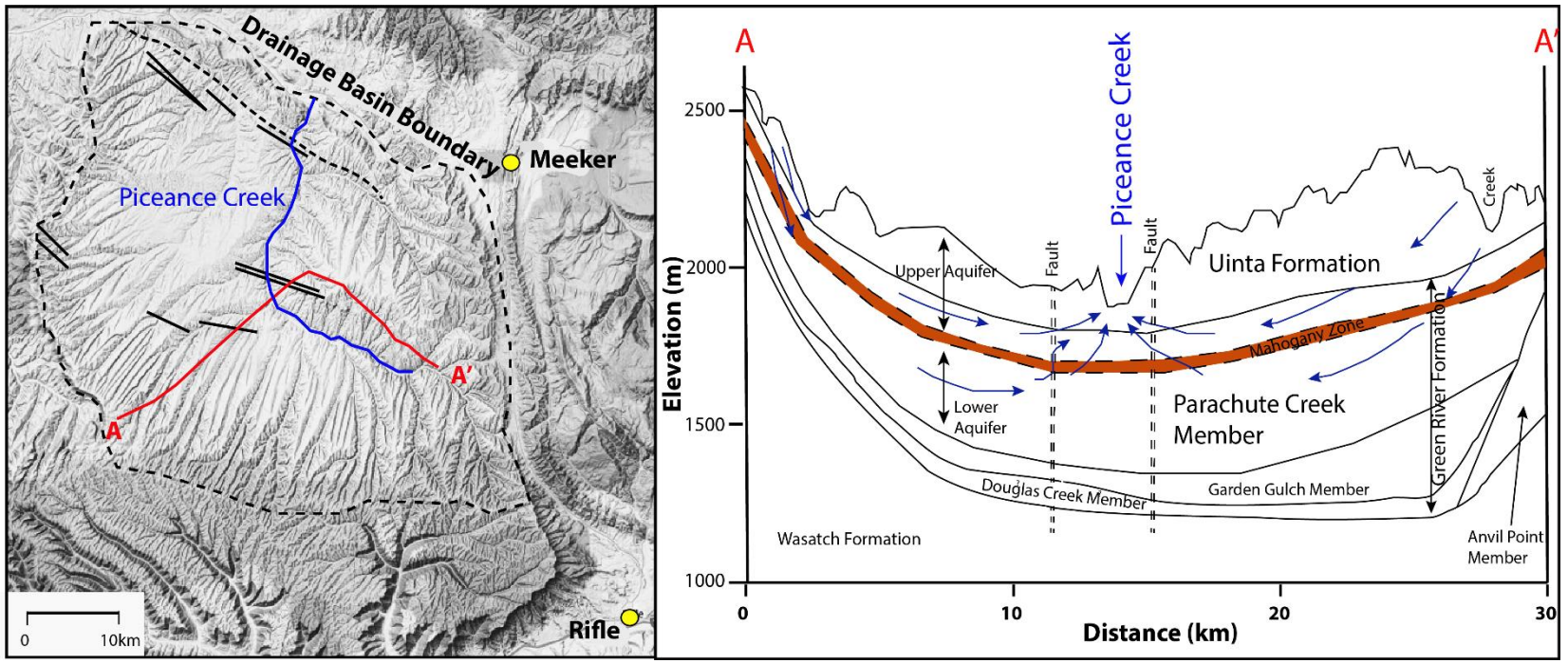

Figure 6. Plan view map (left: modified from Robson and Saulnier, 1981) and cross section (right: modified from Weeks et al., 1974) displaying presumed flow paths in the Piceance Creek Basin. The black lines on the map view depict major faults. The main formations and members are labeled along with the bounds of the upper and lower aquifer. The blue arrows show the presumed groundwater flow paths. The red-colored layer is the Mahogany Zone which acts as a leaky aquitard between the two aquifers.

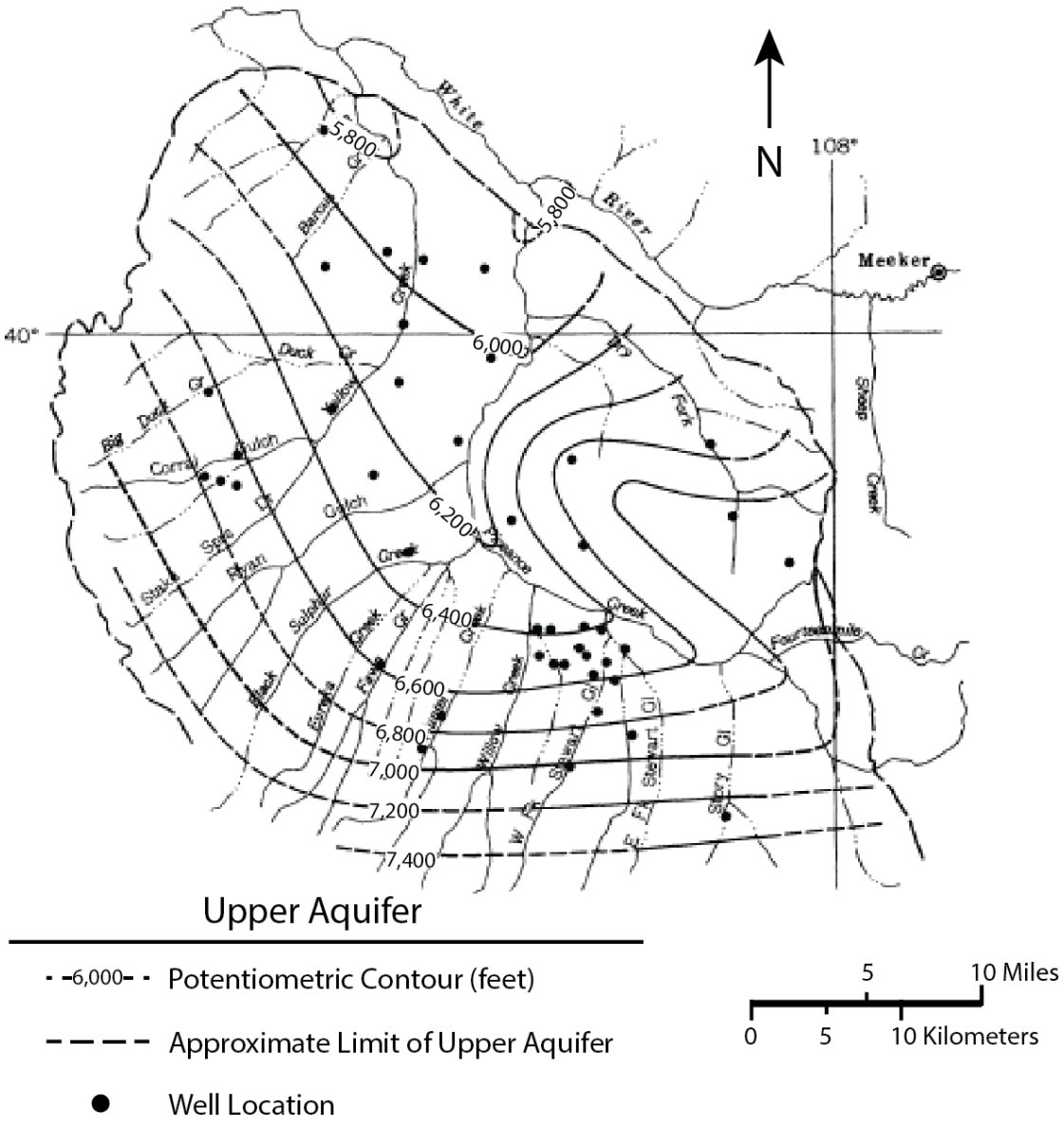

Figure 7. Potentiometric surface contours for the upper aquifer (image modified from Robson and Saulnier, 1981).

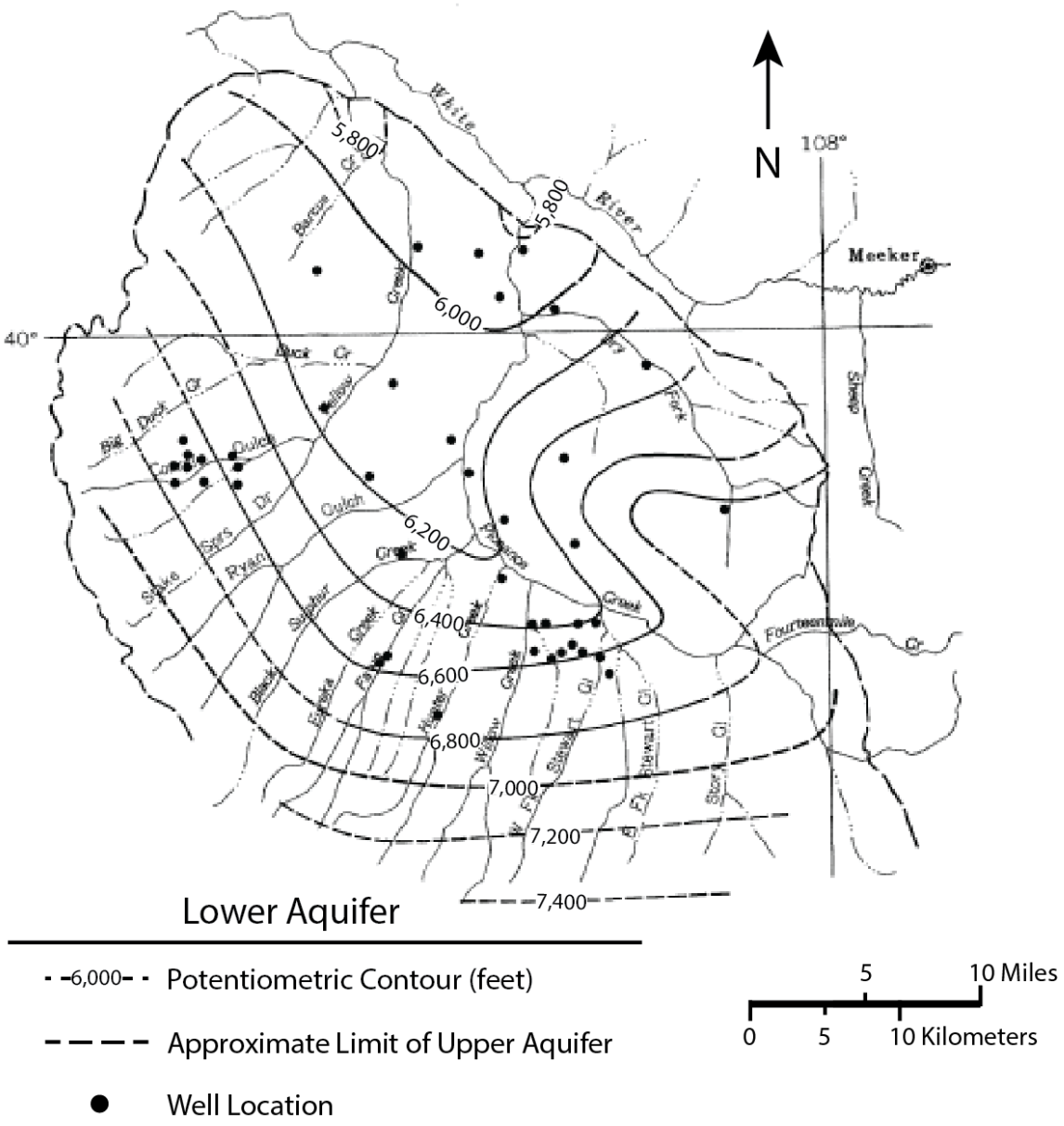

Figure 8. Potentiometric surface contours for the lower aquifer (image modified from Robson and Saulnier, 1981).

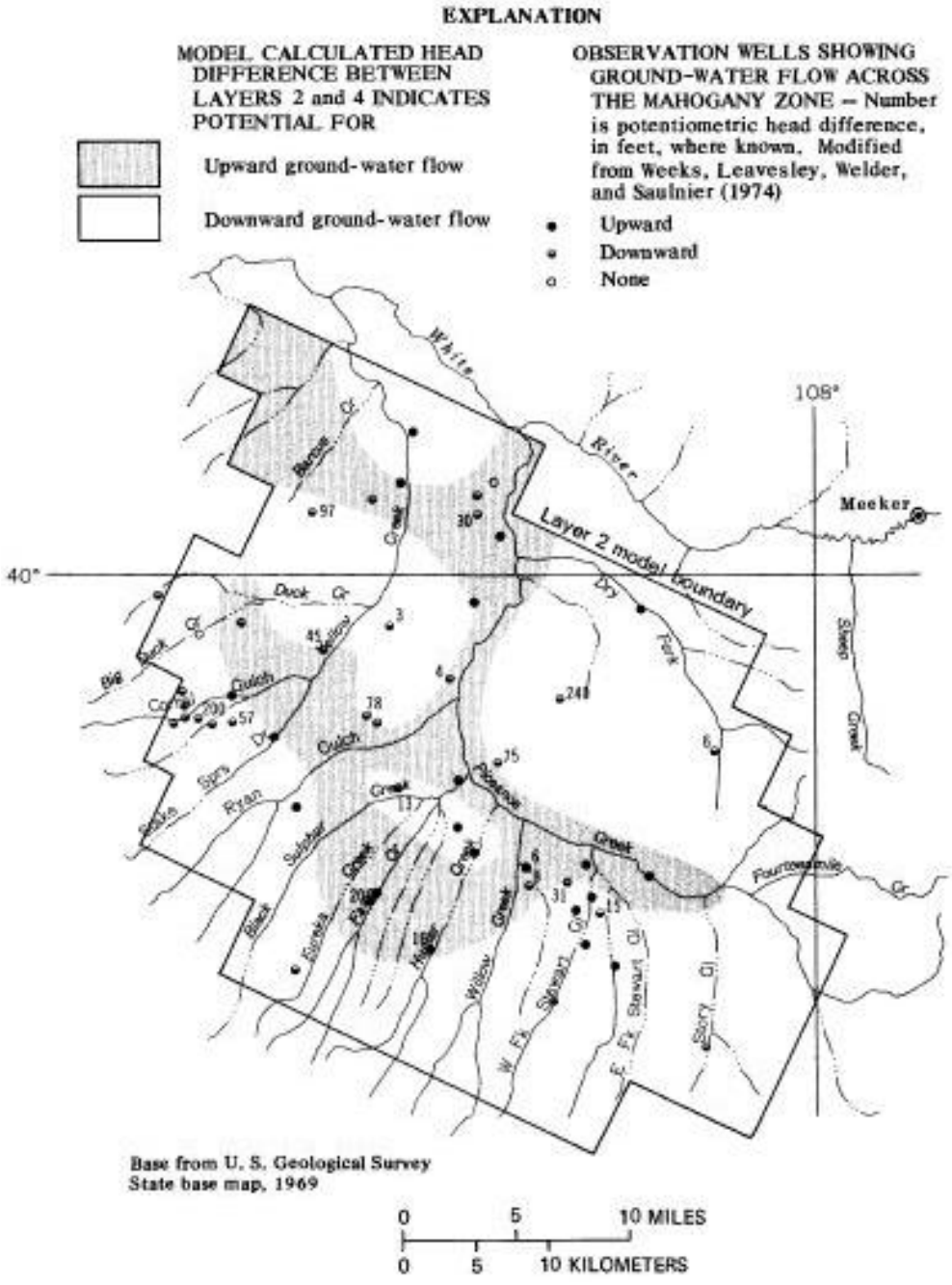

Figure 9. Map displays difference in potentiometric heads between the upper and lower aquifers in the Piceance Creek Basin (image from Robson and Saulnier, 1981).

CHAPTER 2 - SPATIAL DISTRIBUTION OF MAJOR IONS IN PICEANCE BASIN GROUNDWATERS

INTRODUCTION

The Piceance Basin has been of great interest since the Green River Formation was identified in 1874 (Thomas and McMahon, 2012). More recent studies have generally focused on characterizing the grade and extent of recoverable shale oil. Little research has been conducted on the aqueous geochemistry in the basin. Thomas and McMahon (2012) published a groundwater investigation using the same dataset used in this report. They focused on the sources of recharge to wells, comparison of ion concentrations to EPA drinking standards, and describing the distribution of some major, trace, and organic compounds.

This study differentiates itself by focusing on a smaller study area and fewer number of constituents for a more in-depth analysis of groundwater geochemistry. Specific objectives of the study are 1) to select and summarize data, 2) to evaluate groundwater flow paths, 3) to describe the general distribution and source of major and minor ions and, 4) to determine controls on major chemistry changes in the basin.

METHODS

Data Selection

The USGS Piceance Basin Water-Quality Data Repository (USGS, 2009) contains more than 100,000 entries. The dataset was first narrowed by selecting only data in the area of interest - the main watershed of Piceance Creek (Figure 1). In many cases, the analyses of multiple samples collected over time are reported for specific spatial (well) locations. One sample was chosen to represent the water quality at each location, based on two factors. The first was the degree of completeness; a sample analysis ("sample") was considered complete if it contained concentration values for common major ions (defined as calcium, magnesium, sodium, potassium, chloride, sulfate, and either (bi)carbonate or any alkalinity measurement), pH, temperature, and sample depth. If a site did not contain a complete set, the ion and/or parameter values of incomplete sets were still used, but complete sets were chosen preferentially as they are important for assessing mineral equilibrium. The second factor was the sample date – all else being equal, the most recent sample was chosen for analysis.

The resulting subset of data was checked and edited for consistency. For example, well locations were reported by various agencies in decimal degrees, UTM, and DMS format. Non-detect (ND) and minimum detection limit (MDL) values were replaced with one-half the detection limit value per methodology validated by Antweiler and Taylor (2008). Additionally, data were examined for statistical consistency in reporting values for temperature, pH, specific

conductivity, calcium, magnesium, sodium, potassium, chloride, alkalinity, and sulfate between different agencies, decades, and by season. Agency to agency variations may be attributed to differences in methodology, equipment and sampling techniques. Decadal variations may be caused by long-term chemical changes to the system or advancement in sampling and laboratory detection equipment, and seasonal variations may exist due to fluctuation in flow rates and temperature differences. If at all, seasonal variations will likely have the greatest impact on surface samples. To test for evidence of these in the selected data, a t-test was performed for normally distributed data and a Mann-Whitney test was used for non-normally distributed data (APPENDIX A).

After the relevant data were selected, it was important to determine sample depth relative to a datum, such as average sea level, instead of surface elevation. To determine sample elevation, digital elevation models (DEM) of the region were obtained from the U.S. Geological Survey, The National Map (2015), and sutured together via the mosaic tool in ArcGIS (version 10.3; Figure 10). The DEM raster provided a surface with units of meters above mean sea level. The 'extract values to points' function in the spatial analyst toolset extracted the cell values of the raster based on the coordinates of the point features. Thus, for each point in the subdataset, the surface elevation relative to mean sea level was obtained. The sample depths were subtracted from the surface elevations to obtain the sample elevations.

Once sample elevations above mean sea level were ascertained, the next step was to evaluate the samples relative to the position of the Mahogany Zone.

A raster model of the top of the Mahogany Zone was available from a USGS digital data series accompanying a publication by Johnson et al. (2010) (Figure 11). The raster was in units of feet above mean sea level and were converted to meters using map calculation tools in ArcGIS. The 'extract values to points' function was used again to obtain an elevation for the top of the Mahogany Zone at each data point.

The sample elevation was compared to the Mahogany Zone elevation and was assigned one of three categories: Surface samples (samples with depths equal to zero - rivers, streams, and springs, although the database does not accurately distinguish between the specific types), upper aquifer (samples collected above the Mahogany Zone), and lower aquifer (samples collected below the top of the Mahogany Zone).

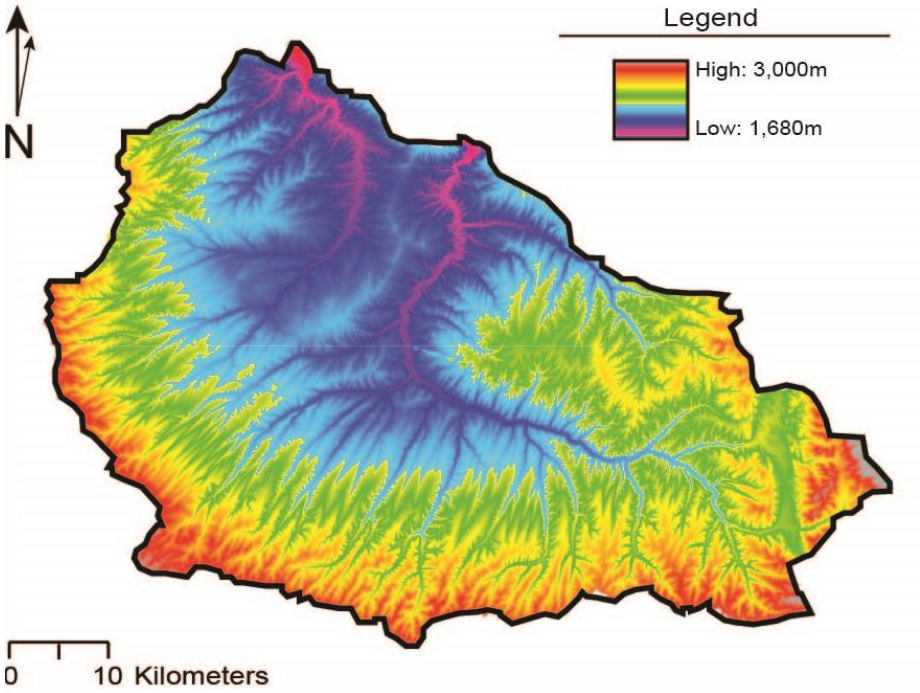

Figure 10. Digital elevation model of the study region. The highest expressions are along the west, south, and southeastern boundary, and the elevation decreases towards the north (USGS, 2015).

Statistical Analysis

Preliminary statistics conducted on the selected dataset include the minimum and maximum concentrations for each analyte/parameter of interest, the number of samples, and sample means for each hydrologic unit. Correlation and factor analyses (FA) were used to evaluate relationships among variables and reduce dimensions to a smaller number of factors based on correlations in the data. Cluster analysis was performed to evaluate homogenous groups of classes and determine the number of groups present in the system. Z-scores were calculated for each observation and used to normalize the data and limit

effects due to relative magnitude of variables. Additionally, outliers were removed prior to analysis by a Grubbs Outlier Test (Grubbs, 1969).

Correlation coefficients were calculated using Pearson's correlation coefficient. The correlation coefficient table is a measure of the linear dependence between to random variables, *A* and *B*; it indicates how strongly two variables are related to each other with +1 being highly positively correlated, 0 indicating no correlation, and -1 indicating high negative correlation (see Table 1 for a more detailed correlation strength breakdown).

FA is a statistical data reduction technique in which values of observed data are expressed as linear combinations that describes variability in terms of a reduced number of unobserved variables, or factors. The results of the factor analysis were used to identify similar groups of variables associated with a particular factor contributing the most variability in the data. The analysis was carried out in Matlab (Version 2011a) with the major ion data, pH, temperature, and depth (APPENDIX B).

The factor analysis implemented the maximum likelihood extraction method and was rotated to make the pattern of loadings more pronounced. Varimax rotation, an orthogonal rotation method which assumes no correlation between the factors, was used in this study as it provided the "simplest" structure (Costello and Osborne, 2005). The loadings for each factor, i.e. the correlation between the observed score and latent score, were evaluated and categorized as very weak, weak, moderate, strong, or very strong according to the values summarized in Table 1 (Evans, 1996). When the loadings or correlation

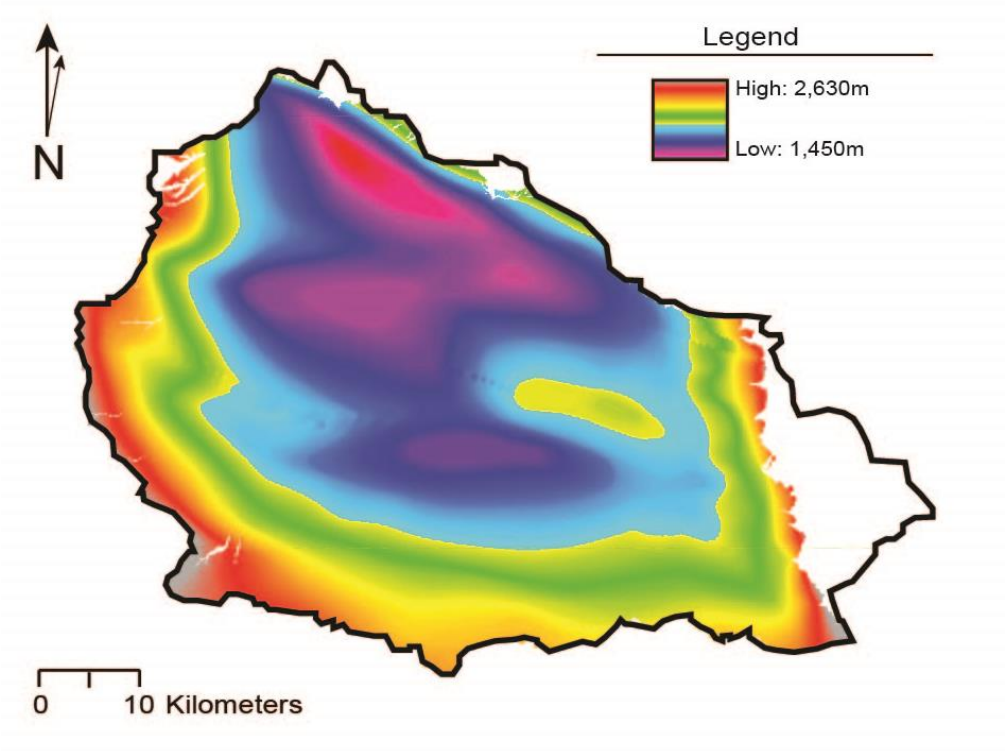

Figure 11. Digital elevation model for the structural contours of the Mahogany Zone (Johnson et al., 2010).

coefficients are positive numbers, the relationship is said to be positively correlated, and the opposite is true for negative values. Loadings that were strong to very strong were considered most influential to the factor. Next, the factor scores were computed. Factor scores are the estimated contribution of each factor to each observation. The factor scores were plotted by depth categories in ArcGIS to assess the spatial distribution of the dominant factors found in this analysis. Between points were interpolated using universal kriging with linear drift (see methodology for concentration distribution maps for information on kriging and the interpolation selection processes).

Table 1. Correlation strength interpretation terms

$\lvert Factor\ Loading\ Values / Correlation\ Coefficient \rvert$	Strength (Evans, 1996)
0.00 – 0.19	Very weak
0.20 – 0.39	Weak
0.40 – 0.59	Moderate
0.60 – 0.79	Strong
0.80 – 1.0	Very strong

Ion Concentration Distribution Maps

Total ion concentrations were evaluated spatially by plotting the concentration values for each hydrologic unit in ArcGIS and interpolating between the points. Careful consideration was given to the type of interpolation method used for this evaluation. Li and Heap (2008) published a comprehensive report addressing the different types of interpolation methods and the limitations and strengths of each per different data types. Based on the decision tree included in their publication, universal kriging as chosen as the best interpolation method for this project. Kriging is a geostatistical method used to predict values in regions with no data and is commonly used in geology, soil science and to model geochemical phenomena (Childs, 2004). Kriging is stochastic and assumes a degree of error in the input values and estimates the output values as statistical probabilities (Childs, 2004). Universal kriging also assumes an overriding trend exists in the data that can be modeled and that the function changes over space. This is appropriate for the dataset as there are known

spatial changes in mineralogy (Cole and Picard, 1986). There is not one perfect interpolation method for each dataset. Rather, a large part of choosing the right interpolation method involves intuition (Li and Heap, 2008); an intimate knowledge of the dataset is required and ultimately, finding an interpolation method that best captures the data variations is the goal. Therefore, different interpolation methods were tested on the same set of data (calcium concentration values from the lower aquifer). The tested interpolation methods included: ordinary kriging (linear, Gaussian, exponential, circular, spherical), universal kriging (linear and quadratic), and trend surface analysis. Only inexact interpolators were considered because the exact input value is not as important to this study as the overall trend of the system.

Upon selection of the best interpolation method (universal kriging), dissolved constituent concentration distribution maps were produced for the following major ions: calcium, magnesium, sodium, chloride, sulfate, and alkalinity. Other mapped parameters include temperature, pH, and specific conductivity. Standard residual errors were calculated for each sample point comparing the measured results value with the interpolated value. Residual errors were added to the map as sample point symbols for three categories: less than one, one to three, and greater than three.

Parameter values displayed on the maps were separated into four different classifications, displayed as different colors. The selected categories were chosen by Jenks natural breaks optimization method (Jenks, 1967). The Jenks method aims to reduce the variance within a class and maximize the

variance between classes. The break values were then rounded up for clean interval values.

Evaluation of Groundwater Evolution Along Flow Paths

Concentrations for major cations and anions were converted to milliequivalents per liter (meq/L) and then converted to a percent of the total cations/anions. For example, the cation percent for calcium in a sample is the meq/L of calcium divided by the sum of meq/L calcium, magnesium, potassium and sodium. The percentages were plotted at specific points along a presumed groundwater flow path. Dominant cations and anions were plotted over relative distance using Microsoft Excel.

RESULTS

Data Selection

Upon refining the dataset, a maximum of 267 sites were included in the final subdataset from three agencies, spanning the time range from 1966 to 2008 (Table 2). Less than 1% of the data used was gathered in the 1960s, 67.6% was sampled in the 1970s, 20.2% was from the 1980s. No data used in this study is from the 1990s and 11.3% was from the 2000s. The reason for the data gap in the 1990s is primarily many wells that were sampled in the 1990s were also sampled in the 2000; thus, the most recent samples were used for this project

leaving a temporal gap in the 1990s. Figure 12 displays the data by decade with different size symbols to represent hydrologic unit.

The samples were placed into one of three hydrologic units (i.e. surface sample, upper aquifer, and lower aquifer), and the average percent of samples in each category and the corresponding depth intervals are summarized in Table 3 below. Surface samples comprised over half the data (54.8%). Approximately 20.1% was sampled from the upper aquifer, and 25.1% from the lower aquifer.

The well locations, agency, and relative depths are displayed in Figure 13. The bottom map displays the USGS data locations in blue with relative symbol sizes corresponding to each hydrologic unit. The top map displays the COGCC and ENCANA data points in orange and purple respectively. Two maps were used to better illustrate the locations of the COGCC and ENCANA data points which are imperceptible when plotted on the same map as the USGS data.

Results from the t-test and Mann Whitney tests comparing agency to agency were unable to distinguish the sets apart with a confidence level of 5%, with the exception of chloride values between EnCana and COGCC, and sulfate values between USGS and COGCC data. EnCana and COGCC sample locations do not overlap geographically, therefore differences between the two are dismissible as ion concentrations are known to vary spatially (Figure 13). Although there are USGS points in close proximity to COGCC well locations, the points do not overlap in three-dimensional space; the sample depths are at least 200m apart. Once again, these differences may be negligible or indiscernible considering the spatial variations expected in the basin.

Results from the t-test and Mann Whitney tests comparing decadal variation report several differences in certain ions with a confidence level of 5%. However, there are confounding factors that may influence this result. For example, data collected in the 2000s is confined a small region in the center of the basin at Piceance Creek where samples were collected from the upper and lower aquifer, and surface samples were collected narrowly at the southern margin. Of all the data collected in the 1980s, less than ten samples were collected from the upper and lower aquifer and data collected in the 1970s contains the most samples from below the surface (Figure 12). These differences may, once again, be negligible or indiscernible considering the spatial variations expected in the basin.

Results for seasonal variations were unable to distinguish the sets apart with a confidence level of 5%, with the exception of temperature, pH, calcium and magnesium. These parameters were further evaluated by hydrologic unit, and significant differences in these parameters occurred only in surface samples. This result is expected as snowmelt contributions and variations in temperature and biologic activity between the seasons will influence the water chemistry. Between summer and winter months, calcium concentrations fluctuated an average of 15 mg/L, magnesium 25 mg/L, temperature 3˚C, and pH an average of 0.25.

To account for potential variations that may results from the aforementioned factors, results in this study implemented additional methods to minimize data discrepancies, such as inexact interpolation (discussed later in this

chapter), and weighted mineral saturation indicies (discussed in Chapter 3). A summary of the results from the t-test and Mann Whitney tests is provided in Appendix A and a comprehensive summary of the data, including the number of samples per each constituent and the value range is provided in Table 4 along with the number of samples and mean value of each constituent in each hydrologic unit.

Piper Diagram

The piper diagram was created using the program GW Chart (Version 1.28.0.0), published by the U.S. Geological Survey (USGS, 2000), and was divided into four main classifications and four sub-classifications based on ones used in a study by Bartos and Ogle (2002). The main classifications include the following: Calcium-magnesium-chloride-sulfate type; calcium-magnesium-bicarbonate-chloride type; sodium-potassium-bicarbonate-chloride type; and sodium-potassium-chloride-sulfate type waters.

Piper diagram results for the three individual hydrologic units as well as all samples combined are displayed in Figure 14 - Figure 17. Surface samples are predominately (bi)carbonate waters, but overall do not have a particular dominant cation, although some tend towards being sodium dominated (Figure 14). Samples from the upper aquifer appear to have cations that range from mixed to nearly 100% sodium and the anions appear to have two distinct groups, one that is a continuum along the bicarbonate-sulfate line and the other along the

bicarbonate-chloride line. The water chemistry of the upper aquifer samples are categorized as Ca-Mg-Cl-SO_4, Ca-Mg-HCO_3-Cl, Na-K-HCO_3-Cl, and Na+K type, with very few samples falling into the Na-K-Cl-SO_4 type (Figure 15).

Table 2. Summary of data sources that contribute to the Piceance Basin Data Repository and were used in this study.

Agency Name	Sites	Date Range	
Colorado Oil and Gas Conservation Commission	3	9/12/77	1/30/02
EnCana Oil and Gas (USA) Inc.	13	8/18/05	8/26/08
U.S. Geological Survey	251	5/24/66	12/7/00

Table 3. Percent of samples per aquifer and corresponding depth interval.

Aquifer	Number of Samples	Percent of Total Samples	Depth Interval (m)	
Surface	146	54.8	0	0
Upper	54	20.1	6.5	390
Lower	67	25.1	6.5	2300

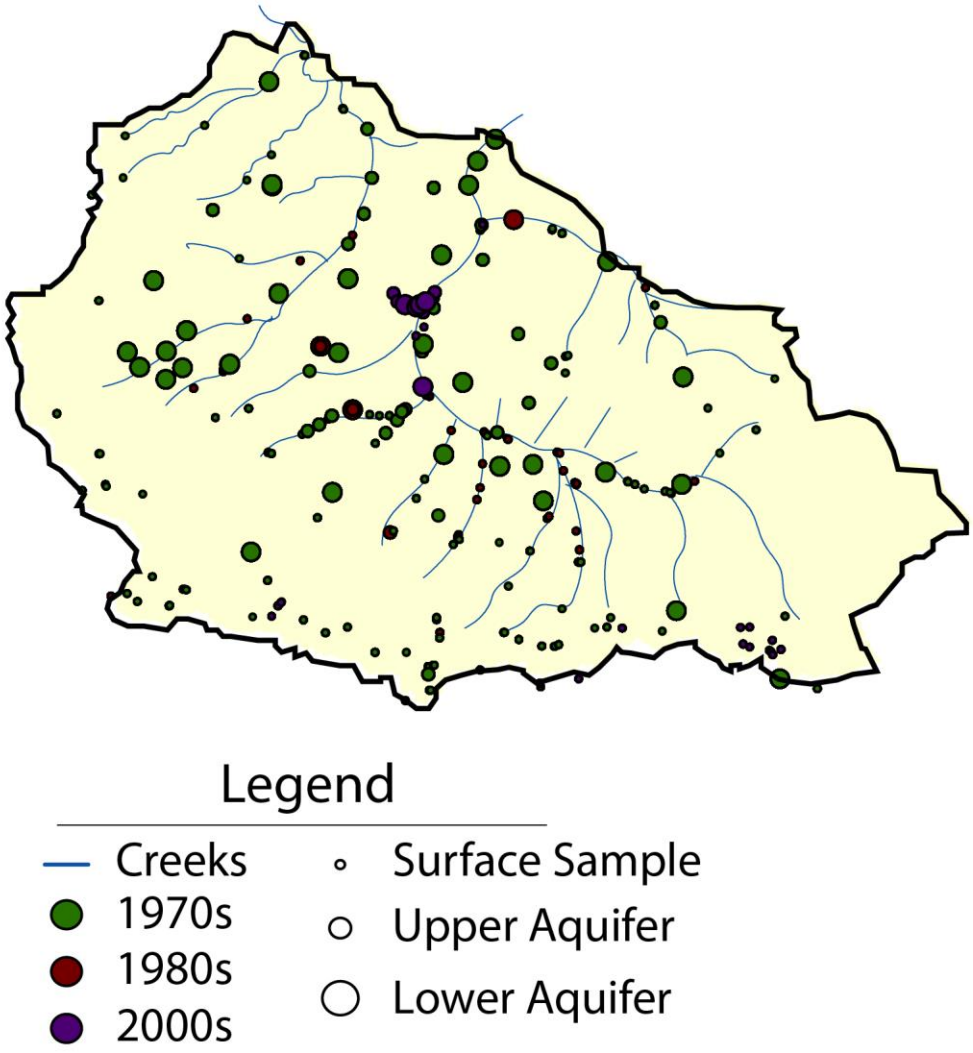

Figure 12. Sample spatial distribution by decade with graduated symbols showing depth. Samples collected in the 1970s are displayed in green on the figure, 1980s are red, and 2000s are displayed in purple.

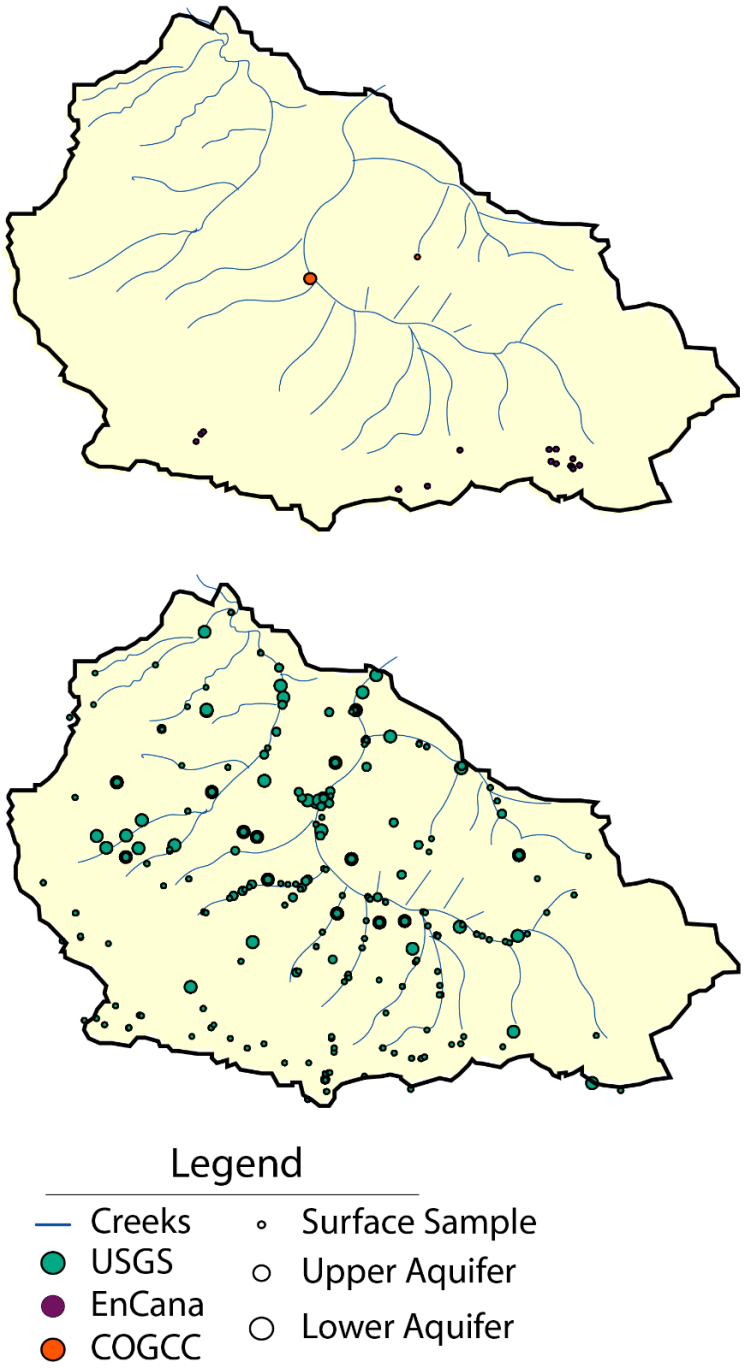

Figure 13. Sample spatial distribution by agency with graduated symbols showing depth. USGS point locations and depths are displayed in green on the figure (bottom) and EnCana is represented with purple and COGCC is red (top). COGCC and EnCana were displayed on a separate map from the USGS due to the large number of samples in the latter data source.

Table 4: Parameter and dissolved concentration value summary by aquifer in the main watershed of the Piceance Creek Basin, Colorado.

Parameters	Units	Total	Value Range		Surface Waters		upper aquifer		lower aquifer	
		Sites	Min	Max	No. Sites	Mean	No. Sites	Mean	No. Sites	Mean
Temperature	° C	250	6	32	149	10.2	43	15.6	58	18.6
pH		267	6.1	9.68	161	7.6	46	7.9	60	8.2
Specific Conductivity	uS/cm 25C	215	416	46300	117	1540	41	3500	57	4870
Calcium *	mg/L	229	1.1	190	122	81.2	46	37.8	61	19.7
Magnesium *	mg/L	230	0.3	245	122	62.9	47	51.2	61	18.4
Sodium *	mg/L	231	29	25418	123	230	47	1040	61	2360
Potassium *	mg/L	230	0.3	729	123	1.43	46	4.23	61	18.2
Chloride *	mg/L	229	0.5	11874	123	32.3	46	150	60	429
Sulfate * ŧ	mg/L	227	0.31	1741	123	290	46	258	58	156
Alkalinity* ŧ	mg/L CaCO3	212	1	49500	108	664	45	2190	59	4997
Fluoride *	mg/L	219	0.05	64	114	0.97	46	8.5	59	18.0
Iron *	ug/L	205	3	49000	103	85.2	46	1660	56	236
Notes:	* Samples filtered									
	ŧ Samples unfiltered									

Samples from the lower aquifer are predominantly sodium (bi)carbonate type waters although some lack a dominant cation or anion and a few are sulfate type waters. The water chemistry of the lower aquifer is primarily categorized as Na-K-HCO_3 and Na+K types, with few samples falling into the categories of Ca-Mg-HCO_3-Cl and Na-K-Cl-SO_4 types (Figure 16).

When plotted on the same ternary diagram (Figure 17), surface samples contain the majority of samples with no dominant cation while the upper and lower aquifer samples increasingly tend towards sodium dominant.

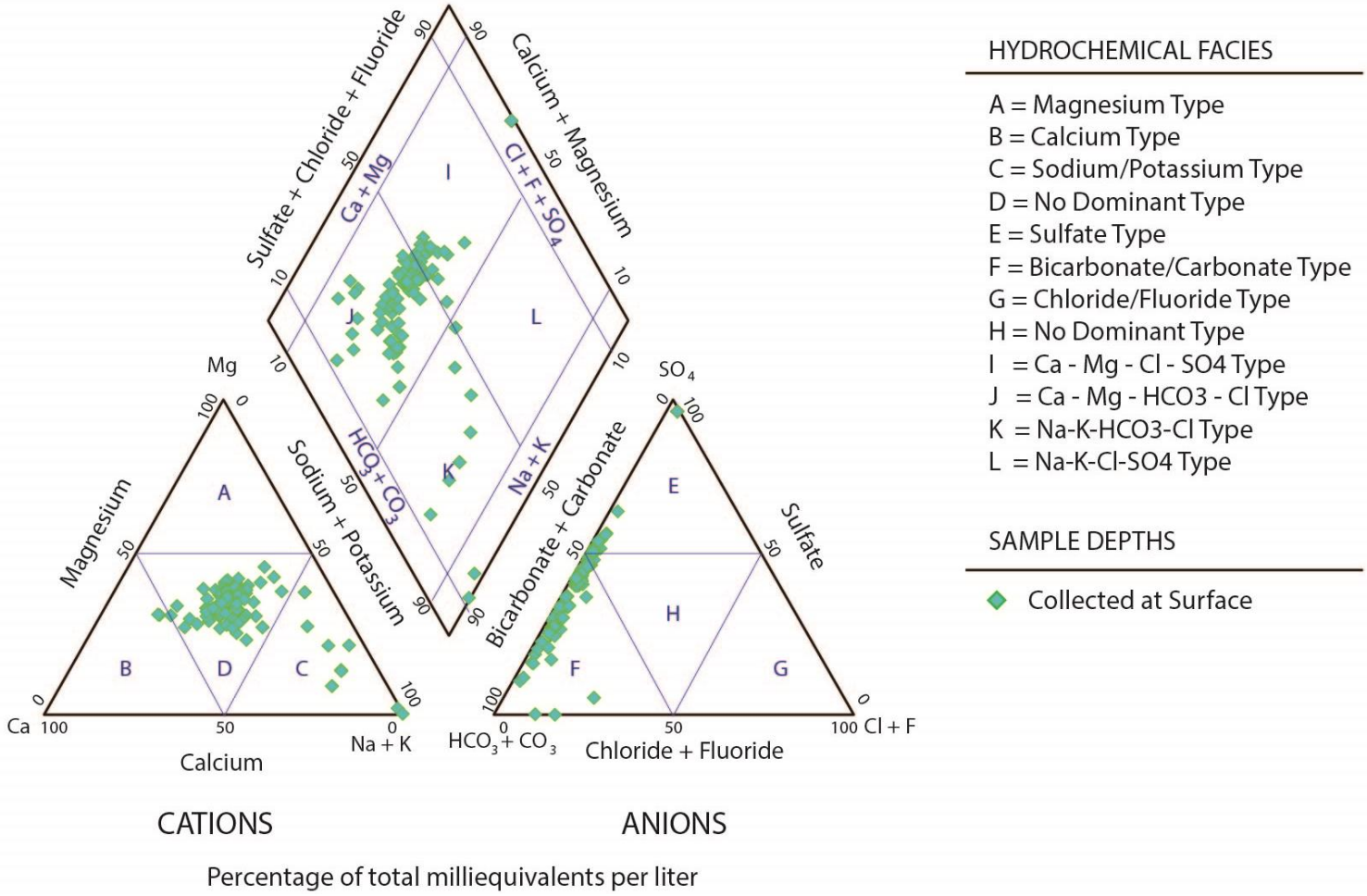

Figure 14. Piper diagram showing water types for surface samples collected from the Piceance Creek Basin.

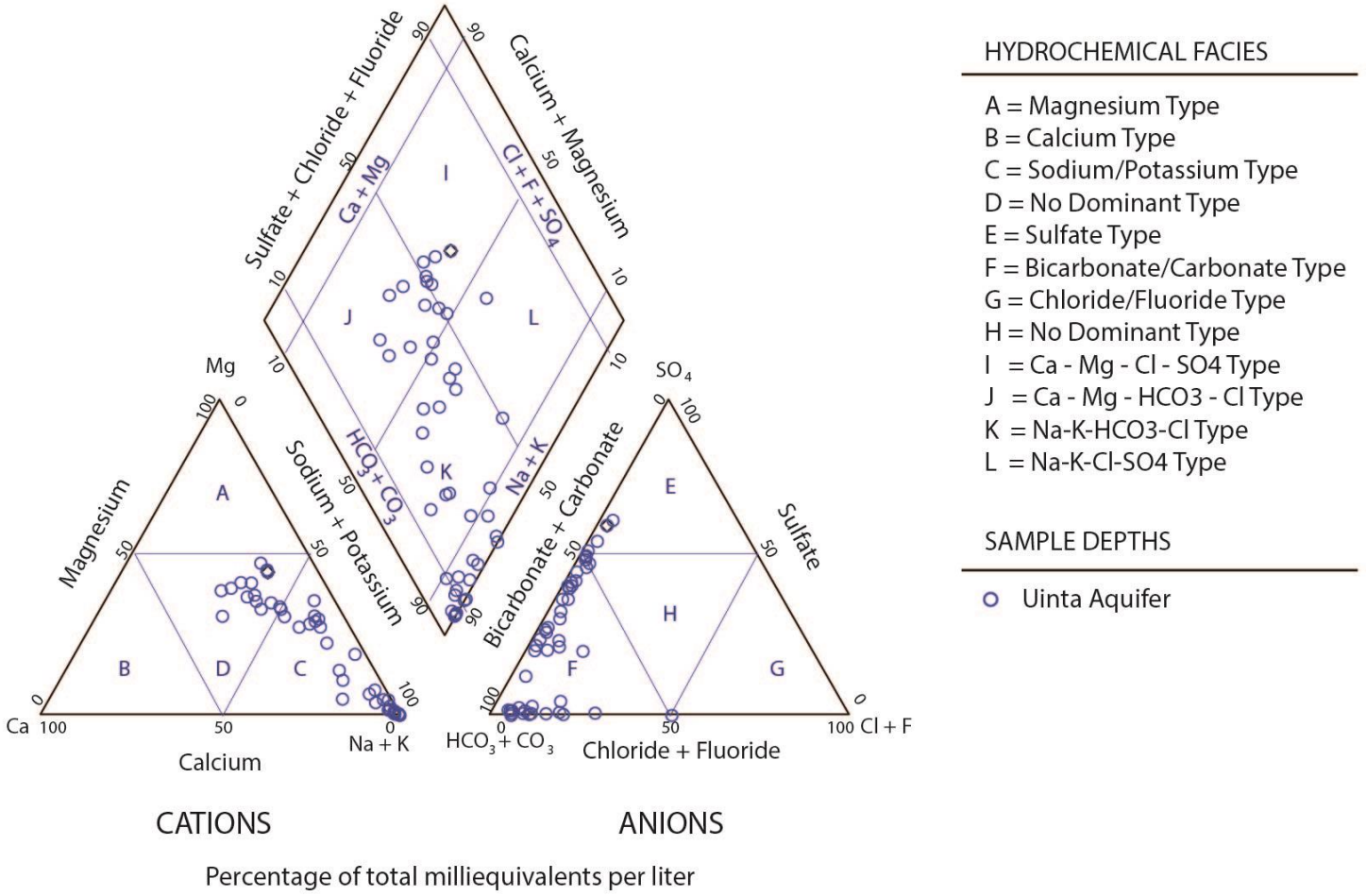

Figure 15. Piper diagram showing water types for groundwater samples collected from the upper aquifer in the Piceance Creek Basin.

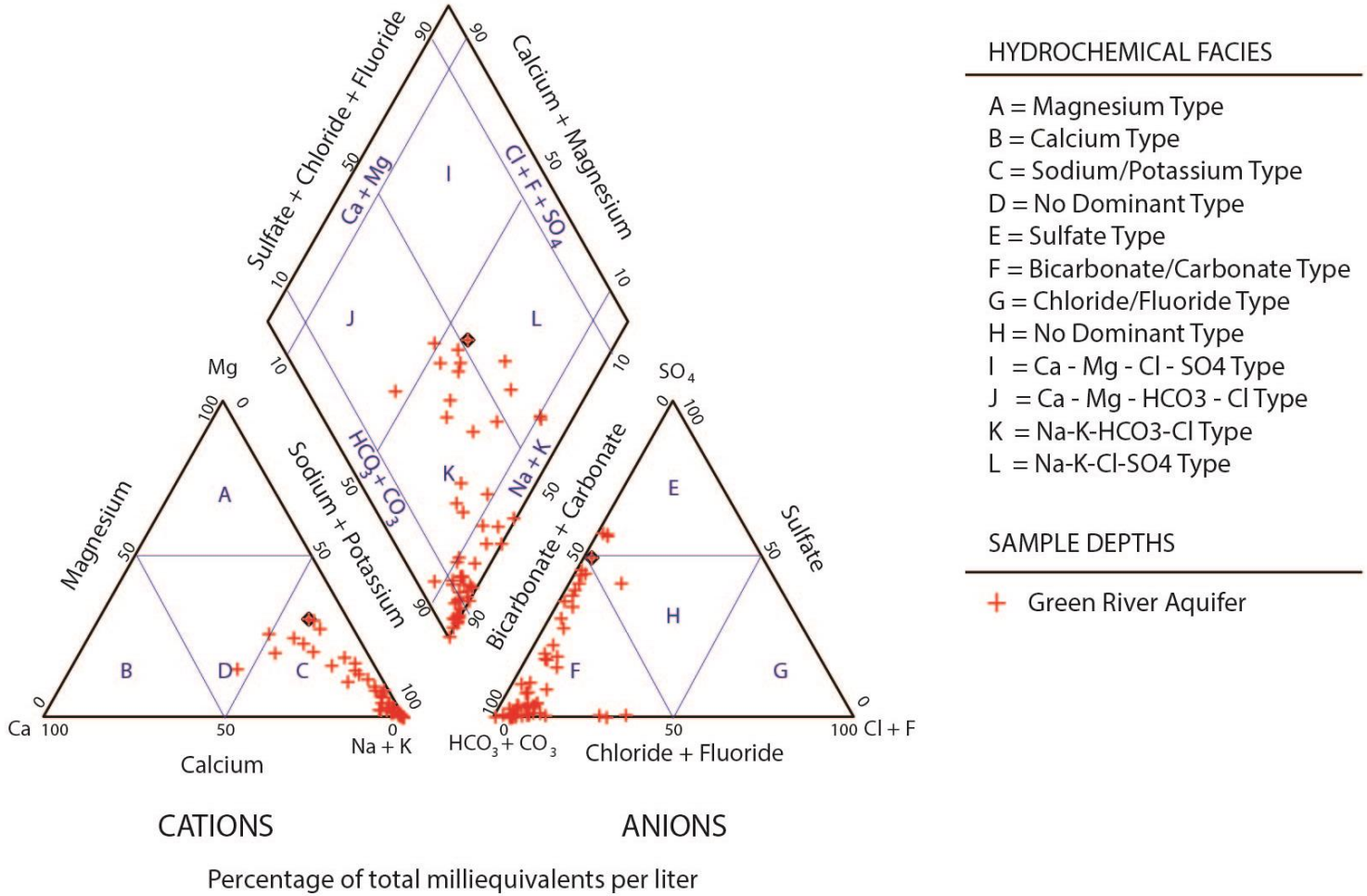

Figure 16. Piper diagram showing water types for groundwater samples collected from the lower aquifer in the Piceance Creek Basin.

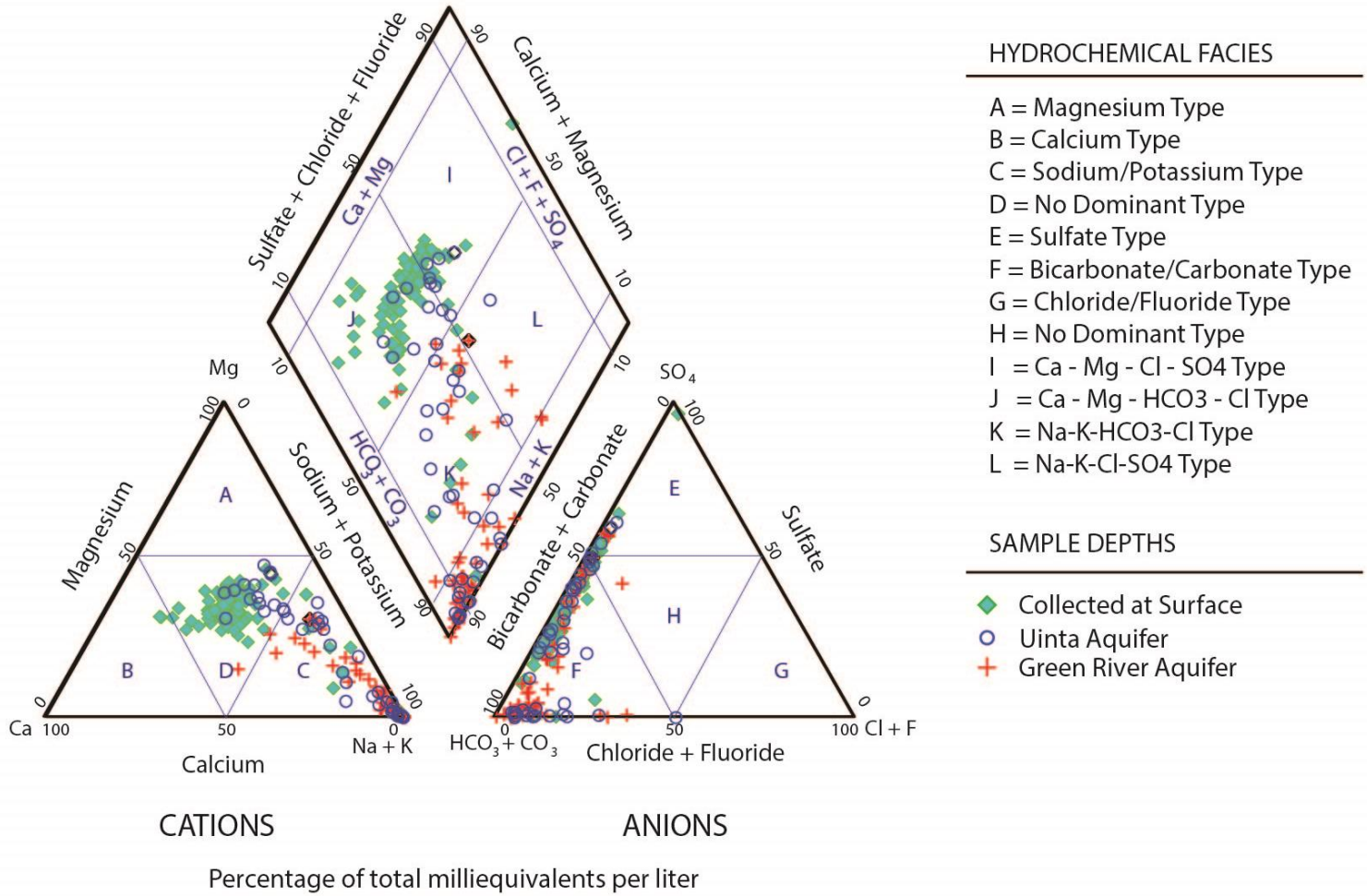

Figure 17. Piper diagram of all water samples in the Piceance Creek Basin. The cyan diamonds represent samples collected at the surface. Blue circles represent samples collected in the upper aquifer, and red plus signs correspond with samples collected in the lower aquifer.

Statistical Analysis

A comprehensive summary of the data, including the number of samples per each constituent and the value range is provided in Table 4 along with the number of samples and mean value of each constituent in each hydrologic unit.

Results from the correlation and factor analyses are summarized below in Table 5 and Table 6. Values with strong to very strong correlation strengths (Table 1) are in bold, additionally, strengths that are considered very strong are highlighted light red.

Table 5. Correlation table results for major ion concentrations and field parameter values, Piceance Creek Basin, Co.

	Depth	Alk	Ca	Cl	K	Mg	Na	pH	SO4	Temp
Depth	1.00	0.17	**-0.68**	0.14	0.12	-0.56	0.20	0.53	-0.39	**0.76**
Alkalinity		1.00	-0.37	**0.85**	**0.75**	-0.24	**0.99**	0.24	-0.25	0.23
Calcium			1.00	-0.30	-0.23	**0.76**	-0.40	**-0.69**	**0.67**	**-0.75**
Chloride				1.00	**0.69**	-0.20	**0.89**	0.20	-0.22	0.18
Potassium					1.00	0.01	**0.76**	0.17	-0.04	0.17
Magnesium						1.00	-0.25	-0.41	**0.91**	-0.58
Sodium							1.00	0.27	-0.26	0.26
pH								1.00	-0.33	0.57
Sulfate									1.00	-0.43
Temperature										1.00

Table 6. Factor loading correlation results for major ion concentrations and field parameter values, Piceance Creek Basin, Co.

(% variance explained)	Factor1 (48.68)	Factor2 (26.90)	Factor3 (10.10)
Depth	0.05	**0.80**	-0.22
Alkalinity	**0.98**	0.12	-0.15
Calcium	-0.22	**-0.75**	0.48
Chloride	**0.86**	0.09	-0.12
Potassium	**0.78**	0.13	0.11
Magnesium	-0.06	-0.45	**0.88**
Sodium	**0.98**	0.15	-0.15
pH	0.15	**0.67**	-0.12
Sulfate	-0.09	-0.27	**0.90**
Temperature	0.10	**0.85**	-0.22

Thurstone (1947) proposed five criteria for selecting the number of factors retained in FA to achieve a simple structure. The five criteria include: 1) Each variable should produce a zero loading on some factor; 2) Each factor should have at least as many zero loadings as there are factors; 3) Each pair of factors should have variables with significant loadings on one and zero loadings on the other; 4) Each pair of factors should have a large proportion of zero loadings on both factors; 5) Each pair of factors should have only a few complex variables, which are variables with notable loadings on two or more factors (Brown, 2009).

Based on these criteria, three factors were chosen for the FA and account for 85.7 percent of the total variance in the data (Table 6).

Factor 1 accounts for 48.7 percent of the data variance and includes a very strong positive correlation with alkalinity, sodium, chloride, and a strong positive correlation with potassium. Factor 2 accounts for 26.9 percent of the variance and contains a very strong positive correlation with depth and temperature, a strong positive correlation with pH, and a strong negative correlation with calcium. Factor 3 accounts for 10.1 percent of the variance and includes a very strong positive correlation with magnesium and sulfate.

The factor loadings were used to calculate factor scores which estimate the contribution of each factor to each observation (APPENDIX B). The factor scores were plotted in ArcGIS within each hydrologic unit and are displayed below in Figure 18 -Figure 20. This allows for analysis of the geospatial location of correlated samples.

Figure 18 displays the factor scores for Factor 1 by hydrologic unit. Higher values indicate more positive correlation between the sample points and the factor. Surface samples overall have high factor scores with the largest values near the discharge point of Piceance Creek and Yellow Creek. In the upper aquifer, values are greatest in the center basin and in areas along the western boundary. The lower aquifer values increase from southeast to northwest.

Figure 19 displays the factor scores for Factor 2 by hydrologic unit. In general, factor scores increase with depth. Surface sample scores are greatest in the basin center to the north. Upper aquifer scores are greatest in the basin

center and factor scores are very high in the lower aquifer except in the northwestern region of the study area.

Factor 3 scores are displayed in Figure 20 by hydrologic unit. Surface sample factor scores increase from the drainage boundaries to the basin center and towards the north. Factor scores in the upper aquifer increase from the southeast to the northwest, and scores are lowest in the lower aquifer in which the score does not increase past zero.

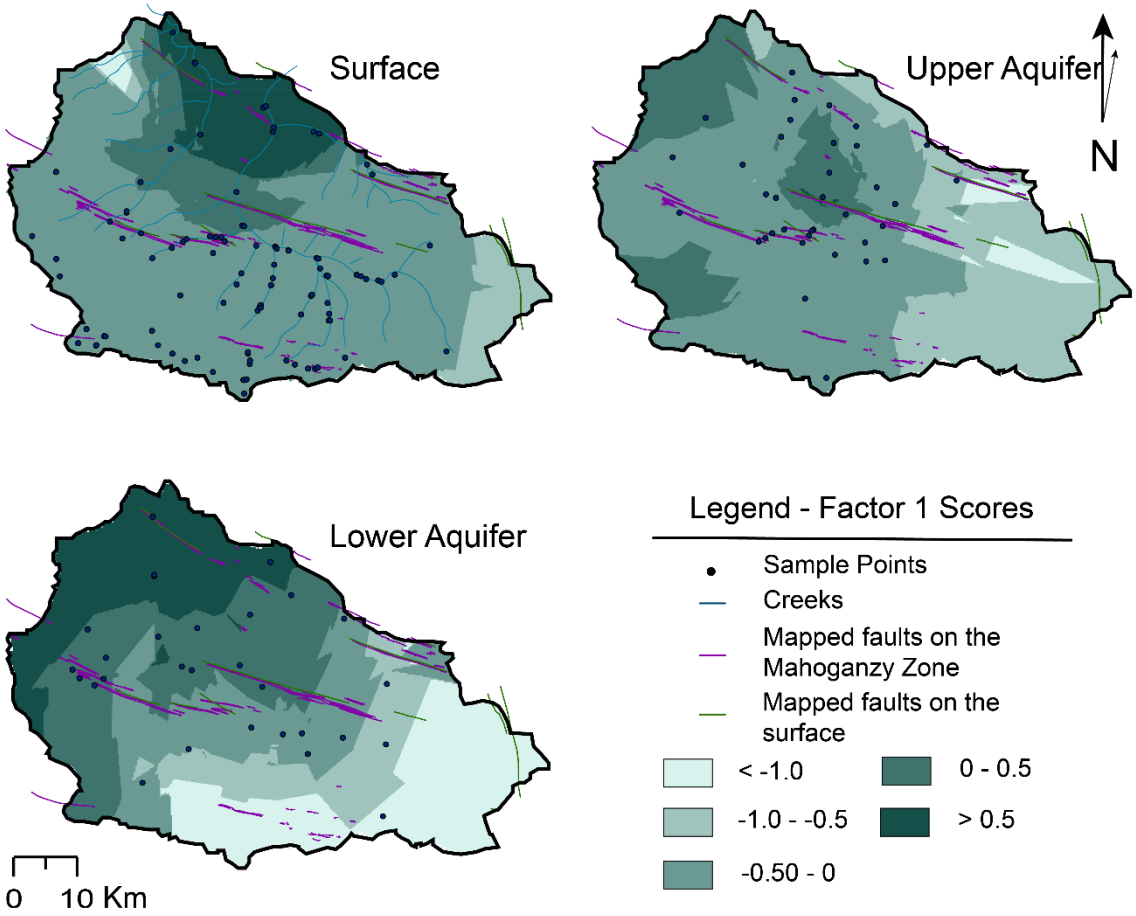

Figure 18. Factor score results for Factor 1, plotted using universal kriging interpolation of points by hydrologic unit. The higher the value, the stronger positive correlation with the factor.

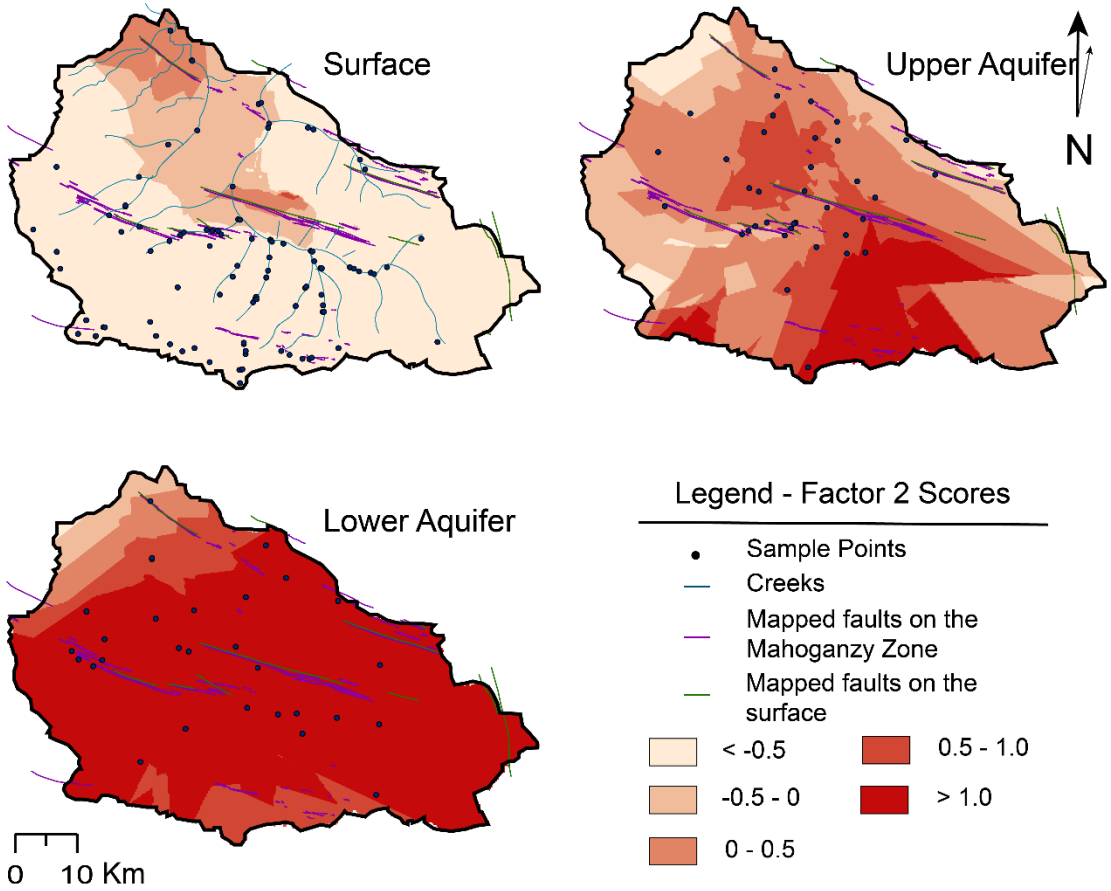

Figure 19. Factor score results for Factor 2, plotted using universal kriging interpolation of points by hydrologic unit. The higher the value, the stronger positive correlation with the factor.

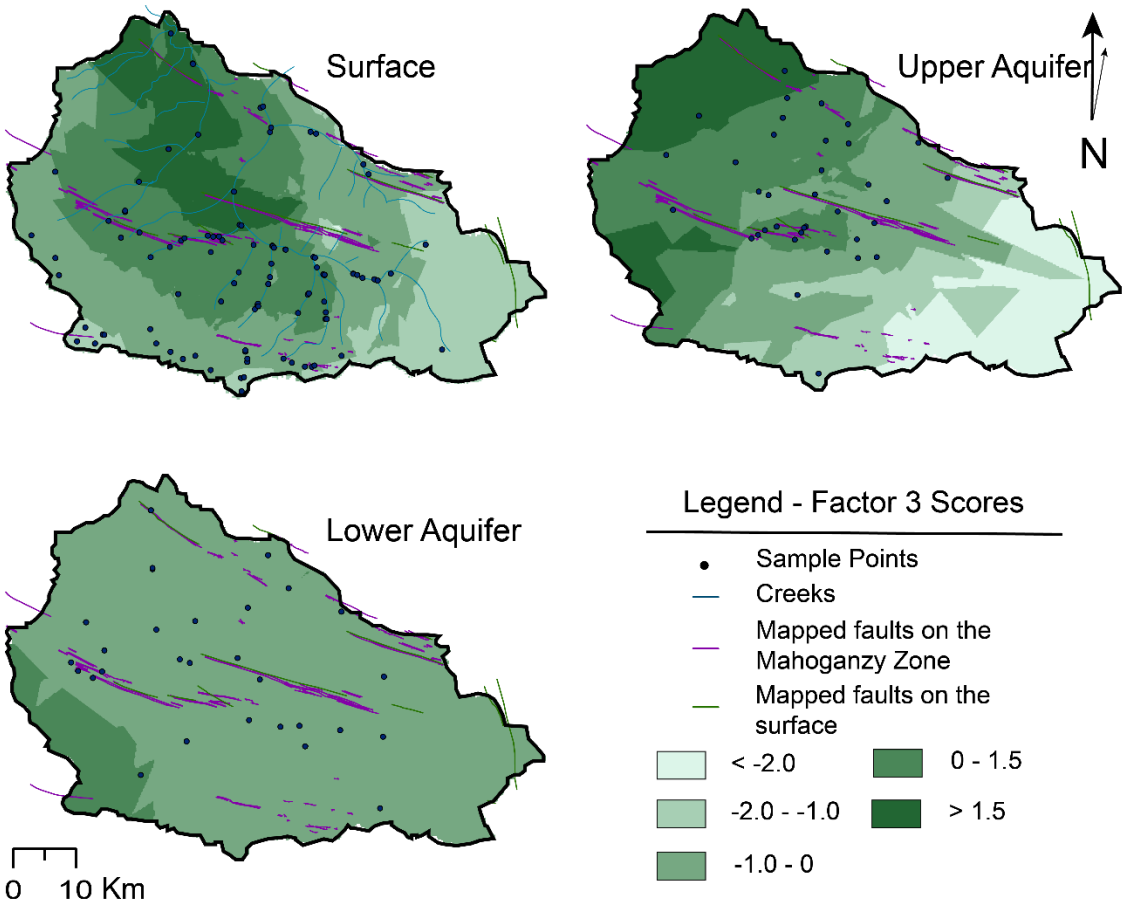

Figure 20. Factor score results for Factor 3, plotted using universal kriging interpolation of points by hydrologic unit. The higher the value, the stronger positive correlation with the factor.

Concentration Distribution Maps

Constituent concentration distribution maps were created for major ions and field-measured parameters for each hydrologic unit. Linear universal kriging was selected as the interpolation method because it was the best method for this particular dataset and modeling objectives based on the Li and Heap (2008) evaluation method, and upon visual observation it was the method that most accurately represented the concentration variations in the system (Figure 21). Measured calcium concentrations in the lower aquifer range from 2.4 to 190 mg/L. Ordinary kriging methods use a global mean for interpolation and ignore localized variations. This kriging method generally estimated a concentration range between 6.5 to about 50 mg/L. Trend surface analysis results in similar ranges from -4 to 40 mg/L, and quadratic universal kriging accentuated the concentration range between -187 and 278 mg/L. Linear universal kriging was closest to encompassing the true variations in calcium concentrations in this aquifer unit (-4 to 112 mg/L) and was used for creating concentration maps in this chapter.

Field parameters

Field-measured parameters include pH, temperature, and specific conductivity. Each parameter result contains three maps showing the interpolated distribution of dissolved constituent concentrations for water in the upper aquifer, lower aquifer and surface samples (Figure 22-Figure 24).

pH values in the basin (Figure 22) generally increase with depth and tend to be lower along the western margin. Specific conductivity values (Figure 23) are generally greatest in the north near the discharge points for the creeks in all hydrologic units with the highest values occurring in the lower aquifer. Temperature in the basin (Figure 24) increases with depth.

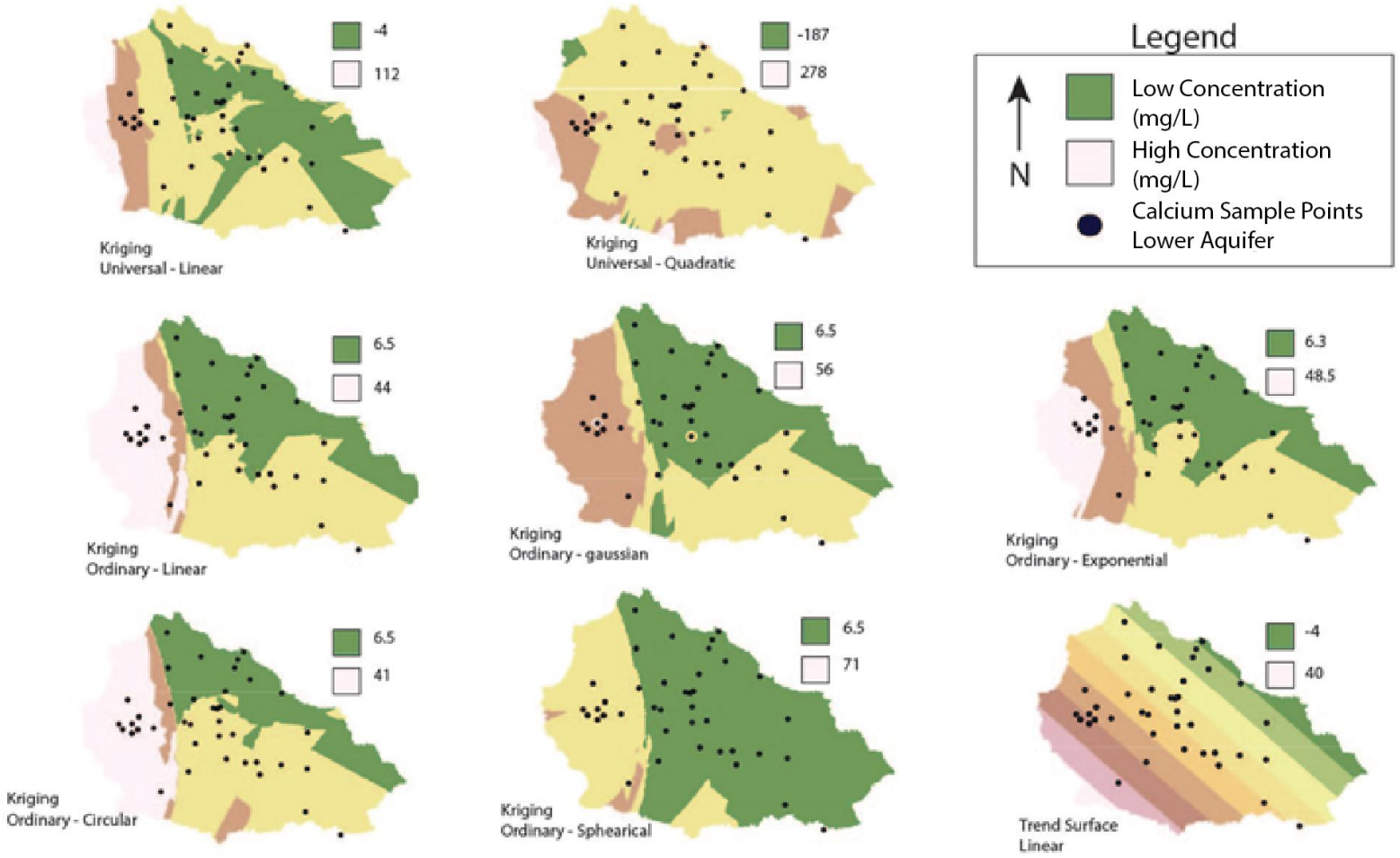

Figure 21. Different interpolation methods, including Ordinary and Universal Kriging, and Trend Surface. All interpolations were performed on the same dataset - calcium concentration values from the lower aquifer. Green represents the lowest concentration ranges and white represents the highest concentration ranges on the map.

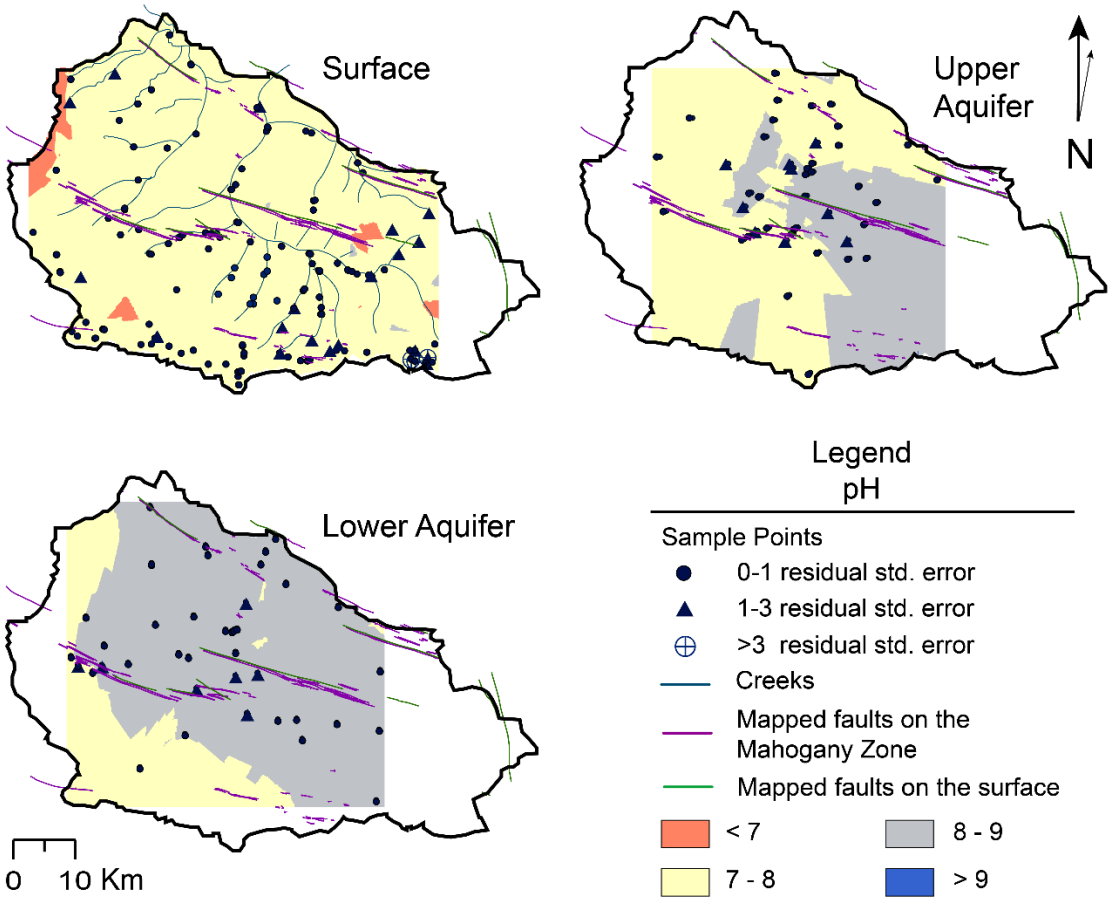

Figure 22. pH distribution maps for surface waters (top left), upper aquifer (top right), and lower aquifer (bottom left), Piceance Basin, Co. Black points represent sample locations and standard residual errors. Purple and green lines represent faults mapped on the Mahogany Zone and surface, respectfully. Dark blue regions represent areas with a pH > 9, light blue indicates pH values between 8-9, light pink represents pH values between 7-8, and red is used for values less than 7.

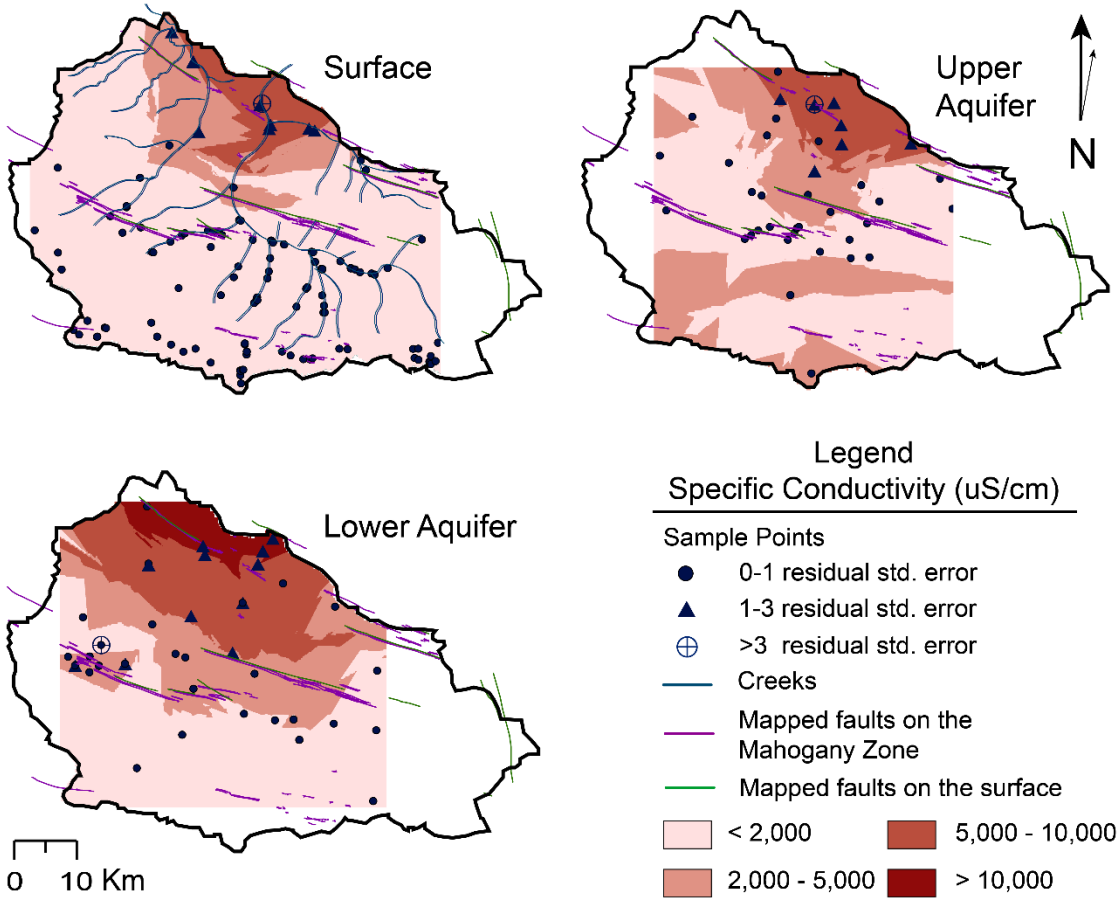

Figure 23. Specific conductivity distribution maps for surface waters (top left), upper aquifer (top right), and lower aquifer (bottom left), Piceance Basin, Co. Black points represent sample locations and standard residual errors. Purple and green lines represent faults mapped on the Mahogany Zone and surface, respectfully. Dark red regions represent areas with a specific conductivity value > 10,000 µS/cm, 25˚C. The shade of red transitions to light pink for specific conductivity values of 5,000-10,000, 2,000-5,000, and < 2,000 µS/cm, 25˚C.

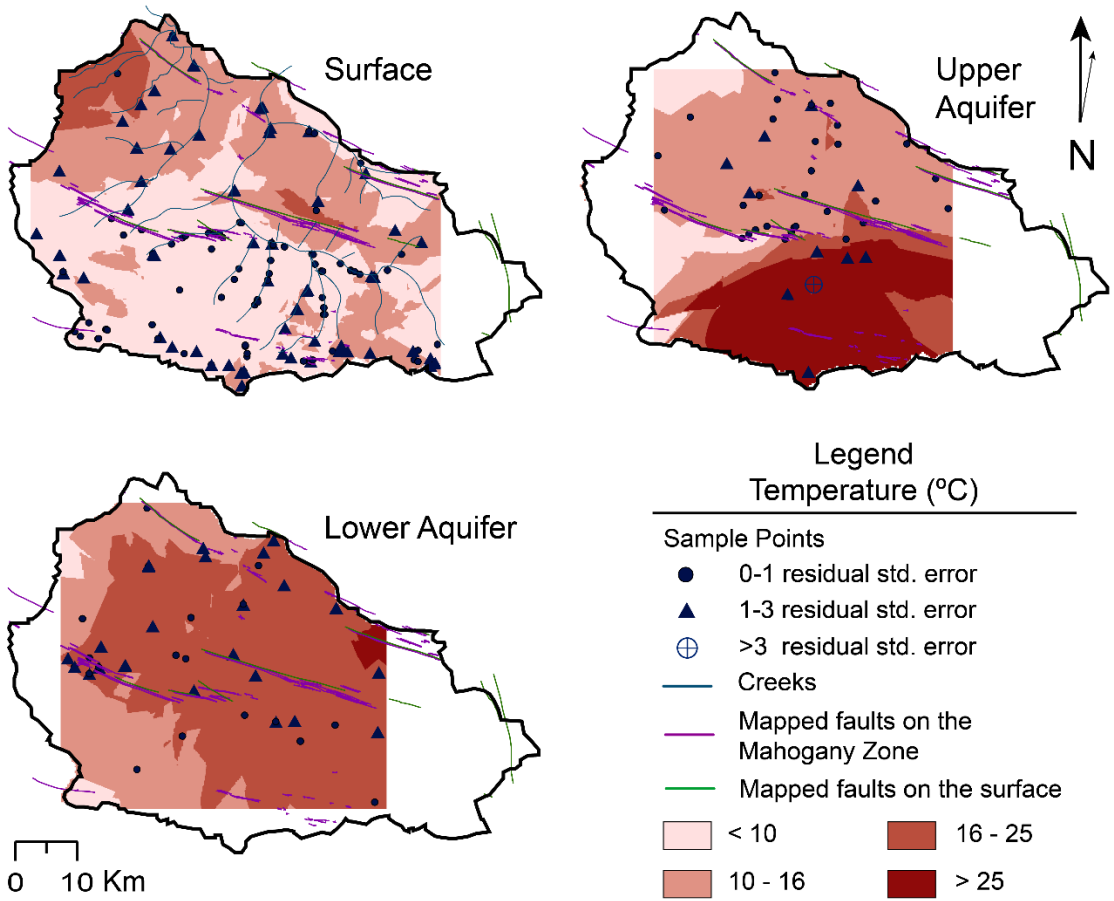

Figure 24. Temperature distribution maps for surface waters (top left), upper aquifer (top right), and lower aquifer (bottom left), Piceance Basin, Co. Black points represent sample locations and standard residual errors. Purple and green lines represent faults mapped on the Mahogany Zone and surface, respectfully. Dark red regions represent areas with a temperature > 25˚C. Dark red shade transitions to light pink with temperature value categories between 16-25, 10-16, and < 10˚C.

Major ions

Three maps showing the interpolated distribution of major dissolved constituent concentrations in groundwater in the upper aquifer, lower aquifer and surface samples are presented in Figure 25-Figure 30. Calcium concentrations in the hydrologic units (Figure 25) overall decrease with depth. Higher concentrations are found on the surface and in the upper aquifer, and concentrations increase toward the west. Magnesium surface sample concentrations are greatest in the north and decrease towards the southeast (Figure 26). Magnesium concentrations in the upper aquifer increase towards the northwest, and values are lowest in the lower aquifer. Sodium concentrations (Figure 27) increase with depth. The greatest values for all hydrologic units are found in the northern region by the creeks discharge points and additionally in the basin center in the lower aquifer.

Alkalinity in the three hydrologic units (Figure 28) are very similar to those of sodium. The largest concentrations in all units are found in the north. In the lower aquifer, high values extend to the basin center. The highest chloride concentrations are found in the north for all hydrologic units and values tend to increase with depth (Figure 29). Sulfate concentrations are greatest for surface samples and increase from the margins to the basin center and to the north (Figure 30). Upper aquifer sulfate concentrations increase from the southeast to the northwest, and values are consistently low in the lower aquifer with the exception of higher values along the west-southwestern margin and in the north.

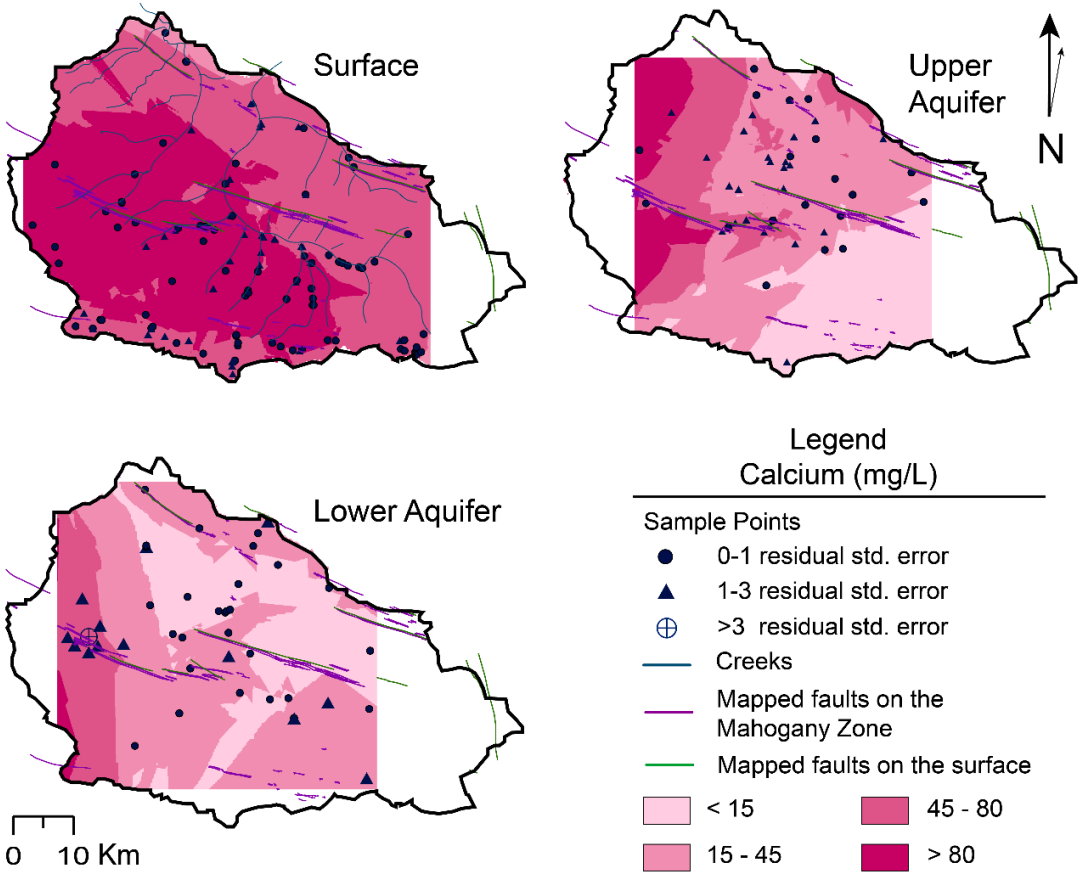

Figure 25. Calcium concentration distribution maps for surface waters (top left), upper aquifer (top right), and lower aquifer (bottom left), Piceance Basin, Co. Black points represent sample locations and standard residual errors. Purple and green lines represent faults mapped on the Mahogany Zone and surface, respectfully. Dark magenta regions represent areas with dissolved calcium concentration values > 80 mg/L. The shading saturation decreases to light pink with concentration categories between 45-80, 15-45, and < 15 mg/L.

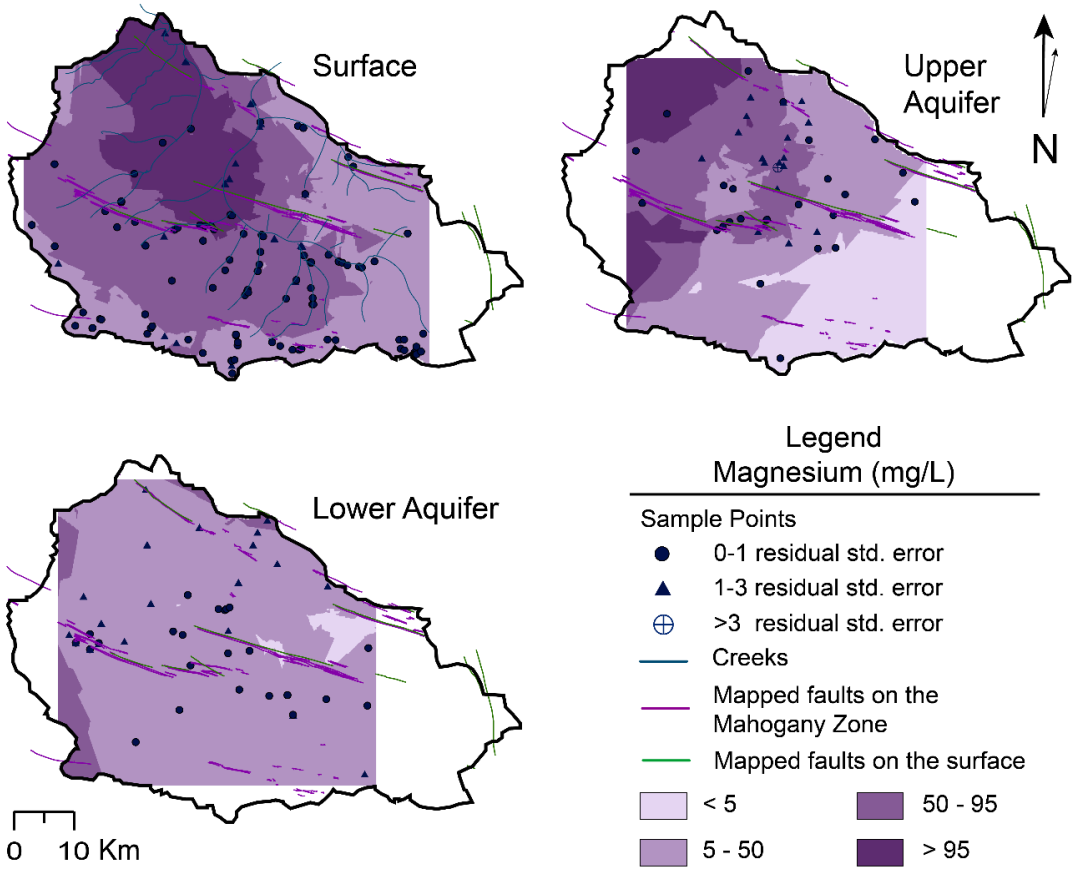

Figure 26. Magnesium distribution maps for surface waters (top left), upper aquifer (top right), and lower aquifer (bottom left), Piceance Basin, Co. Black points represent sample locations and standard residual errors. Purple and green lines represent faults mapped on the Mahogany Zone and surface, respectfully. Dark purple regions represent areas with dissolved magnesium concentration values > 95mg/L. The shading saturation decreases to light purple with concentration categories between 50-95, 5-50, and < 5mg/L.

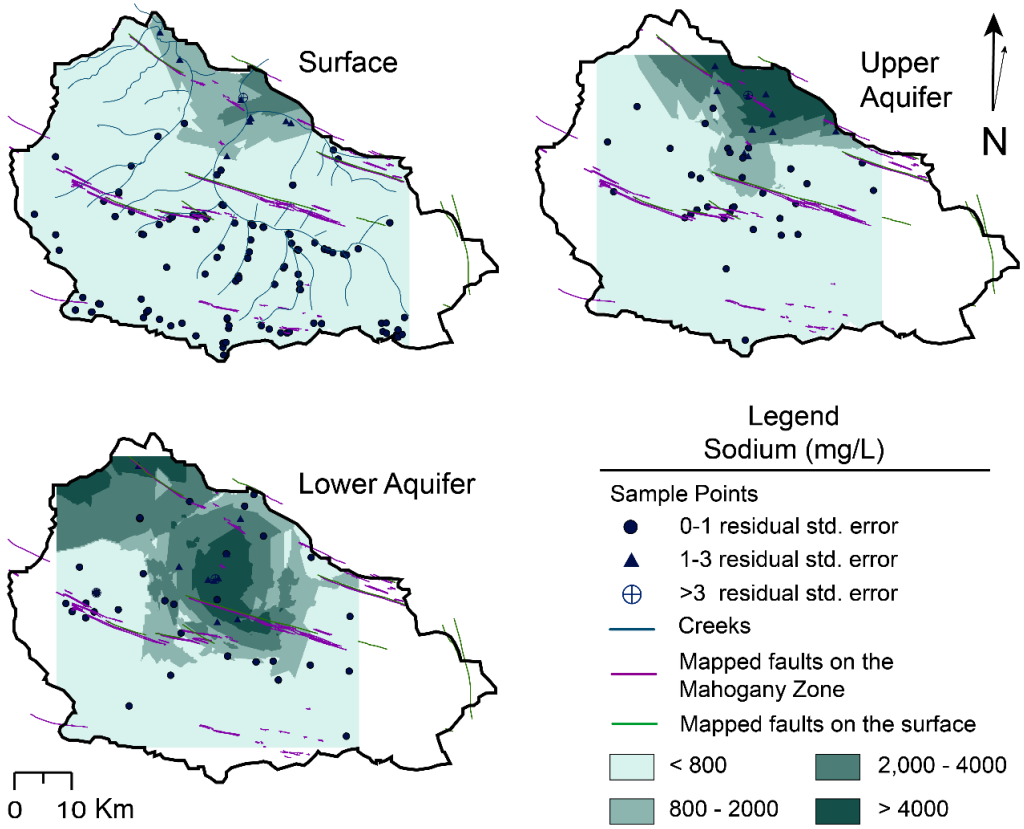

Figure 27. Sodium distribution maps for surface waters (top left), upper aquifer (top right), and lower aquifer (bottom left), Piceance Basin, Co. Black points represent sample locations and standard residual errors. Purple and green lines represent faults mapped on the Mahogany Zone and surface, respectfully. Dark teal regions represent areas with dissolved sodium concentration values > 4,000 mg/L. The shading saturation decreases to light teal with concentration categories between 2,000-4,000, 800-2,000, and < 800 mg/L.

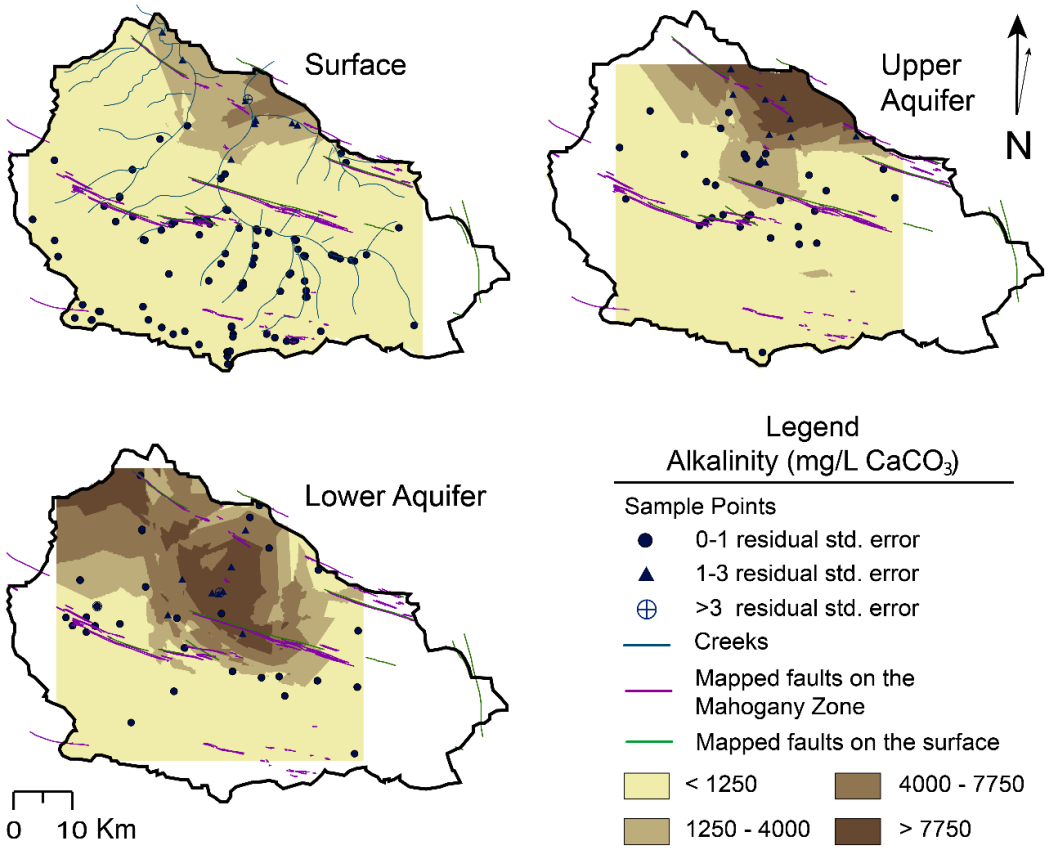

Figure 28. Alkalinity distribution maps for surface waters (top left), upper aquifer (top right), and lower aquifer (bottom left), Piceance Basin, Co. Black points represent sample locations and standard residual errors. Purple and green lines represent faults mapped on the Mahogany Zone and surface, respectfully. Dark brown regions represent areas with dissolved alkalinity concentration values > 7,750 mg/L $CaCO_3$. The shading saturation decreases to light brown with concentration categories between 4,000-7,750, 1,250-4,000, and < 1,250 mg/L $CaCO_3$.

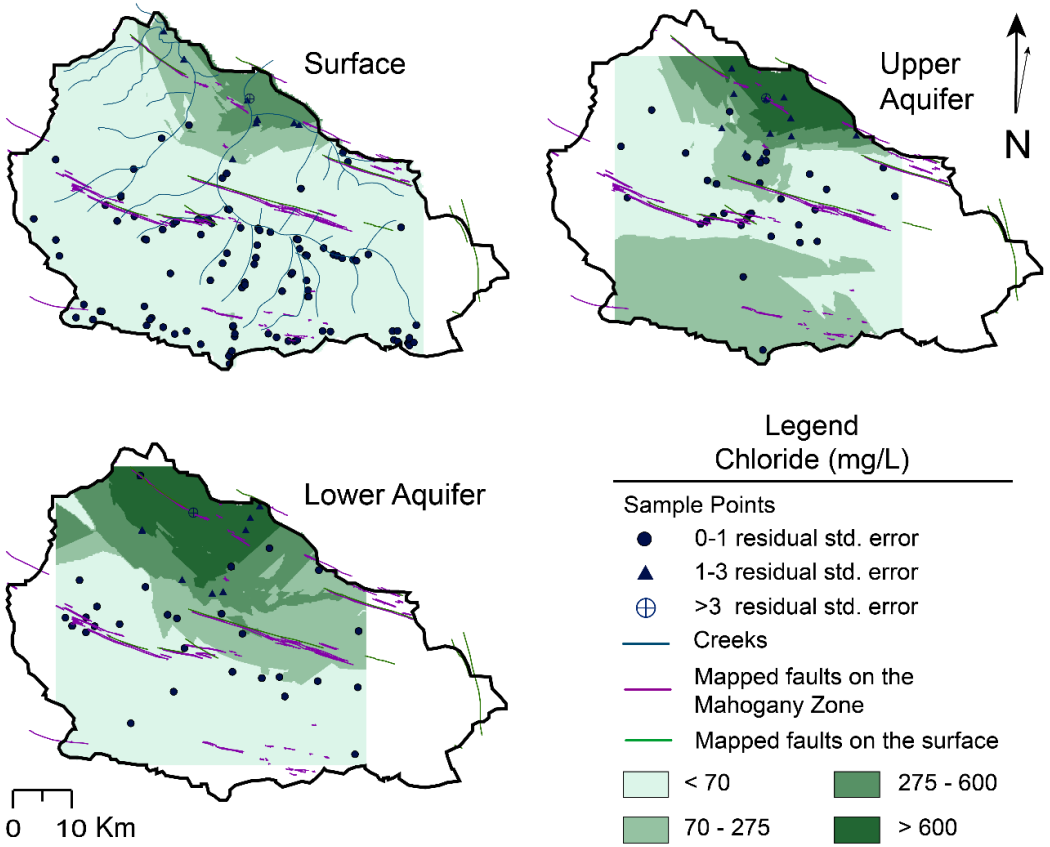

Figure 29. Chloride distribution maps for surface waters (top left), upper aquifer (top right), and lower aquifer (bottom left), Piceance Basin, Co. Black points represent sample locations and standard residual errors. Purple and green lines represent faults mapped on the Mahogany Zone and surface, respectfully. Dark teal regions represent areas with dissolved chloride concentration values > 600 mg/L. The shading saturation decreases to light teal with concentration categories between 275-600, 70-275, and < 70 mg/L.

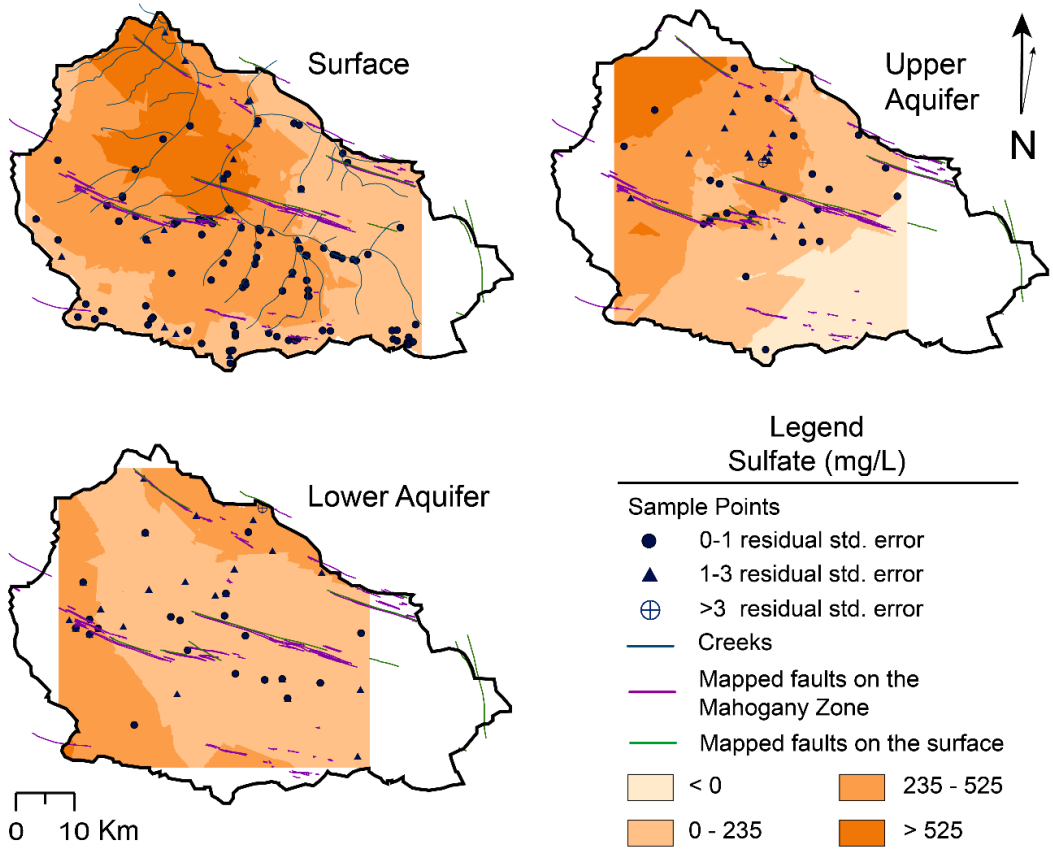

Figure 30. Sulfate distribution maps for surface waters (top left), upper aquifer (top right), and lower aquifer (bottom left), Piceance Basin, Co. Black points represent sample locations and standard residual errors. Purple and green lines represent faults mapped on the Mahogany Zone and surface, respectfully. Dark orange regions represent areas with dissolved sulfate concentration values > 525 mg/L. The shading saturation decreases to light orange with concentration categories between 235-525, 0-235, and 0 mg/L.

Dominant Geochemistry Along Groundwater Flow Paths

Figure 31-Figure 35 display the major ion evolution along different groundwater flow paths. Groundwater flow paths for surface samples (Figure 31) were based on the three largest creeks in the basin and their associated tributaries: Piceance Creek, Yellow Creek, and Dry Fork (Figure 1) and given flow path numbers 1, 2, and 3, respectfully (Figure 31). The quantity of surface samples is much greater than the number of subsurface samples, thus, data points were placed into sections along each flow path starting at headwaters and progressing downstream to the discharge point in the north. For example, points within the Piceance Creek drainage boundary were separated into four sections (1.1, 1.2, 1.3 and 1.4) and ion percentages were averaged for points in each section. Cation percentages are only displayed for the first flow path because the trend and values were similar for all surface flow paths.

Groundwater flow paths for the upper and lower aquifer were chosen with consideration of previous literature on the hydrology of the Piceance Creek Basin (Thomas and McMahon, 2012; Kimball, 1984; Taylor, 1982; Robson and Saulnier, 1981; Weeks et al., 1974) and the distribution of specific conductivity (Figure 23). Robson and Saulnier (1981) published water level data for several wells in the basin and contoured the potentiometric surface of the upper and lower aquifers (Figure 7 - Figure 8). The potentiometric surface in both aquifers indicates general groundwater movement from recharge areas along the western

and southern margin to the north. Groundwater movement from recharge areas along the eastern margin is more to the northwest.

The concentration distribution map for specific conductivity (Figure 23) shows the highest values in the northern region of the basin near the discharge points of Yellow Creek and Piceance Creek which indicates a flow path from the margins towards the basin center and to the north. This result agrees with the potentiometric map created by Robson and Saulnier.

Combining these observations with the flow model created by Weeks et al. (1974), two groundwater flow paths were selected for the upper aquifer (Figure 32 and Figure 33) and two for the lower aquifer (Figure 34 and Figure 35). Although the selected points may not be in an exact flow line, they do represent a general downgradient flow of water in the aquifers.

The first data point along the flow path in Figure 35 contained data from two different depths: 135m and 355m below ground surface (bgs). The latter is referred to as 1b in the figure.

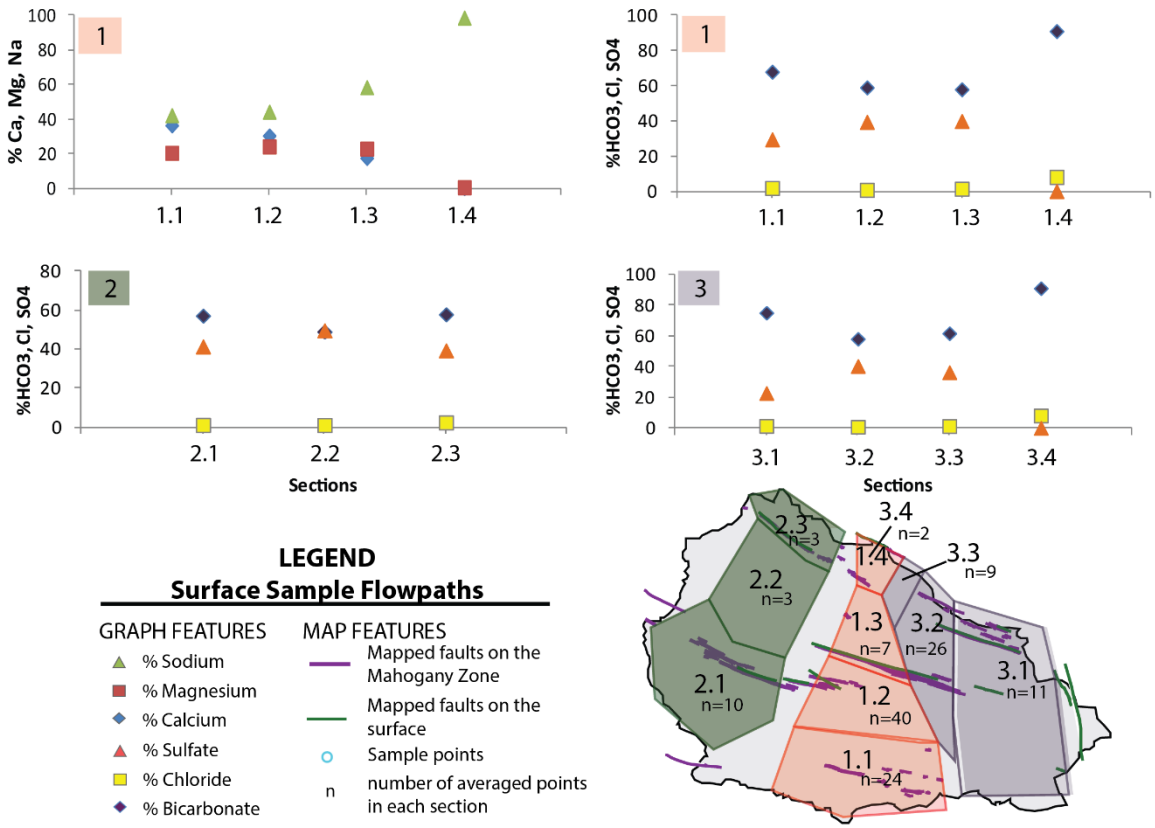

Figure 31. Groundwater ion evolution along presumed flow paths for surface samples. Graph points represent ion percentages in meq/L for cation and anion. Map inset displays the flow path followed and circles represent the sample points. Numbers on inset refer to general flow path associated with the drainage basins for Piceance Creek (1), Yellow Creek (2), and Dry Fork (3). The section numbers indicate progression towards the discharge point and the ion percentages for each section were averaged and then plotted in the graphs above. n refers to the number of points averaged in each section.

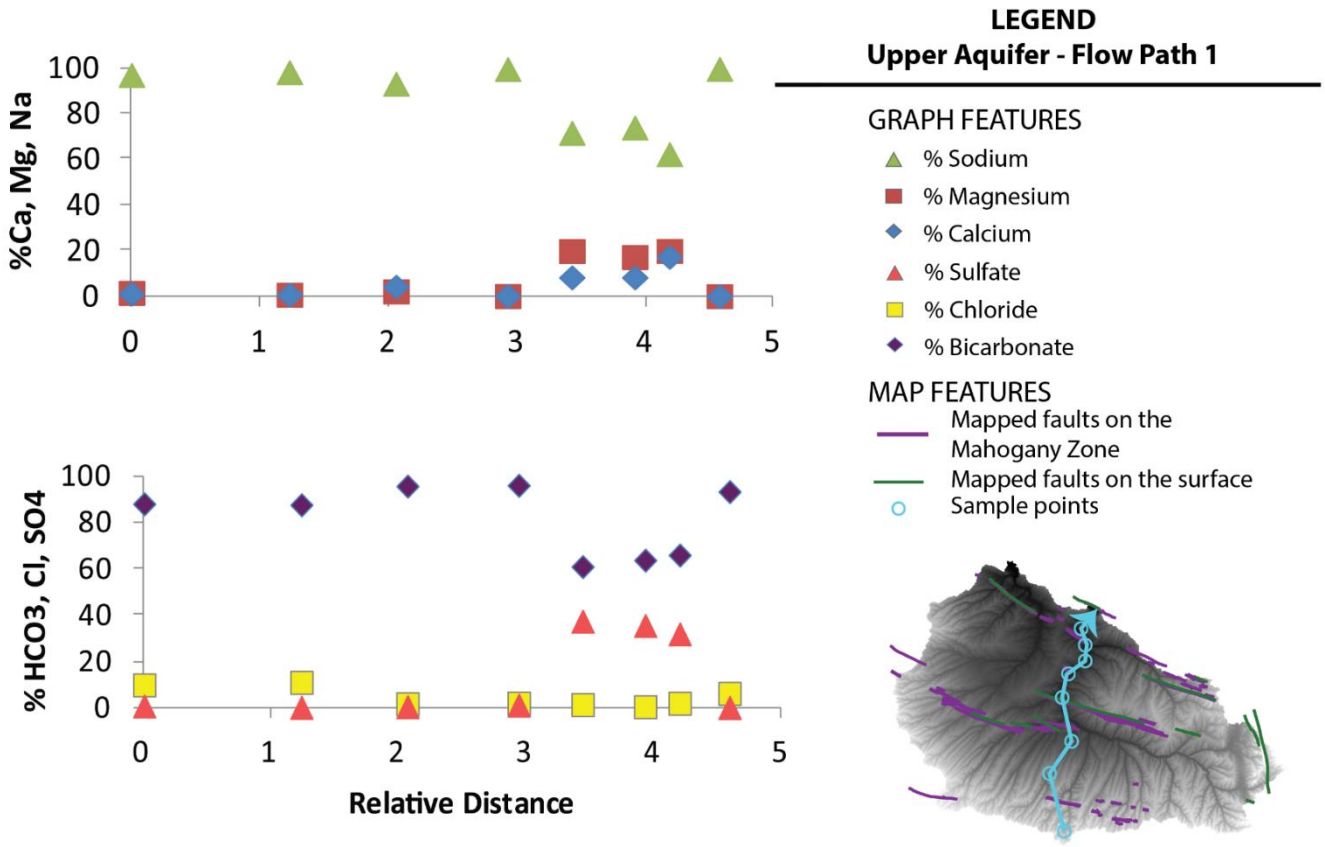

Figure 32. Groundwater ion evolution along a potential flow path for the upper aquifer – Flow Path 1. Graph points represent ion percentages in meq/L for cation and anion. Map inset displays the flow path followed and circles represent the sample points.

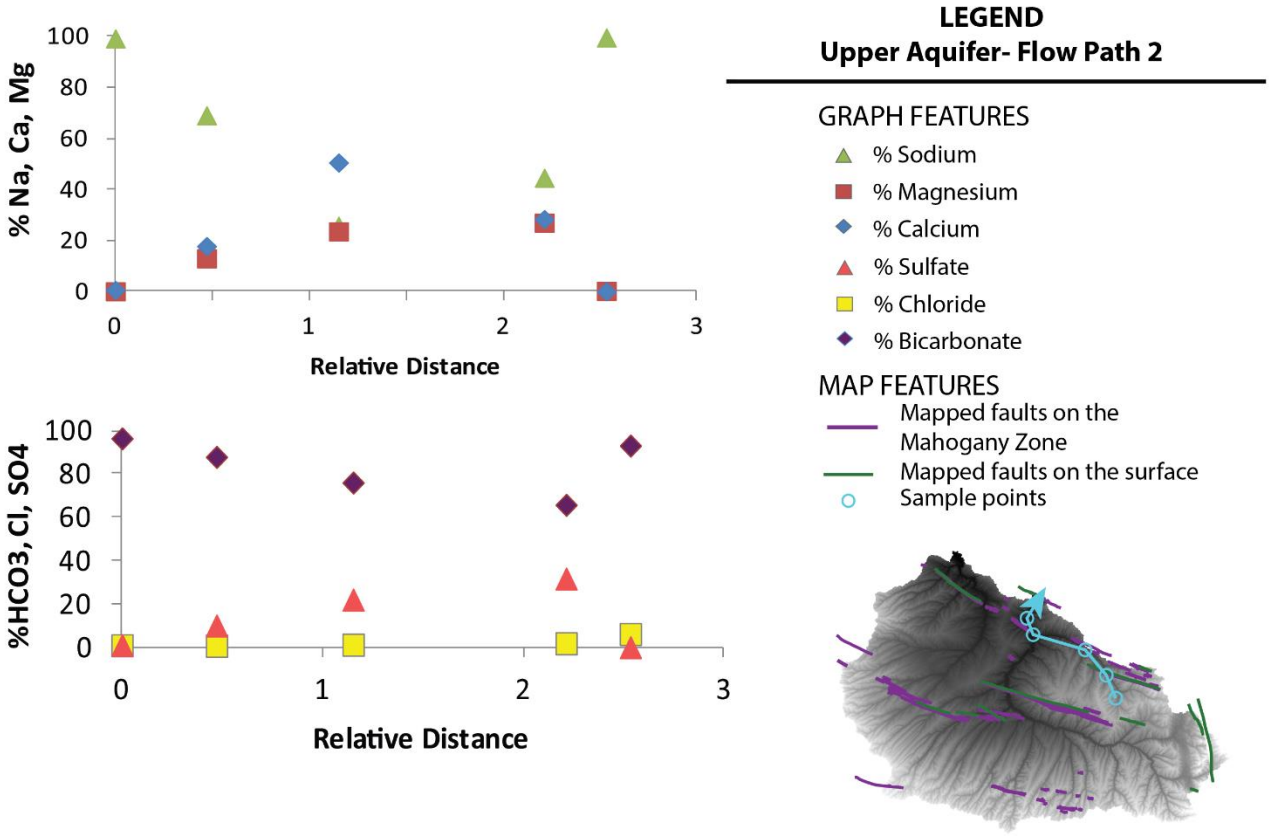

Figure 33. Groundwater ion evolution along a presumed flow path for the upper aquifer – Flow Path 2. Graph points represent ion percentages in meq/L for cation and anion. Map inset displays the flow path followed and circles represent the sample points.

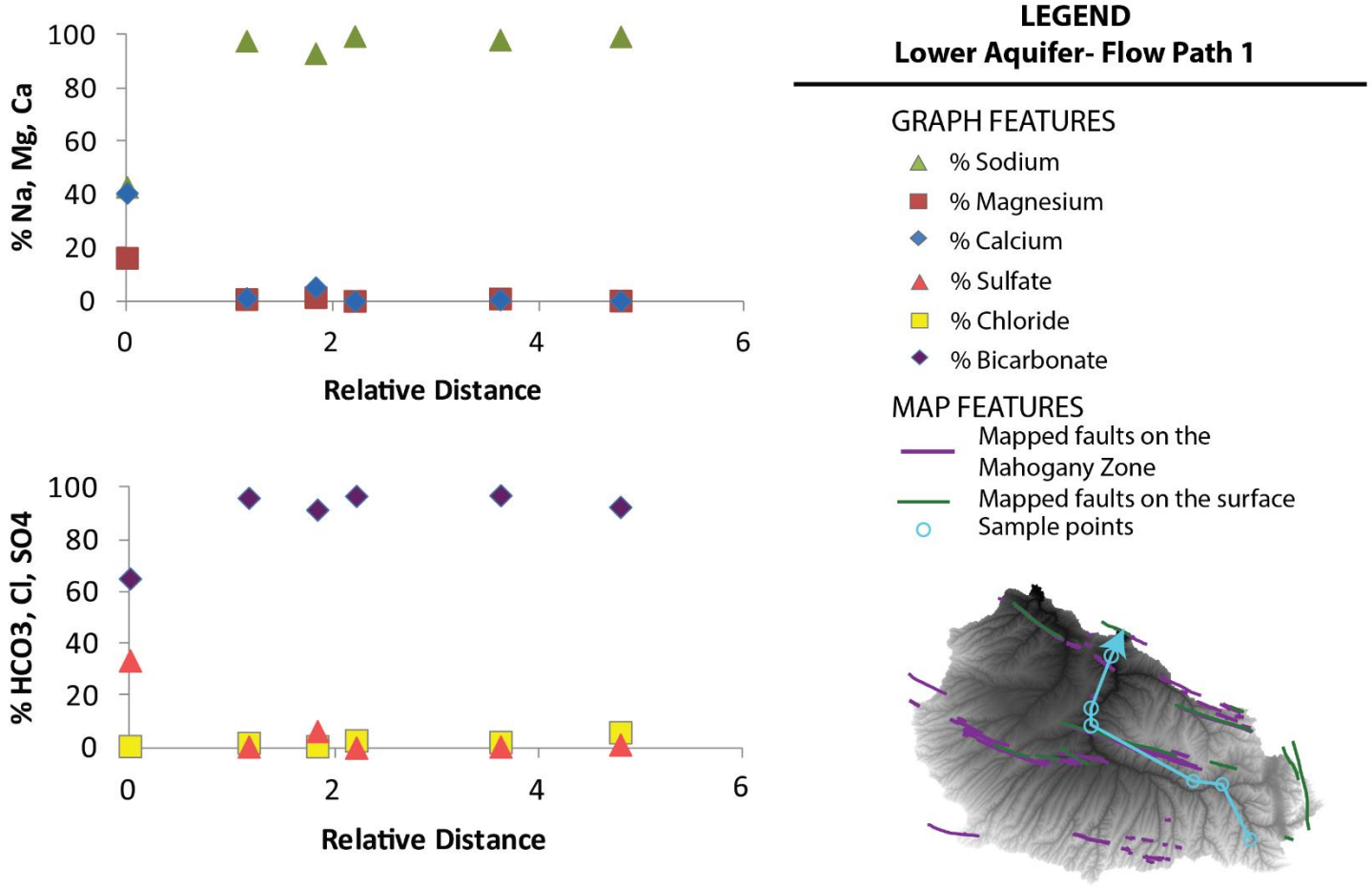

Figure 34. Groundwater ion evolution along a presumed flow path for the lower aquifer – Flow Path 1. Graph points represent ion percentages in meq/L for cation and anion. Map inset displays the flow path followed and circles represent the sample points.

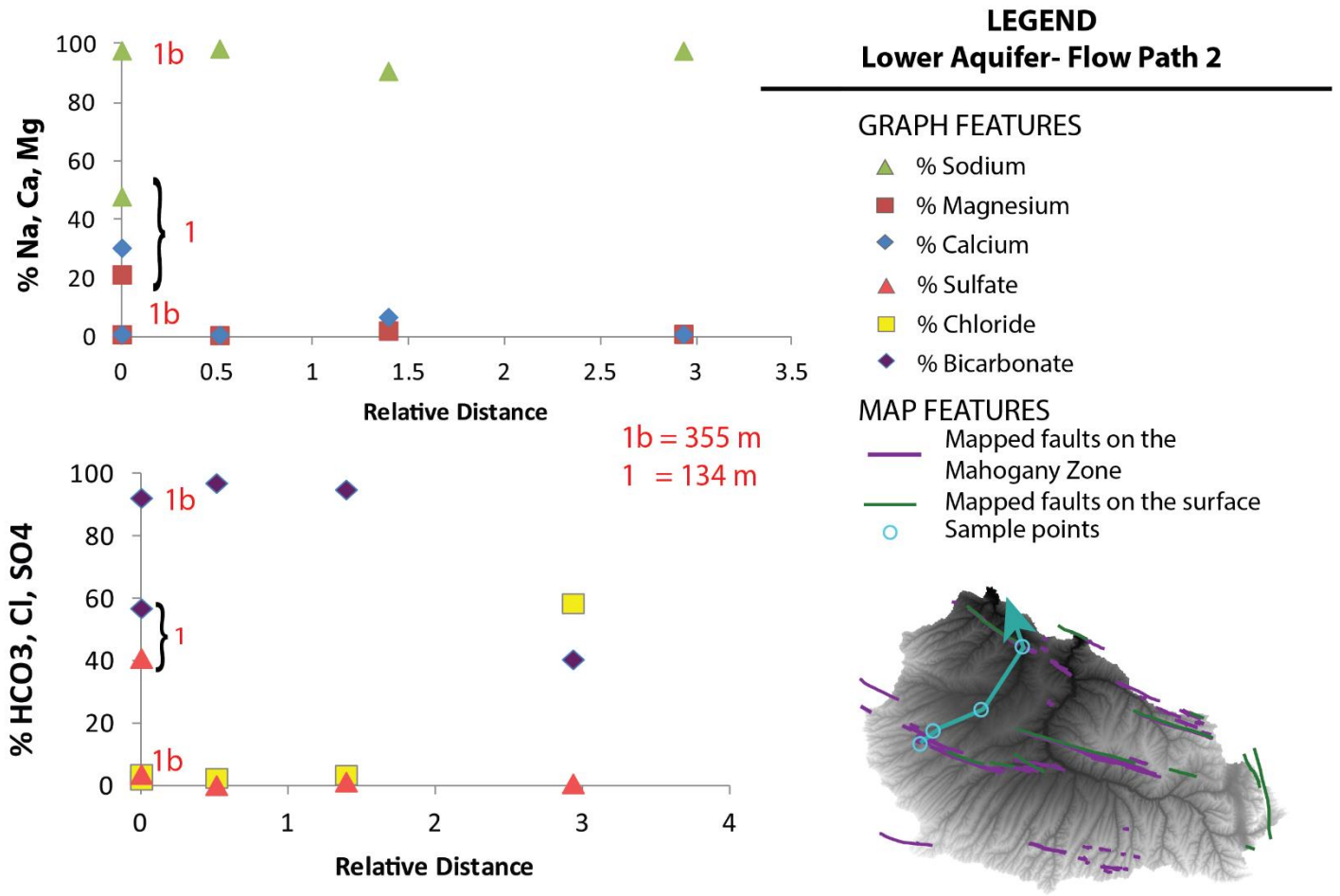

Figure 35. Groundwater ion evolution along a presumed flow path for the lower aquifer – Flow Path 2. Graph points represent ion percentages in meq/L for cation and anion. Map inset displays the flow path followed and circles represent the sample points.

DISCUSSION

Groundwater Flow Paths

Based on specific conductivity values and some ion concentration distribution patterns (e.g., magnesium, sodium, alkalinity, chloride, and sulfate), the general groundwater flow in the system is in agreement with previously published research (Kimball, 1984; Robson and Saulnier, 1981; Weeks et al., 1974). Water states that water enters the system as recharge water along the western, southern, and eastern margin, where conductivity and ion concatenations are generally at their lowest. Surface water drains into one of three creeks: Yellow Creek in the west, Dry Fork in the east, and Piceance Creek in the center. In the upper and lower aquifer, water flows from the margins toward the northern discharge regions of Piceance Creek and Yellow Creek. There are regions of upward water migration from the lower aquifer to the upper aquifer along the lower tributaries and main stem of Piceance Creek due to pressure gradients from the bowl-shaped structure of the basin. Along Piceance Creek and toward the northern discharge points, lower aquifer water is migrating upward through the leaky aquitard and possibly along fault pathways, and mixing with upper aquifer water before discharging through the groundwater-fed Piceance Creek. Elevated specific conductivity values between 2,000 - 5,000 µS/cm are found towards the basin center and demonstrates the convergence of upper and lower aquifer waters, with much higher concentrations, exiting the subsurface into the creek.

Major Geochemistry Overview

Surface samples are the most distinct of the three hydrologic units due to the mixed dominant cations. Surface recharge water is high in calcium and bicarbonate but increases in sulfate and sodium along flow paths. Therefore, the anions on the piper diagram grade between bicarbonate and sulfate (Figure 14). There still are some samples with characteristics more closely aligned with the upper and lower aquifer waters (e.g., sample points that plot as Na-K-Cl-SO_4 type waters on surface sample piper diagram; Figure 14) which can be explained by upper and lower aquifer water exiting the subsurface through preferential flow paths and mixing with each other and surface waters.

Almost all samples in the lower aquifer are categorized as Na-K-HCO_3-Cl to Na-HCO_3 type, but there are a few samples dominated by calcium and magnesium and others with sulfate as the main anion (Figure 16). The deviations from nearly 100 percent sodium-bicarbonate type can be explained by the elevation variation of the lower aquifer and presumed flow paths. Since the system is bowl-shaped, groundwater sample elevations vary from relatively shallow (6.5 m below ground surface (bgs)) to 2300m bgs (Table 3). Samples nearer the surface and recharge zone will be influenced by the recharge waters to a greater degree than deeper samples, resulting in higher calcium and sulfate concentrations.

The upper aquifer is influenced by upwelling lower aquifer water and shallow subsurface groundwater movement. The piper diagram in Figure 15

demonstrates these influences with two distinct transitions in anion composition in the bottom right pyramid; one is a continuum of points along the bicarbonate-sulfate line and the second is a separate continuum along the bicarbonate-chloride line. The latter represents the upward flow of groundwater from the lower aquifer and the mixing with upper aquifer water prior to exiting the system. The bicarbonate-sulfate line in the anion trilinear diagram is similar to the same transition displayed in surface sample and is likely shallow subsurface groundwater flow that has lower residence times and therefore has not evolved much further from recharge water.

The mixed water types in the hydrologic units are primarily due to permeation of lower aquifer water through the Mahogany Zone aquitard and/or preferential fault conduits. However, some of the variance may be due to the boundary between the Green River Formation and the Uinta Formation not being exact; stratigraphic units interfinger. Additionally, dolomitic oil shales of the Green River Formation are present above the Mahogany Zone, thus is it not unreasonable to have some water samples with signatures that mimic the Green River Formation water chemistry.

Major Ion Evolution

Chebotarev (1955) observed that water tends to evolve chemically towards the composition of seawater. He argued that this evolution generally follows changes in the dominant anion: $HCO_3^- \rightarrow HCO_3^- + SO_4^{2-} \rightarrow SO_4^{2-} + HCO_3^- \rightarrow$

$SO_4^{2-} + Cl^- \rightarrow Cl^- + SO_4^{2-} \rightarrow Cl^-$, where age and distance increase along the flow path. For sedimentary basins, Chebotarev identified three zones that generalize this evolution: 1) the Upper Zone – which is characterized by active flushing of groundwater with bicarbonate as the dominant anion; 2) an Intermediate Zone – characterized by longer residence times. This zone has higher total dissolved solids and sulfate is the dominant anion; and 3) the Lower Zone – wherein groundwaters have had the longest residence times with little recirculation. This zone is very high in total dissolved solids with the occurrence of more saline minerals. Chloride is the dominate anion in this zone.

Freeze and Cherry (1979) emphasize that this evolution sequence is a generalization that needs to be viewed in terms of the regional geology and is ultimately controlled by mineral availability and solubility. In the Piceance Basin, the surface samples and the upper aquifer samples follow similar anion trends, from bicarbonate, to bicarbonate and sulfate, followed by a reversal back to bicarbonate (Figure 31-Figure 33): $HCO_3^- \rightarrow HCO_3^- + SO_4^{2-} \rightarrow HCO_3^-$. The lower aquifer (Figure 34 and Figure 35) anion trend starts with bicarbonate and sulfate and progresses to nearly 100 percent bicarbonate ($HCO_3^- + SO_4^{2-} \rightarrow HCO_3^-$). The anion water chemistry in the basin does not evolve past bicarbonate and sulfate dominant water with the exception of a few discrete samples. There are many processes contributing to the spatial variations observed in the basin including mineral composition of the stratified sedimentary units, groundwater flow paths and mixing zones, and sulfur redox and occurrence.

Groundwater flow paths and preferential fault pathways

The last point on the ion percent graphs for surface sample flow paths 1 and 3 (Figure 31) and upper aquifer flow paths 1 and 2 (Figure 32 and Figure 33), is located after the intersection of Piceance Creek and the Alkali Flats fault. At this point the water chemistry transitions from bicarbonate and sulfate dominant anions to nearly 100 percent bicarbonate with no significant sulfate percentage. At this region, the sodium-bicarbonate dominant lower aquifer water is flowing upward to the surface and increases the concentration of bicarbonate, resulting in a decrease in percent sulfate. This is supported by the ion concentration distribution maps for sodium and alkalinity (Figure 27 and Figure 28). The concentration maps for the two constituents are incredibly similar to each other and the highest concentrations for surface samples and samples in the upper aquifer are located near the norther discharge point and along the main stem of Piceance Creek. In the upper aquifer, there are some high concentrations in the basin center which is likely from mixing zones created by upward migration of lower aquifer waters.

Anions in the lower aquifer begin as bicarbonate and sulfate dominant waters and transition to nearly 100 percent bicarbonate. At the surface along the basin boundary, water begins as predominately bicarbonate and as it flows downward through the upper aquifer and into the lower aquifer, the residence time and age of the groundwater increases and begins to increase in sulfate

concentration. However, as the water continues to move through the lower aquifer, mineral abundance and redox conditions take on a greater influence.

Stratified sedimentary basin, mineral abundance and solubility

The dominance of sodium-bicarbonate waters is common in stratified sedimentary basins. Freeze and Cherry (1979) argue that these dominant ions can be explained by the combined processes of cation exchange and calcite or dolomite dissolution. First, cation exchange between calcium and sodium takes place via the following reaction:

$$Ca^{2+} + 2Na_{(ad)} \leftrightarrow 2Na^{+} + Ca_{(ad)}, \quad (2.1)$$

where *(ad)* denotes cations adsorbed to clays. For every one mole calcium adsorbed, two moles of sodium are released into the water column. Evidence of cation exchange is seen on the ion evolution flow path graph for surface samples (Figure 14). The graph for cations shows an incremental increase in sodium as calcium and magnesium decreases. This process actively removes calcium from the water, causing the water to be understatured with respect to calcite or dolomite, thereby enabling calcite or dolomite dissolution to continue. These two processes can continue until the water is no longer undersaturated with respect to the carbonate minerals, or the exchangeable sodium is exhausted.

The dissolution of saline minerals in the saline zone also contributes to the sodium-bicarbonate dominant water type. The saline zone is comprised of halite and nahcolite. The dissolution of nahcolite contributes to the dominant water

chemistry in the lower aquifer which effects the rest of the basin. However, this zone is impermeable, thus, only the top of the unit in contact with flow paths will be subjected to dissolution. Water enriched in sodium and bicarbonate from the lower aquifer flows up through mixing zones and increases the concentrations in other hydrologic units.

Chloride concentrations are surprisingly low considering the presence of halite in the saline zone. Only nine samples have chloride anion percentages greater than 10, with the largest being 36 percent, and the average dissolved chloride concentration in the basin is only 102 mg/L. However, if the nahcolite insulates the halite from active groundwater flow paths, the unit may not readily dissolve. Chloride concentrations are greatest in the northern region by the discharge point of the Piceance Creek Basin (Figure 29). This may be due to the Alkali Flats fault which is known to penetrate down to the saline zone. This fault may allow water to actively circulate through a limited region of the halite deposit, increasing chloride values in this region of the basin. The northern region of the basin is the discharge point for the creeks and the longest flow paths in the system; chloride concentrations are expected to be greatest in this region regardless of the fault. However, in all three hydrologic zones, sample points at the fault have much greater concentrations than points also in discharge regions but away from the fault. Chloride concentrations at the fault range from 1600 mg/L at the surface to 2400 in the lower aquifer and the concentrations at discharge points away from the fault range from 31 to 310 mg/L. This indicates

the Alkali Flats fault is an influential conduit for upward flow of lower aquifer waters that may be in contact with the saline zone.

Stratified sedimentary chemical processes and mineral abundance alone cannot account for the variation observed in the basin. For example, there are regions that are not dominated by sodium-bicarbonate waters.

Sulfur Occurrence

Anion evolution variations can be partially explained by the redox behavior of sulfur. Overall, sulfate concentrations decrease with depth (Figure 30). This is expected as sulfate is the oxidized sulfur species (sulfate(VI)), so likely it will be most abundant near the surface where dissolved oxygen concentrations are greater. Sulfide(-II), the stable reduced species of sulfur, is also found in the basin, most abundantly in the organic-rich Green River Formation. Sulfide concentrations were not reported in the database used for this study, but Kimball (1984) reported six samples from the Uinta and Green River Formation with hydrogen sulfide concentrations ranging from 0.5 to 1.7 mg/L. The oxidation of sulfides, such as pyrite, can contribute to the increased concentration of sulfate found at the surface and in the upper aquifer. The oxidation of pyrite is as follows:

$$FeS_{2(s)} + \frac{15}{4}O_2 + \frac{7}{2}H_2O \rightarrow Fe(OH)_{3(s)} + 4H^+ + 2SO_4^{2-}, \quad (2.2)$$

where pyrite is oxidized to an iron-hydroxide solid phase, two sulfates, and four free hydrogen ions. However, there is a limit to the oxidizing ability of

groundwater. If groundwater is near saturation with respect to O_2 (e.g. contained 10 mg/L or 3.124E-4 moles/L O_2,), then it could oxidize 8.33E-5 moles/L of iron in pyrite, resulting in less than 20 mg/L sulfate. At the surface, sulfate concentrations over 1,000 mg/L are present, indicating that pyrite oxidation alone cannot account for the sulfate source in the system. However, this calculation assumes a closed system for oxygen, which may be more accurate for the upper aquifer (located below the water table) then for surface samples. Oxidation in the vadose zone has the potential to generate more sulfate, but will likely not be enough to account for sulfate concentrations as high as 1,000 mg/L. Other processes must be contributing.

Gypsum dissolution may contribute to the sulfate concentrations in the basin. Previous research by Robson and Saulnier (1981) that focused on the primary drainage basin of Piceance Creek did not report the presence of gypsum in the basin (Robson and Saulnier, 1981). However, calcium and sulfate do have similar concentration distributions (Figure 25, Figure 30) and have a strong positive correlation value of 0.67 (Table 5) which favors a relationship between the two. If gypsum was present in the system, the resulting concentrations of sulfate would be extremely high given gypsum's solubility, likely resulting in sulfate-type waters. Freeze and Cherry (1979) argue that when carbonate and sulfate minerals are both abundant, the water evolves to an intermediate stage quickly (dominated by sulfate anions) and does not evolve further. Our results show only a handful of samples in which sulfate is dominant, mostly the water will

evolve to bicarbonate + sulfate. Thus, gypsum is not likely a major source of sulfate in the system.

Dissolution of sulfate-bearing carbonates in the basin may be an additional contributor of sulfate to the system. Previous studies have found sulfate in saline calcites, present as structurally substituted sulfate ions within the carbonate lattice; the sulfate ion is not a sulfate mineral inclusion, but rather a part of the carbonate crystal (Kampschulte and Strauss, 2004; Pingitore et al., 1995). The quantity of sulfate in the carbonates can range from tens of ppm in inorganic precipitates to thousands of ppm in biogenic carbonates (Kampschulte and Strauss, 2004). Carbonate formation in the basin occurred under brackish to hypersaline conditions, and dolomite, in particular, is thought to be of biogenic origin (Desborough, 1978). It is therefore viable that structurally substituted sulfate ions are present in the Piceance Basin's carbonate minerals and dissolution sources sulfate to the system.

Previous research in the basin has determined a reduced environment in the Uinta and Green River Formation of the basin (Hansen et al., 2010; Thomas and McMahon, 2009; Kimball, 1984; Robson et al., 1981). Therefore, sulfate concentrations decrease with depth due to the reduction of sulfate. Sulfate reduction is key to the major dominant anion patterns in the basin. Bicarbonate and sulfate dominated anions are mainly present in the surface and the upper aquifer. In the lower aquifer, the presence of sulfate is almost non-existent except along the basin boundaries, but since the system is bowl-shaped, those points have a higher elevation and are closer to the infiltration of recharge water. The

depth dependence of sulfate is well demonstrated in the ion percent graph along lower aquifer flow path 2 (Figure 35). The first sample point on this graph had two sample results taken at very different depths. The first sample (point 1) was taken 134 m bgs and the second sample (point 1b) was taken 355 m bgs. The shallower sample has chemistries closer to the surface samples and upper aquifer samples; there is not a dominate cation, rather a close mix of calcium, magnesium and sodium, and the anions are bicarbonate and sulfate. The deeper sample does not include the bicarbonate and sulfate zone, but rather goes straight to bicarbonate waters. Between 134 m and 355 m, sulfate was removed from the system by biochemical reduction, likely from sulfate-reducing bacteria which has been shown in previous studies to facilitate dolomite formation under anoxic conditions (Deng et al., 2010; Van Lith et al., 2003). The reduction of sulfate and oxidation of organic material can result in increased bicarbonate concentrations. For example:

$$2CH_2O + SO_4^{2-} \rightarrow HCO_3^- + HS^- + CO_2 + H_2O. \quad (2.3)$$

This process reduces the sulfate (lowering the concentration percent) and increases the concentration of bicarbonate.

Discussion Summary

Recharge water enters the Piceance Basin along the western, southern, and eastern margin and flows to the north where Piceance Creek and Yellow Creek meet the east to west flowing White River. Recharge waters are

characterized by having mixed cation and bicarbonate and sulfate anions and flows either as surface runoff, or infiltrates down to the upper and lower aquifers. Groundwater movement in the basin flows downward toward the northern discharge points of Piceance and Yellow Creek. Pressure gradients force the lower aquifer water to move upward in the center and towards the north and exit the subsurface through the groundwater-fed creeks. This upward flow causes mixing zones in the upper aquifer and surface samples. The lower aquifer waters are primarily sodium-bicarbonate type and the upper aquifer represents a mix of water types between the two other hydrologic units.

Many processes contribute to the geochemical distribution of ions in the basin. Stratified sedimentary units in the presence of nahcolite and other carbonates aid in continuing a bicarbonate dominant water type in the lower aquifer. Cation exchange actively removes calcium and releases sodium to the system. Sulfate-bearing carbonate dissolution increases sulfate concentrations in the upper aquifer and at the surface and sulfate reduction in the lower aquifer removes sulfate concentrations and increases bicarbonate. Groundwater flow paths in the north cause lower aquifer water to flow upward through the upper aquifer and to the surface. This path brings groundwater high in sodium and bicarbonate to these hydrologic zones and dominates the water chemistry in this region.

CHAPTER 3 - MINERALOGICAL CONTROLS ON WATER CHEMISTRY

INTRODUCTION

Cole and Picard (1978) related mineralogic variations, specifically quartz, albite, K-feldspar, analcime, calcite, dolomite, ankerite, dawsonite, nahcolite, and halite, to a depositional model in the Green River Formation (Figure 4). The most prominent spatial patterns are those between the carbonate minerals and evaporites; dolomite was found to be the dominant carbonate mineral and occurs in abundance in all regions except the basin margins. Calcite is abundant along the margin but is far less abundant, even rare, in the basin center. Ankerite is absent along the margin and abundant in the basin center. Similarly, nahcolite and halite are absent from the basin margin to the proximal open lacustrine region and are abundant in only very narrow regions in the basin center. Poole (2014) analyzed core samples in the basin and found results in agreement with Cole and Picard. In the saline zone of the Green River Formation, Poole found abundant dawsonite, nahcolite, halite, and buddingtonite ($(NH_4)AlSi_3O_8 \cdot O.5H_2O$). Poole reported higher quantities of analcime along the margins, and dolomite and ferroan dolomite abundant throughout. Poole characterized the upper part of the Green River Formation by increased feldspar, analcime, ferroan dolomite and calcite, along with decreased saline minerals (Poole, 2014).

In the Uinta Formation, the dominant clastic mineralogy includes quartz and feldspar, while marlstones contain calcite, illite, and analcime (Day et al.,

2010). However, the spatial distribution of these minerals has not been as thoroughly established.

Groundwater moves slowly in the basin; Kimball (1984) used corrected carbon-14 dating to estimate the age of groundwaters that ranged from 750 years for water near recharge zones to more than 20,000 years for water further down the hydrologic gradient. During this transit, the groundwater is in contact with the formation sediments for considerable periods of time. Given this ample time, groundwater solutions should be in equilibrium with minerals present in the system. Therefore, it is expected that SI values should reflect the mineral spatial distribution outlined by Poole (2014) and Cole and Picard (1978), for Green River Formation, and the predominant Uinta Formation mineralogy identified by Day et al. (2010).

Specific objectives of this study are 1) to describe the distribution of water chemistries in the Piceance Basin in terms of major mineral equilibrium, 2) compare mineral saturation indicies results to the expected mineralogic trends determined by Cole and Picard (1978), Poole (2014), and Day et al., (2010).

METHODS

PHREEQC

PHREEQC Interactive is a software program developed by the U.S. Geological Survey (Parkhurst and Appelo, 2013) that performs a large number of

aqueous geochemical calculations, including speciation, batch-reactions, one-dimensional transport, and inverse geochemical calculations. For this study, PHREEQC was used to calculate the saturation indicies for all possible mineral combinations for each given sample using the Lawrence Livermore National Laboratory database.

Each sample in the study area was processed in PHREEQC as a separate solution and not as a batch because system parameters such as temperature and pH cannot be changed in a batch sample analysis. The default conditions were accepted for redox (pe = 4), solution density (1.0 g/cm^3) and water mass (1 kg). Elemental (basis species) concentrations were entered as milligrams per liters unless otherwise defined. After the program processed the sample solutions, the ionic strengths, charge balance errors, and saturation indicies and formula for possible minerals were extracted and saved as a text file. Using Microsoft Access, the PHREEQC data was related to location data to include Cartesian coordinates, depth bgs, and hydrologic unit.

Redox species

Reduction potential measurements (pe or Eh) were not included in the dataset, at least for data within the study area that contained sample depths. Two data points contained dissolved oxygen values, but both were surface samples. Additionally, the availability of reliable redox pairs was few to none; only two samples contained nitrate/nitrite concentrations, one sample contained

sulfate/sulfide values and all were located at the surface. Most often, redox elements were reported as totals. Therefore, the program default pe value of 4 was used to compute speciation of redox elements with the exception of iron.

Iron redox was treated differently due to the importance of iron carbonate (e.g. ankerite) in the basin (Figure 4). Previous research has concluded a reduced environment in the Green River Formation (expectedly, given the high organic carbon contents), and evidence of such in the Uinta Formation (Hansen et al., 2010; Thomas and McMahon, 2009; Kimball, 1984; Robson et al., 1981). Iron samples with depths equal to zero meters bgs were input in PHREEQC with default conditions (total iron subject to speciation with a pe value of 4). Iron concentrations in samples with depths greater than zero meters bgs, were input as Fe^{2+}, the reduced form of iron.

Charge balance errors

Aqueous solutions are electrically neutral by nature. Analytical errors and unanalyzed constituents in a chemical analysis are the common causes that account for discrepancies between sum of cations and anions. Charge balance errors (CBE) are used to measure the quality of the water analysis. PHREEQC is programmed to calculate the CBE percent for each solution, by the following equation:

$$CBE = \frac{\sum cations - |\sum anions|}{\sum cations + |\sum anions|} \; x \; 100. \qquad (3.1)$$

Samples with charge balance errors (CBE) outside of ±30% were removed.

Ankerite Solubility Product

Ankerite, $Ca(Fe^{2+}, Mg, Mn)(CO_3)_2$, is a major carbonate mineral in the Green River Formation (Figure 4; Cole and Picard, 1978). Ankerite thermodynamic data was not part of the databases incorporated in PHREEQC. In a study by Pham et al., (2011; 2012), the ankerite solubility product (K_{ss}) was estimated by assuming a 60/40 pure phase ankerite-dolomite mix along with a theoretical value for the Gibbs free energy of formation for pure phase ankerite from Woods and Garrels (1992). They estimated the K_{ss} for ankerite to be $10^{-19.51}$. In other reports, researchers have assumed the K_{ss} to be near that of dolomite and have used that value as an estimate (Chai and Navrotsky, 1996). In this study, a separate estimate of the K_{ss} for ankerite was developed.

The Lippman total solubility model, which is widely accepted for carbonate minerals, was used to calculate the saturation indicies for ankerite in this study (Glynn and Reardon, 1990). The Lippman total solubility model is a stoichiometric saturation model in which there is an equilibrium between a solution and a solid solution of a fixed composition (Appelo and Postma, 2010). The general formula and stoichiometric range for natural ankerite is defined by Chai and Navrotsky (1996) and Davidson et al. (1993) as:

$$Ca(Fe_xMg_{1-x})(CO_3)_2,\ 0 \leq x \leq 0.7. \qquad (3.2)$$

By formal definitions, the stoichiometric range proposed above includes ferroan dolomite; ankerite is formally defined as having more moles of iron than magnesium (Fe > Mg) (www.mindat.org). However, ankerite minerals with an iron

mole fraction greater than 0.7 have never been found in nature (Goldsmith et al., 1962; Chia and Navrotsky, 1996; Davidson et al., 1993). For simplification, ferroan dolomites will here be referred to as ankerite.

Two methods were employed to estimate the solubility product for ankerite. The first method calculated the ion activity products for each sample at different iron mole fractions to determine the best stoichiometry and estimated K_{ss} for the data. The second method assumed the iron mole fraction is not constant throughout the basin and used a linear regression model to determine these parameters separately for each hydrologic unit and cluster. Both methods are described in more detail in the subsections to follow.

Ion Activity Product Method

Cole and Picard (1978) found abundant ankerite in the basin center of the Green River Formation. Assuming that groundwaters in that part of the basin are in equilibrium with ankerite, then the ion activity product (IAP) of those samples can be used to estimate the equilibrium solubility product of ankerite assuming a fixed iron mole fraction.

The equilibrium solubility product is temperature dependent. Thus, the measured temperature of a solution may be a potential source of error as temperature can change in transit from origin to surface. However, the geothermal gradient in the basin is low (temperature ranges from 6 to 31˚C) and so impacts to the mineral equilibrium calculation are negligible.

Ankerite IAP values were computed from ion activities in Matlab for all samples located in the lower aquifer with a charge balance error within ±5 percent to ensure usage of the best quality samples (APPENDIX C). IAPs were computed with an x range of 0 to 0.7 by increments of 0.1, along with histograms, normplots, and basic statistics, to include standard deviation, mean, mode, and medium.

In the case of a constant iron mole fraction, the IAPs should converge on a particular value of x. Convergence was defined as having a high IAP value frequency and low standard deviation for the set. Such convergence was not observed. Therefore, a constant mole fraction of iron was assumed at 0.5 as it has been assumed in previous literature (Scott et al., 2014; Giere and Stille, 2004; Wenk et al., 1991).

When data are normally distributed, the mean value can be used as the best sample representative, however, the IAP data was non-normal. Therefore, the corresponding IAP values were transformed to a normal distribution by a Box-Cox transformation. Box-Cox transformations convert non-normally distributed data to a set of data that has approximately normal distribution by power transformations where λ represents the raised power that best transforms the data. When λ ≠ 0, the data can be transformed via the following equation:

$$data(\lambda) = \frac{data^{\lambda}-1}{\lambda}$$ (Box and Cox, 1964). (3.3)

Of the transformed data, the mean was selected and then returned to a regular data value by reversing the equation above,

$$data = ((data(\lambda) * \lambda) + 1)^{1/\lambda}, \quad (3.4)$$

where *data(λ)* is the mean data point found after the Box-Cox transformation to normal distribution, and *data* is the mean data point converted back to the regular data range.

Linear Regression Model

An alternative method to determine the solubility product for ankerite was implemented under the idea that regions with different mole fractions of iron exist in the system. Higher concentrations of Fe(II) may be present in the deeper regions of the basin, leading to ankerite with higher fractions of iron. To explore this possibility, the equation for ankerite was changed to log form:

$$Log(K_{ss}) = log\{Ca^{+}\} + \mathrm{X}\log\{Fe^{2+}\} + (1 - X)\log\{Mg^{2+}\} + 2\{CO_3^{-}\}, \quad (3.5)$$

where {} denotes activities and *X* denotes the mole fraction of iron. By algebraic manipulation, the formula can be written in slope-intercept form:

$$Log\{Ca^{2+}\} + Log\{Mg^{2+}\} + 2Log\{CO_3^{-}\} = X(Log\left({\{Mg^{2+}\}}/{\{Fe^{2+}\}}\right) + LogK_{ss}. \quad (3.6)$$

Samples were plotted using Matlab and Excel and the slope and y-intercept were calculated. From Equation 3.6, the slope represents the mole fraction of iron that best fits the data and the y-intercept represents the solubility product. Samples were first evaluated by hydrologic unit, however, results did not fit a linear trend and were associated with very high standard errors. A cluster analysis was then conducted to determine the number of clusters and possible causes for the grouping. A Ward's minimum variance method was used to cluster

data in groups in which the variance within each group was minimized. Prior to analysis, ion and field parameter concentrations were normalized by means of standard normalization. Each cluster group was evaluated by linear regression for estimates of the solubility product and iron mole fraction.

Mineral Weighting Scheme

Intrinsic errors are present in the SI calculation and includes both the accuracy of reported solubility products and the chemical analyses. These uncertainties are sufficiently compensated by considering a range of saturation values near zero to be within the equilibrium zone for a mineral. It is very common to consider SI values between ±0.3 to be in equilibrium for simple minerals, such as evaporites (Deutsch and Siegel, 1997). However, this range is too narrow for more complex minerals and minerals that contain elements for which analytical uncertainties are likely relatively high (including H^+ derived from pH measurements).

A mineral weighting scheme devised by Palmer (2015) was implemented to calculate a weight for each mineral based on measurement accuracy and mineral complexity. The weighting scheme is an error propagation equation with the following formula:

$$w_k \sim 1/\left[\sum_{i=1}^{nc} v_{ik}\left(\frac{S_{ci}}{C_i}\right)^2\right]^{1/2}, \tag{3.7}$$

where w_k is the weighting factor for the *kth* mineral, v_{ik} is the stoichiometric coefficient of the *ith* component in the *kth* mineral, and $\left({}^{S_{ci}}/_{C_i}\right)$ is the coefficient

of variation of the *ith* basis species. A table of the different coefficients of variations for ions are displayed in APPENDIX D (Palmer, 2015).

The weighted saturation index (WSI) was calculated by taking the inverse of the weighting factor ($1/w_k$). Equilibrium was considered to be ±3xWSI. A mineral was considered over/undersaturated within ±10xWSI and *highly* over/undersaturated for WSI values above and below that threshold (APPENDIX D). When the weighted equilibrium range was less than ±0.3, ±0.3 was used as the minimum range and ±1.0 was used as the threshold for over/undersaturated.

Mineral Saturation Maps and Cross Sections

The results from the PHREEQC SI calculations were input to Microsoft Access and georeferenced. The referenced results were exported to ArcGIS and the SI values for major minerals were interpolated by hydrologic unit. Previously, universal kriging method was used to interpolate between measured valued for major ion concentrations and field parameters. However, the mineral weighting scheme differs by grouping data points and centering values around zero for equilibrium, as opposed to a linear increase in values. Thus, a different interpolation technique was used to best fit the data. An Inverse Difference Weighted (IDW) interpolation scheme was used to produce the maps in this section. IDW is an exact interpolator and determines cell values using a linear-weighted combination set of sample points and assigning a weighting factor to each point based on distance from the cell. Therefore, points close to the cell have more influence on the cell value then points further away (Childs, 2004).

Cross sections were created for major minerals for two transects: One transect going north-south across the basin, and the other going east-west. Points were selected in ArcGIS by location; points within 0.3 decimal degrees (dd) of the transect were selected and exported to Excel. In some cases, point density in areas were sparse. In this case, the nearest point outside of 0.3 dd was selected for completeness. In Excel, the SI values and longitude or latitude was plotted for different minerals by hydrologic unit. The creek location and faults were added to the graphs for a more comprehensive look at the system.

RESULTS

Ankerite Solubility Product

Ion Activity Product Method

Histogram of different stoichiometric values for x in the ankerite IAP equation are displayed below in Figure 36. A summary of preliminary statistics for different values of x are located in Table 7. The histograms and standard deviations were very similar for the different values of x; convergence was not observed. A value of x = 0.5 was used as the stoichiometry of the equation as assumed in previous studies (Scott et al., 2014; Giere and Stille, 2004; Wenk et al., 1991).

At x = 0.5, the transformed IAPs of the solution resulted in a log(IAP) value of -17.97.

Table 7. Ankerite IAP summary table based on different stoichiometric coefficients

X value	Standard dev.	Mean	Mode	Median	Log(IAP)
0.00	0.734	-15.72	-15.95	-15.90	-15.78
0.10	0.685	-16.15	-16.46	-16.33	-16.21
0.20	0.659	-16.57	-16.96	-16.80	-16.65
0.30	0.656	-17.00	-17.47	-17.23	-17.09
0.40	0.677	-17.43	-17.97	-17.60	-17.53
0.50	0.721	-17.85	-18.48	-17.97	-17.97
0.60	0.783	-18.28	-18.98	-18.32	-18.39
0.70	0.860	-18.71	-19.49	-18.79	-18.82

Linear Regression Method

The linear regression method was calculated for each hydrologic unit and cluster. Hydrologic units resorted in poor linear fits with high errors. Analysis by cluster produced better results. A Ward's cluster analysis was performed and truncated to include five clusters. Group 1, 2, and 4 represent a mix of upper and lower aquifer samples and Group 3 and 5 are primarily surface samples.

Group 1 is defined by having high sodium and alkalinity concentrations (on average around 95 percent of the total anion/cations content), high calcium to magnesium ratio (average 1.8), and low sulfate concentrations. Group 2 also has high sodium and alkalinity concentrations (on average between 90 and 98

percent of the total anion/cations), lower calcium to magnesium ratio (average 1.2) and low sulfate. Group 4 has an average depth less than the previously defined groups and is defined by less sodium and alkalinity (making up approximately 65 to 75 percent of total ions), a calcium to magnesium ratio of approximately 1.0, and an increase in sulfate (on average 30 percent of total anions). Group 3 samples are high in calcium, alkalinity, and contain approximately 30 percent sulfate anions. This group is located narrowly along the southern boundary and comprised of almost entirely surface samples. This group represents the recharge water in the basin. Group 5, also comprised mostly of surface samples, differs from Group 3 by containing less calcium and more sodium, less alkalinity, and more sulfate. These samples are located towards the center and northern region of the basin and represents the evolution of the groundwater as it flows from recharge regions to its discharge location in the north. Since Group 3 and Group 5 are primarily surface samples, these clusters were not used in further analysis due to concerns with respect to the loss of CO2 and the oxidation of ferrous iron. In addition, previous studies have not reported the presence of ankerite at the surface of the basin. A summary of results for the three remaining cluster groups are in Table 8 below.

Group 1 samples are generally located along the lower reaches of Piceance Creek tributaries (in the zone of upward groundwater movement between the lower and upper aquifer), along the southern margin at shallow depths (zone of downward groundwater movement), and are absent from the

northern discharge region. Some well locations, particularly the locations along the southern boundary, are in regions with no known ankerite deposits.

Table 8. Ankerite solubility product summary per cluster group by linear regression method.

Group	Log(K_{ss})	Std error	Fe mole fraction	Std error	Description
1	-19.72 ±	1.167	1.45 ±	0.465	Mostly lower aquifer
2	-16.25 ±	0.337	0.48 ±	0.132	Mostly lower aquifer
3	-16.51 ±	0.439	0.34 ±	0.154	Mostly upper aquifer

This combined with possible effects of groundwater mixing, resulted in Group 1 having an unrealistic iron mole fraction and the greatest standard error of any other group. The results from this group were disregarded. Group 2 and 4 have close results with log(K_{ss}) values of -16.25 ±0.337 and -16.51 ±0.439 respectfully. The calculated mole fractions for these two clusters are 0.48 ±0.132 and 0.34 ±0.154. These solubility product values are similar to that of disordered dolomite (-16.54) and slightly greater than the reported value of -17.09 for dolomite (Visual MINTEQ database). Group 2 contains mostly lower aquifer samples with upper and surface samples located in the far north near the discharge point of Piceance Creek. This group represents a lower aquifer flow path that flows to the north and then exists through the upper aquifer and surface. Group 4 is comprised mostly of upper aquifer samples located away

from the margins in the basin center, and lower aquifer samples located closer to the southern and western margin. Graphs of the two groups in which slope and y-intercept (i.e. iron mole fraction and K_{ss}) where calculated are displayed in Figure 37.

Upon further investigation of the cluster groups, it was observed that the average IAPs for Groups 2 and 4 were commonly near equilibrium with respect to siderite and magnesite, but not disordered dolomite, while Groups 1, 3 and 5 were generally near equilibrated with disordered dolomite, magnesite, siderite (for Group 1), and calcite and aragonite (for Group 3). As Groups 1, 3, and 5 are near equilibrium with respect to disordered dolomite, they are less likely to be in equilibrium with ankerite. Groups 2 and 4 are oversaturated with respect to disordered dolomite and fit the linear regression formula with reasonable standard errors. Thus, it is likely that these two groups are near equilibrium with ankerite. A table summarizing the average IAPs for each group with respect to different carbonate minerals is provided in Table 9 below. Bolded values indicate the average IAPs are within one standard deviation of the reported solubility product (in parenthesis next to the mineral name).

Both methods of estimating the ankerite solubility product provide reasonable values. The second method's calculated iron mole fraction from Group 2 is approximately 0.5 which is a value used in previous research (Scott et al., 2014; Giere and Stille, 2004; Wenk et al., 1991) and used in the first method of analysis. However, mineralogic research on the basin has recorded ankerite in the Green River Formation with no mention of the mineral in the Uinta Formation

or on the surface. Group 2 and Group 4 contain various upper aquifer samples, and even some surface samples. These are outside of stratigraphic controls, thus, estimating the K_{ss} based on sample IAPs with good CBEs (±5 percent) only from the lower aquifer seems to be a reasonable choice. However, to make a more informed valuation, both solubility products were added to the PHREEQC database (-17.97 and -16.25) and used in further analysis for comparison.

Table 9. Summary of average IAPs by cluster group with respect to common carbonate minerals.

Group	Siderite (-10.24)			Dolomite (-17.09)			Dis-Dolomite (-16.54)		
	Log(IAP)		Stdev	Log(IAP)		Stdev	Log(IAP)		Stdev
1	**-10.528**	**±**	**0.407**	-16.127	**±**	0.837	**-16.127**	**±**	**0.837**
2	**-9.769**	**±**	**0.616**	-15.099	**±**	0.614	-15.099	**±**	0.614
3	-12.016	**±**	0.277	**-16.553**	**±**	**0.575**	**-16.553**	**±**	**0.575**
4	**-10.369**	**±**	**0.814**	-15.582	**±**	0.783	-15.582	**±**	0.783
5	-11.935	**±**	0.486	-16.061	**±**	0.552	**-16.061**	**±**	**0.552**

Group	Magnesite (-7.46)			Calcite (-8.48)			Aragonite (-8.30)		
	Log(IAP)		Stdev	Log(IAP)		Stdev	Log(IAP)		Stdev
1	-8.040	**±**	0.513	-8.085	**±**	0.352	**-8.085**	**±**	**0.352**
2	**-7.362**	**±**	**0.451**	-7.738	**±**	0.249	-7.738	**±**	0.249
3	-8.327	**±**	0.305	**-8.226**	**±**	**0.275**	**-8.226**	**±**	**0.275**
4	**-7.636**	**±**	**0.444**	-7.946	**±**	0.365	**-7.946**	**±**	**0.365**
5	-7.928	**±**	0.337	-8.132	**±**	0.238	**-8.132**	**±**	**0.238**

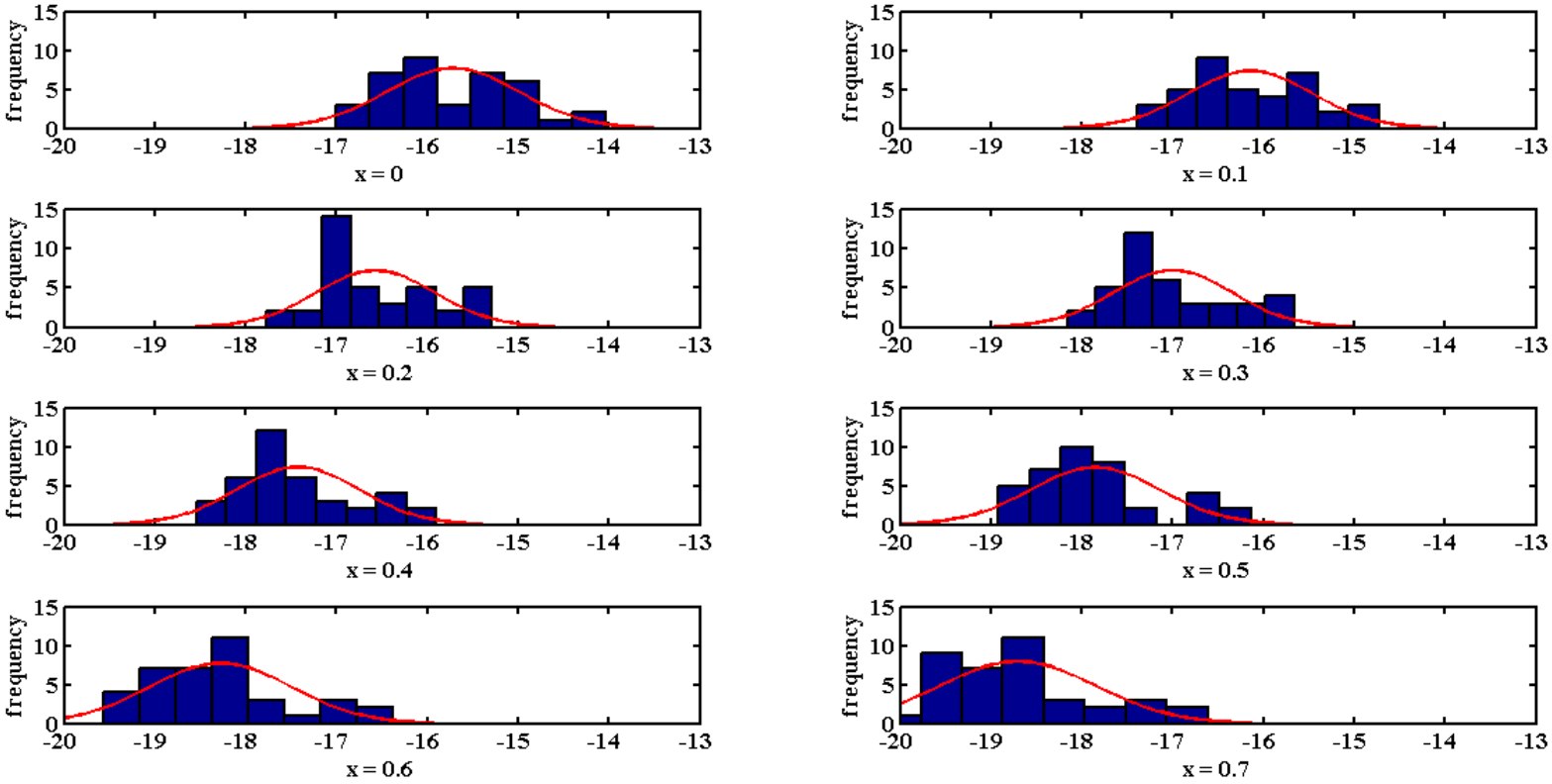

Figure 36. Ankerite log(IAP) histograms (prior to Box-Cox transformations) for varying stoichiometric ranges when x goes from 0 to 0.7 by 0.1 increments. A red line was added to show the approximate normal fit of the data.

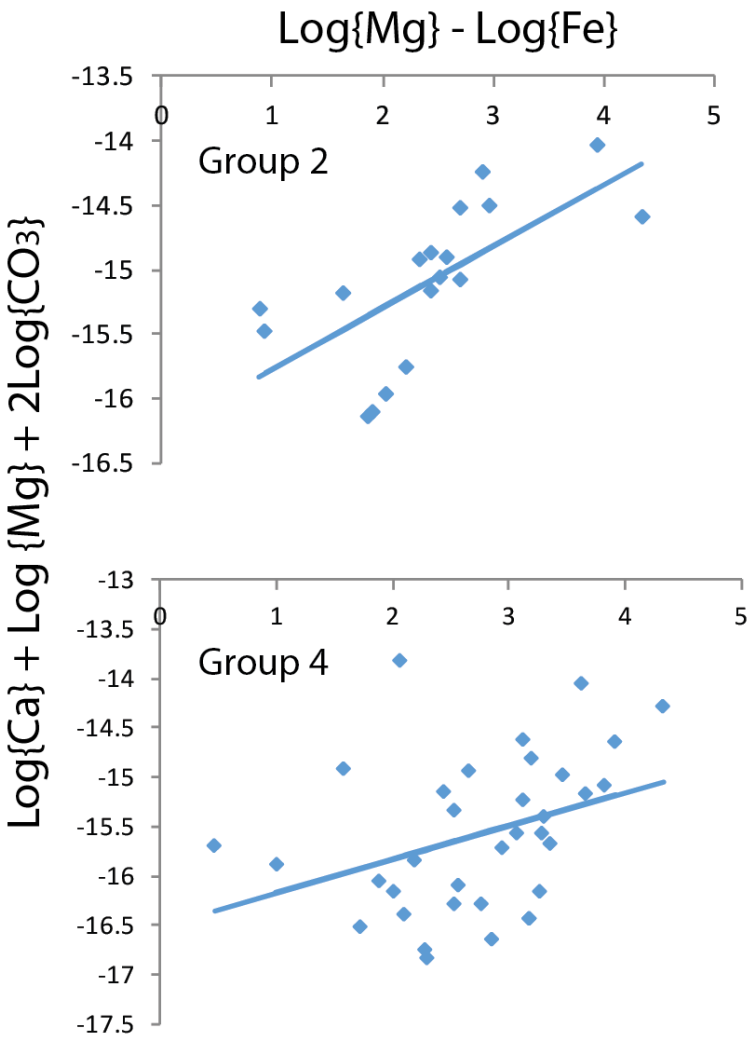

Figure 37. Linear regression results for estimating the solubility product for ankerite. The regression was performed on two clusters. The top graph corresponds to Group 2 and the lower, Group 4.

Mineral Saturation Indicies Maps

Mineral saturation indicies maps were created for major minerals outlined by Cole and Picard (1978). Maps are displayed below in Figure 38 - Figure 48 and are separated by mineral class and sometimes group.

Carbonates

Carbonate SI distribution results contain three maps showing the interpolated saturation indicies in the upper aquifer, lower aquifer and surface samples (Figure 38 - Figure 43). Maps are presented for calcite, dolomite, disordered-dolomite, ankerite, and dawsonite. Two ankerite mineral saturation distribution maps (Figure 41 and Figure 42) were created using one of the two methods for estimating the solubility product for ankerite. As evident from the figures, method one (Figure 41) resulted in the majority of samples in equilibrium to oversaturated with respect to ankerite, and the second method (Figure 42) resulted in the majority of samples undersaturated with few regions in the upper and lower aquifer in equilibrium. The points in which equilibrium is reached coincides strictly with the samples associated with that particular cluster. Based on known mineralogy in the basin (Cole and Picard, 1978; Poole, 2014), the first method best represents known spatial distributions of ankerite. A log(K_{ss}) value of -17.97 best fits the data for this study and was used in further analysis to follow.

Although not displayed in figures, nahcolite and halite SI values were highly undersaturated in all hydrologic units. Water is closest to being in equilibrium with nahcolite in the lower aquifer, near the Alkali Flats fault. In this region, the largest SI value was calculated at -0.46.

Upon evaluation of results, regions of high oversaturation were observed for all carbonate minerals, especially around Piceance Creek in the basin center.

High oversaturation is not expected as carbonates are buffers that adapt quickly to restore equilibrium conditions. Error associated with the field pH measurement was thought to contribute to this finding. Due to the difference in CO_2 partial pressure between the aquifer water and the surface, the hydrogen concentration will fluctuate to equilibrate with atmospheric CO_2 when a sample is drawn from depth and brought to the surface. This results in overestimated pH values. In an attempt to correct for this occurrence, pH values were calculated in PHREEQC along with the associated SI values assuming equilibrium with calcite. Calcite was chosen because it is a simple carbonate mineral and is recorded in literature as being present in the Uinta and Green River Formation (Poole, 2014; Day et al., 2010; Cole and Picard, 1978). For most of the samples, this method resulted in decreased pHs, decreased SI values, and little to no change in charge balance errors. Carbonate mineral saturation values were generally in equilibrium to undersaturated. The regions of undersaturation conflicted with regions of known mineral presence, and for quite a few samples, the method increased pH values to implausible values (up to 13.66). For these reasons, the estimated pH values were not used further in this study. A table demonstrating the estimated verse reported pH values and CBEs is included in Appendix E.

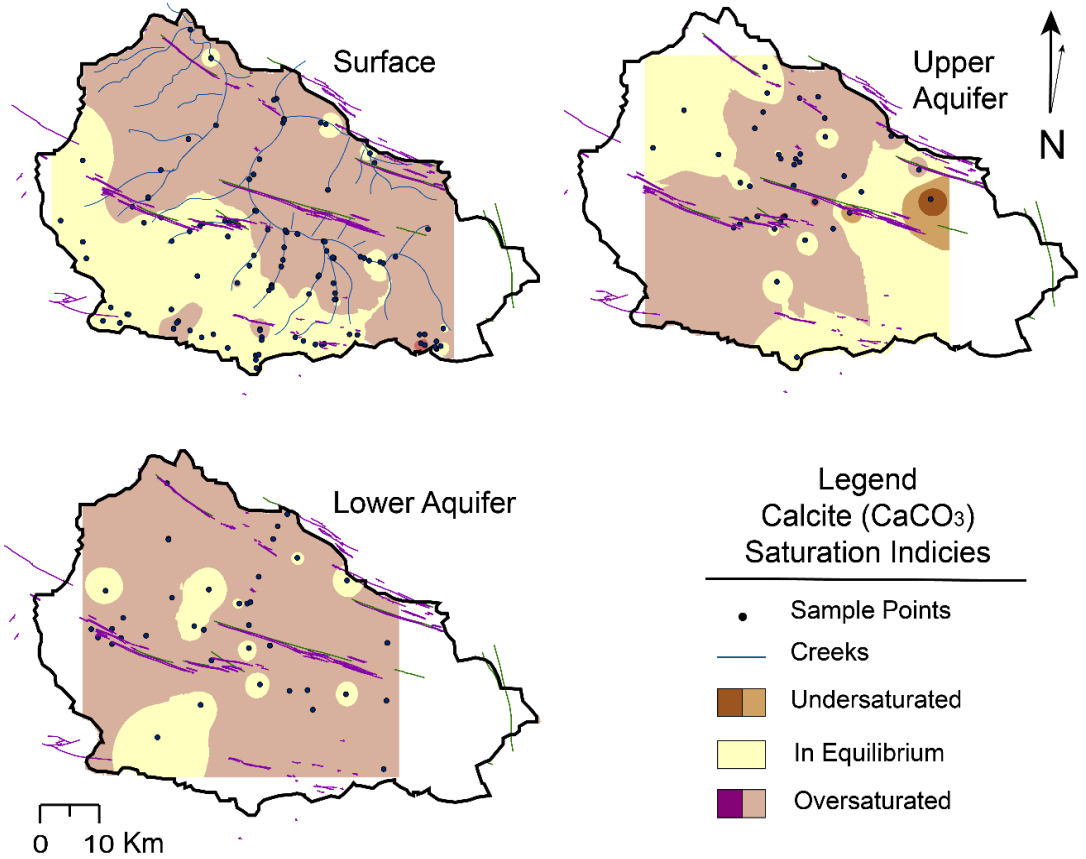

Figure 38. Calcite SI distribution maps for surface waters (top left), upper aquifer (top right), and lower aquifer (bottom left), Piceance Basin, Co. Black dots represent sample locations. Purple regions represent areas that are undersaturated with respect to the mineral and green regions represent areas that are oversaturated. Off-white represents regions in equilibrium with the mineral. Darker colors represent highly over/undersaturation, which is defined as values greater or less than 10 times the weighted SI. Purple and green lines represent faults mapped on the Mahogany Zone and surface, respectfully.

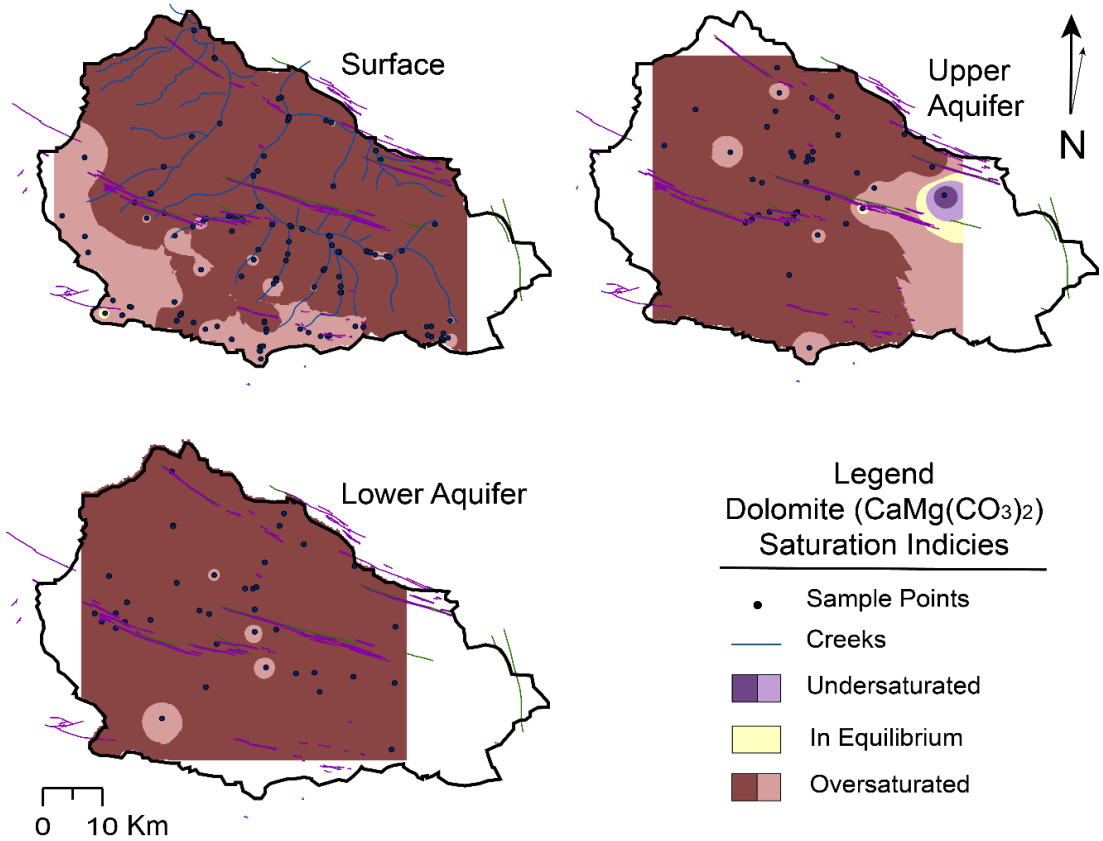

Figure 39. Dolomite SI distribution maps for surface waters (top left), upper aquifer (top right), and lower aquifer (bottom left), Piceance Basin, Co. Black dots represent sample locations. Blue regions represent areas that are undersaturated with respect to the mineral and red regions represent areas that are oversaturated. Off-white represents regions in equilibrium with the mineral. Darker colors represent highly over/undersaturation, which is defined as values greater or less than 10 times the weighted SI. Purple and green lines represent faults mapped on the Mahogany Zone and surface, respectfully.

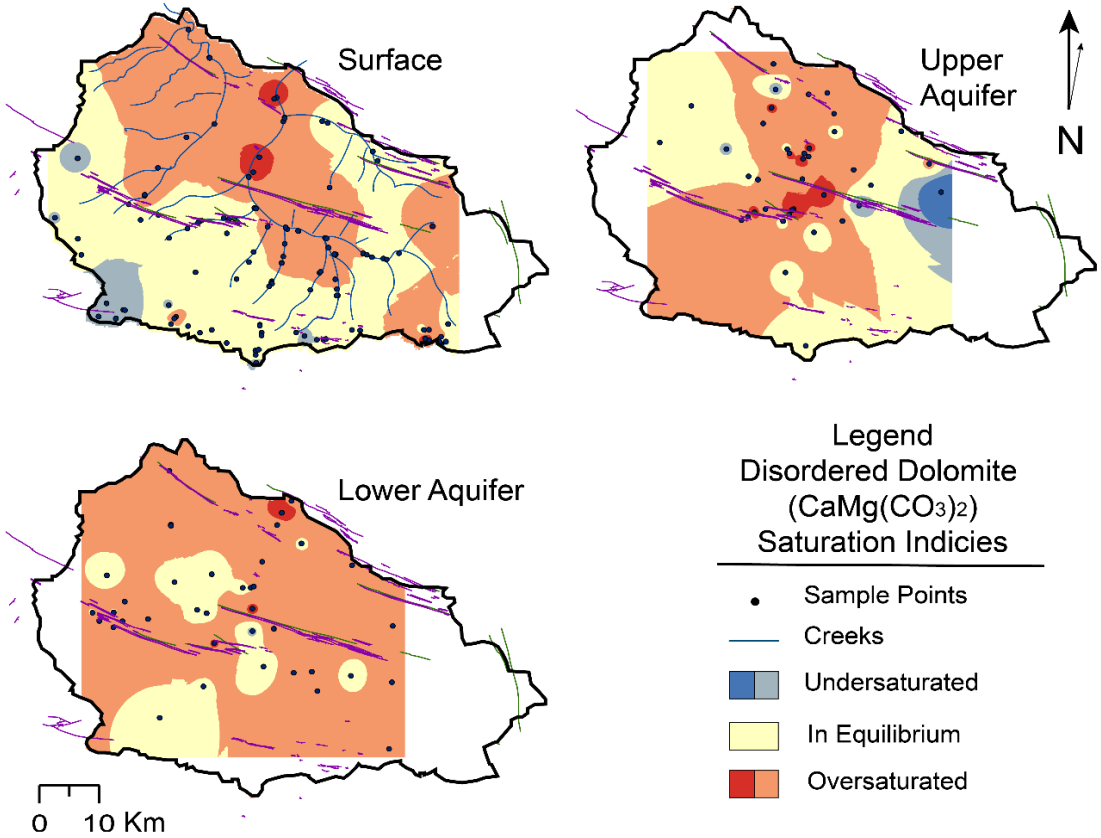

Figure 40. Disordered Dolomite SI distribution maps for surface waters (top left), upper aquifer (top right), and lower aquifer (bottom left), Piceance Basin, Co. Black dots represent sample locations. Purple regions represent areas that are undersaturated with respect to the mineral and red regions represent areas that are oversaturated. Off-white represents regions in equilibrium with the mineral. Darker colors represent highly over/undersaturation, which is defined as values greater or less than 10 times the weighted SI. Purple and green lines represent faults mapped on the Mahogany Zone and surface, respectfully.

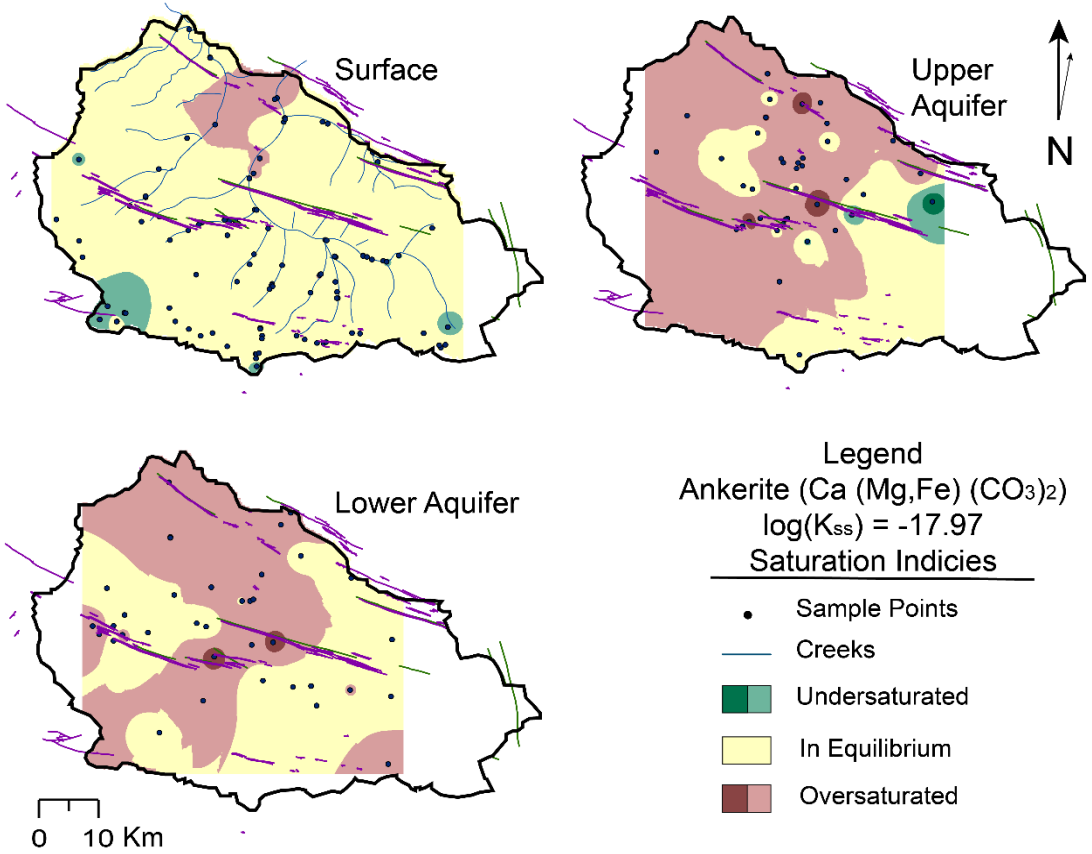

Figure 41. Ankerite SI distribution maps ($\log K_{ss}$ = -17.97) for surface waters (top left), upper aquifer (top right), and lower aquifer (bottom left), Piceance Basin, Co. SI values are based on an estimated solubility product. Black dots represent sample locations. Blue regions represent areas that are undersaturated with respect to the mineral and red regions represent areas that are oversaturated. Off-white represents regions in equilibrium with the mineral. Darker colors represent highly over/undersaturation, which is defined as values greater or less than 10 times the weighted SI. Purple and green lines represent faults mapped on the Mahogany Zone and surface, respectfully.

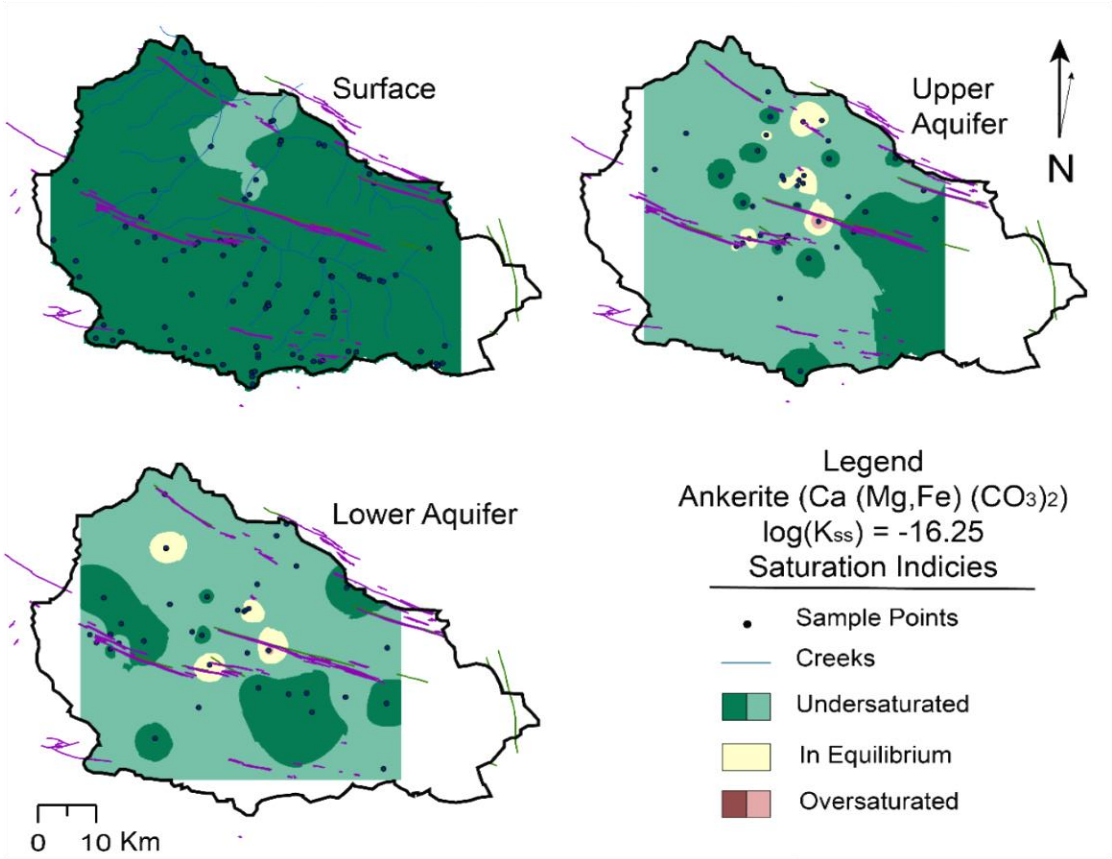

Figure 42. Ankerite SI distribution maps ($logK_{ss}$ = -16.25) for surface waters (top left), upper aquifer (top right), and lower aquifer (bottom left), Piceance Basin, Co. SI values are based on an estimated solubility product. Black dots represent sample locations. Blue regions represent areas that are undersaturated with respect to the mineral and red regions represent areas that are oversaturated. Off-white represents regions in equilibrium with the mineral. Darker colors represent highly over/undersaturation, which is defined as values greater or less than 10 times the weighted SI. Purple and green lines represent faults mapped on the Mahogany Zone and surface, respectfully.

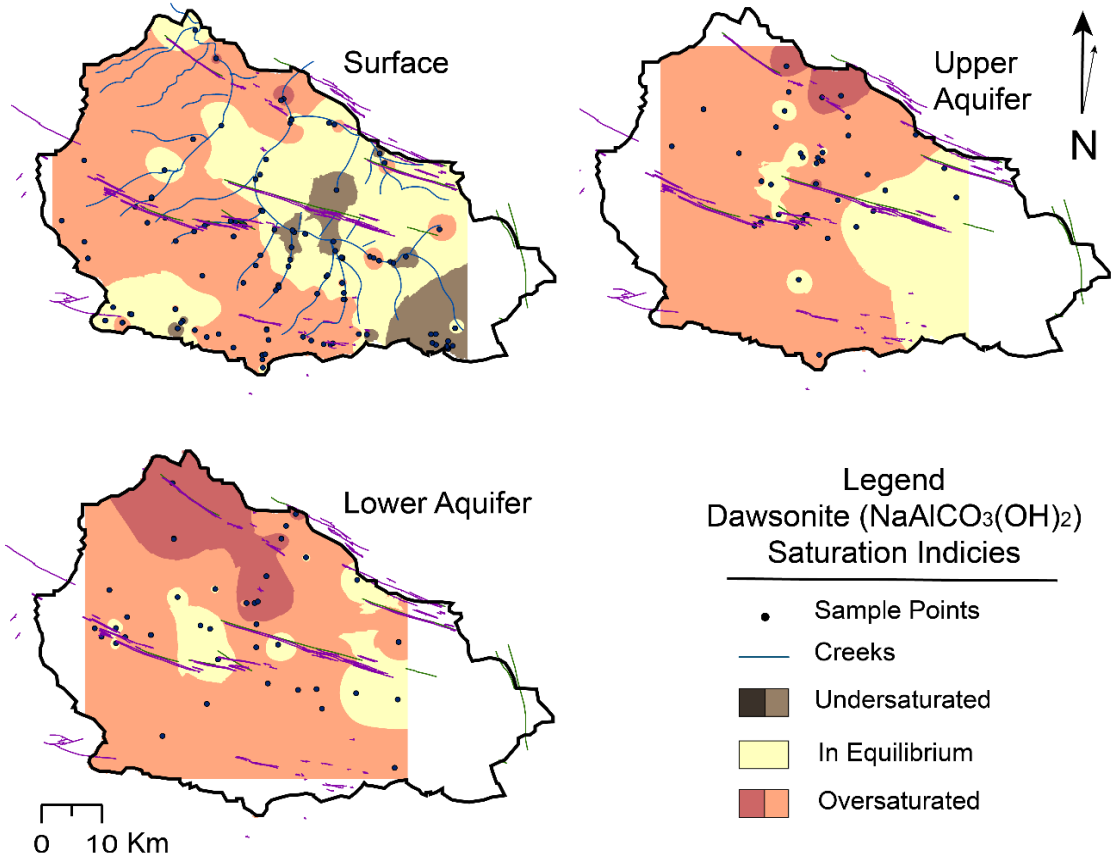

Figure 43. Dawsonite SI distribution maps for surface waters (top left), upper aquifer (top right), and lower aquifer (bottom left), Piceance Basin, Co. Black dots represent sample locations. Purple regions represent areas that are undersaturated with respect to the mineral and green/blue regions represent areas that are oversaturated. Off-white represents regions in equilibrium with the mineral. Darker colors represent highly over/undersaturation, which is defined as values greater or less than 10 times the weighted SI. Purple and green lines represent faults mapped on the Mahogany Zone and surface, respectfully.

Sulfates

All sulfates (gypsum, anhydrite, jarosite, and tiemmanite) are highly undersaturated (as much as 70 times less than the WSI) in all three hydrologic units.

Silicates

Analcime SI distribution maps for the three hydrologic units are displayed in (Figure 44). Albite and K-feldspar SI distribution maps (Figure 45 and Figure 46) show that albite SI values are generally oversaturated to highly oversaturated in each hydrologic unit. A few regions are in equilibrium or understatured. K-feldspar SI values are generally highly oversaturated, but SI values decrease to just oversaturated in the lower aquifer.

Quartz SI distribution results contains three maps showing the interpolated saturation indicies in the upper aquifer, lower aquifer and surface samples (Figure 47). In general, quartz is oversaturated everywhere in the basin, except for a few small regions in the lower aquifer where quartz is in equilibrium or undersaturated. Chalcedony SI distribution results (Figure 48) show the water as oversaturated on the surface and much of the upper aquifer. The mineral is generally in equilibrium with groundwater in the lower aquifer although it is oversaturated along the southern margin and undersaturated in the north.

Mineral Saturation Cross Section

Mineral SI values along two transects are displayed for calcite, disordered dolomite, and ankerite in Figure 49, and albite, K-feldspar, and analcime in Figure 50. Different symbology is used to distinguish surface, upper aquifer, and lower aquifer samples (red square, green triangle, and blue diamond, respectfully).

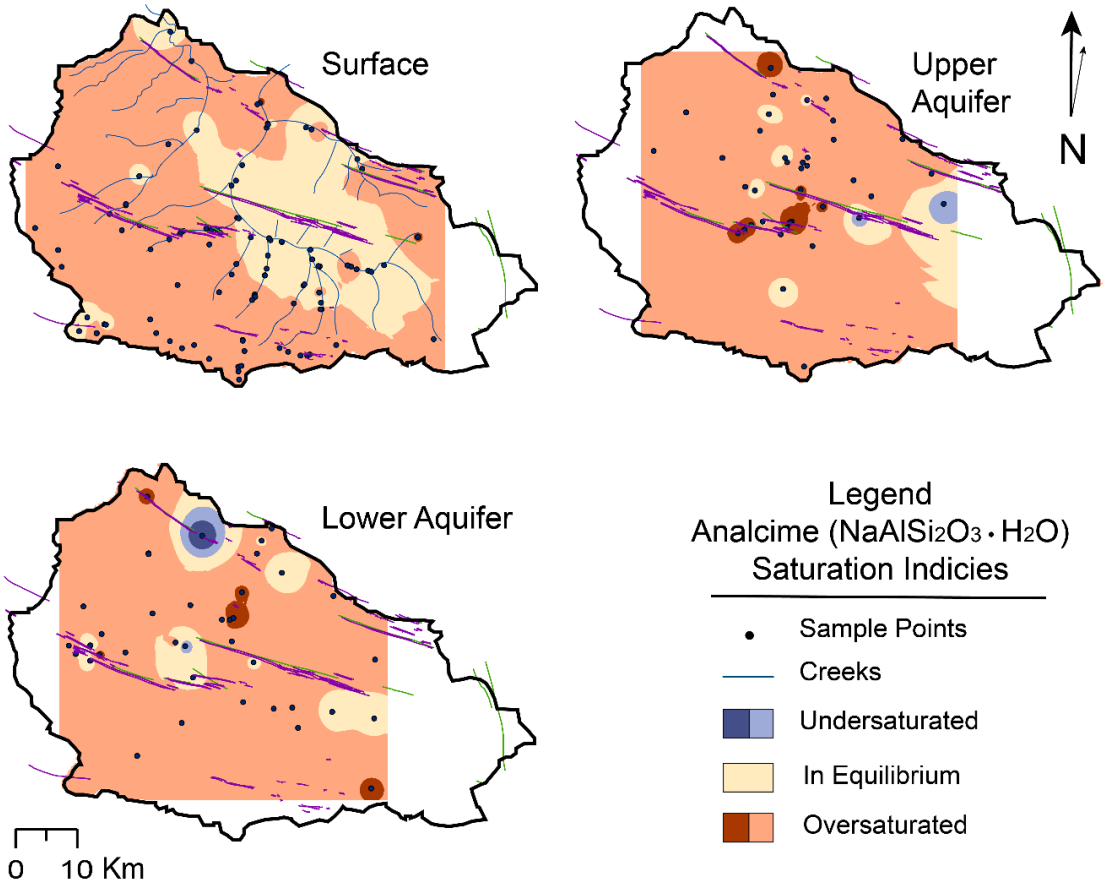

Figure 44. Analcime SI distribution maps for surface waters (top left), upper aquifer (top right), and lower aquifer (bottom left), Piceance Basin, Co. Black dots represent sample locations. Blue regions represent areas that are undersaturated with respect to the mineral and red regions represent areas that are oversaturated. Off-white represents regions in equilibrium with the mineral. Darker colors represent highly over/undersaturation with SI values greater or less than 10 times the weighted SI. Purple and green lines represent faults mapped on the Mahogany Zone and surface, respectfully.

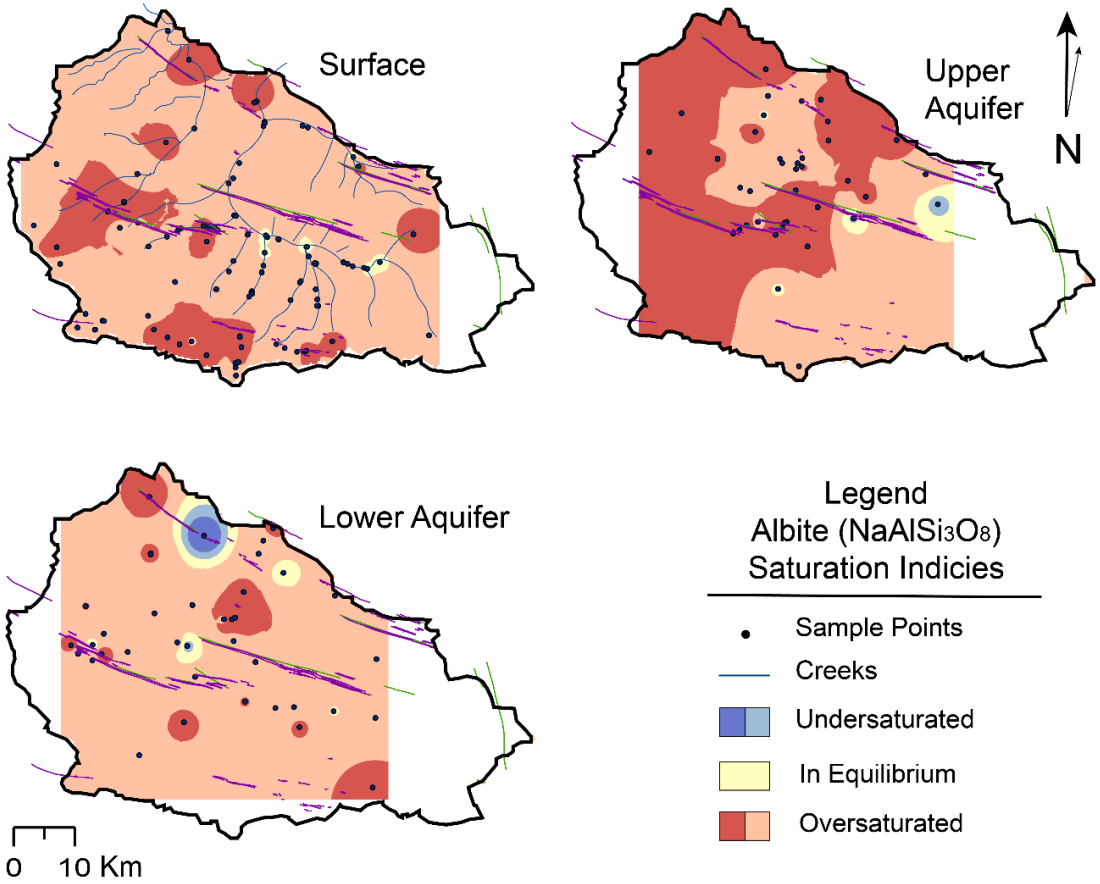

Figure 45. Albite SI distribution maps for surface waters (top left), upper aquifer (top right), and lower aquifer (bottom left), Piceance Basin, Co. Black dots represent sample locations. Blue regions represent areas that are undersaturated with respect to the mineral and red regions represent areas that are oversaturated. Off-white represents regions in equilibrium with the mineral. Darker colors represent highly over/undersaturation with SI values greater or less than 10 times the weighted SI. Purple and green lines represent faults mapped on the Mahogany Zone and surface, respectfully.

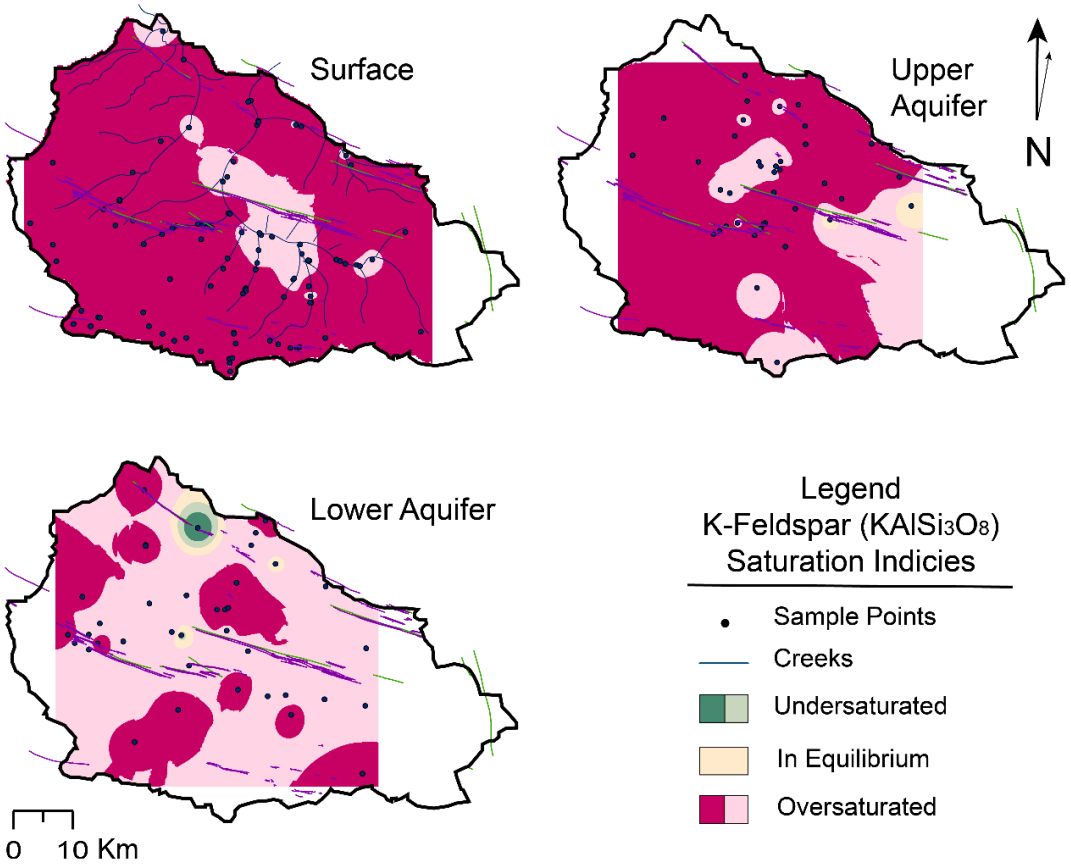

Figure 46. K-feldspar SI distribution maps for surface waters (top left), upper aquifer (top right), and lower aquifer (bottom left), Piceance Basin, Co. Black dots represent sample locations. Purple regions represent areas that are undersaturated with respect to the mineral and green regions represent areas that are oversaturated. Off-white represents regions in equilibrium with the mineral. Darker colors represent highly over/undersaturation with SI values greater or less than 10 times the weighted SI. Purple and green lines represent faults mapped on the Mahogany Zone and surface, respectfully.

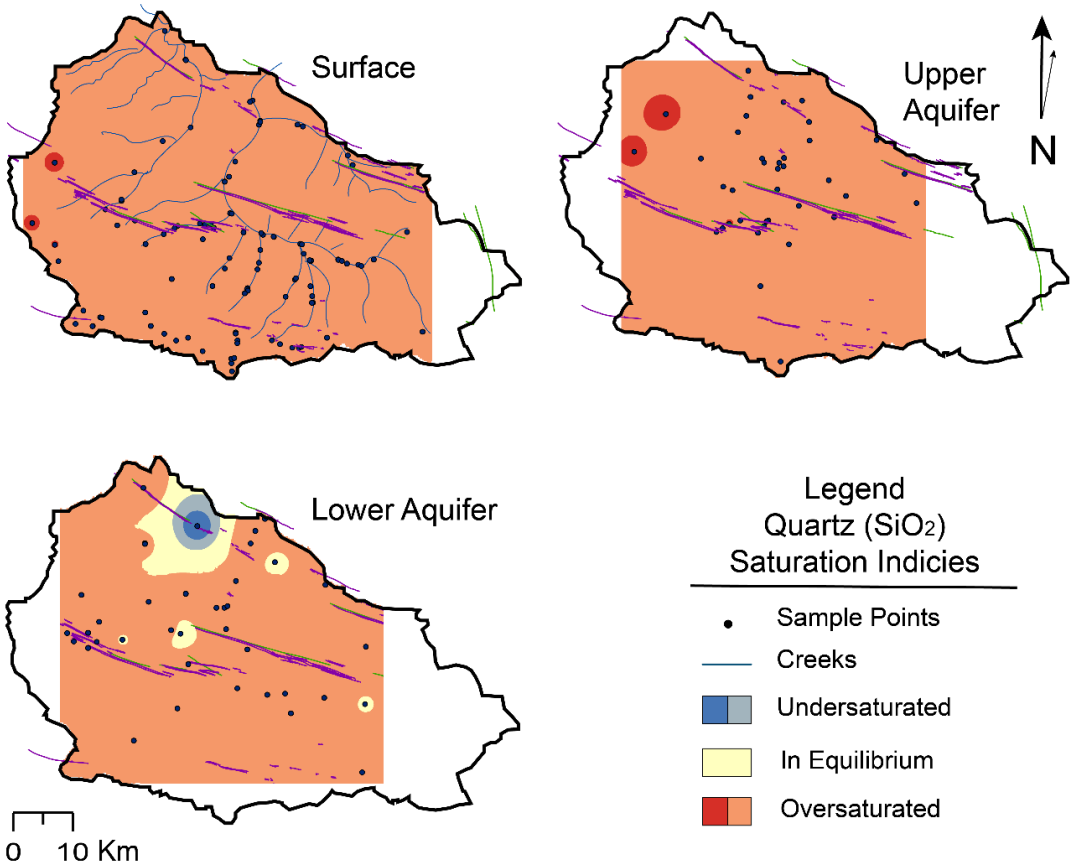

Figure 47. Quartz SI distribution maps for surface waters (top left), upper aquifer (top right), and lower aquifer (bottom left), Piceance Basin, Co. Black dots represent sample locations. Purple regions represent areas that are undersaturated with respect to the mineral and red regions represent areas that are oversaturated. Off-white represents regions in equilibrium with the mineral. Darker colors represent highly over/undersaturation with SI values greater or less than 10 times the weighted SI. Purple and green lines represent faults mapped on the Mahogany Zone and surface, respectfully.

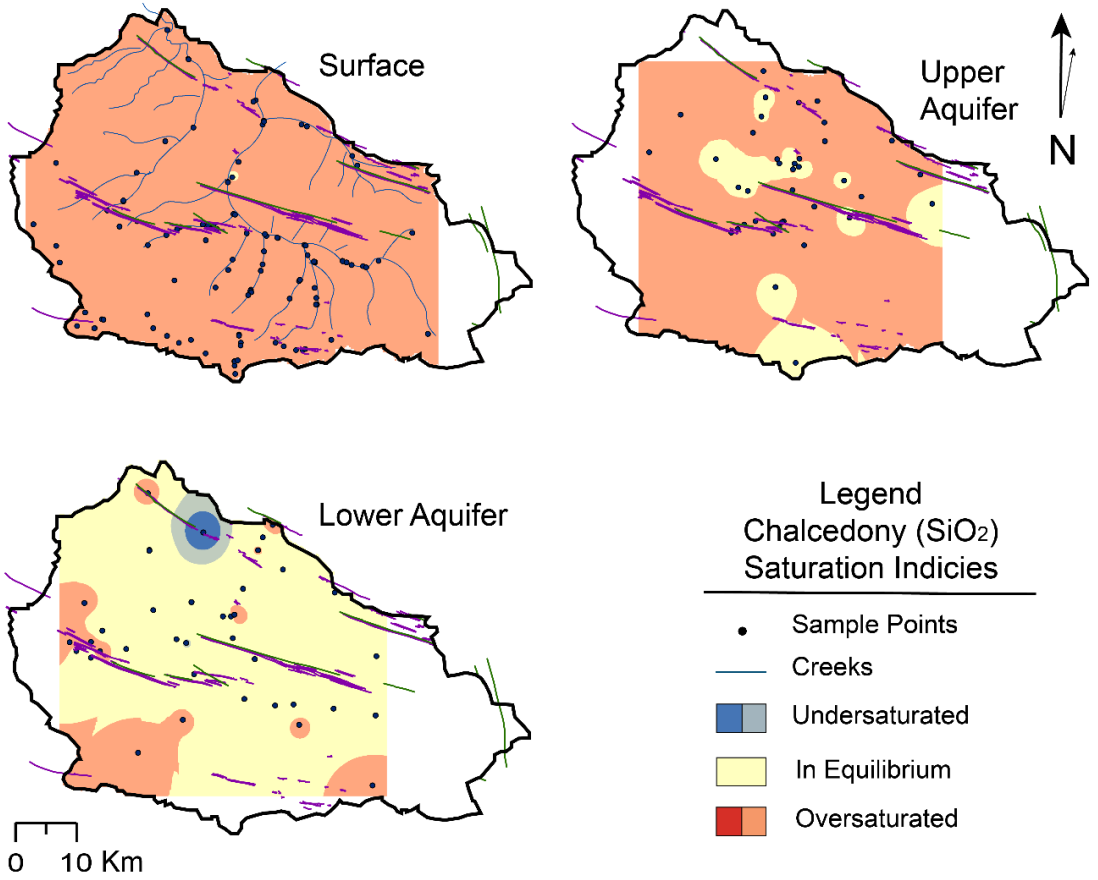

Figure 48. Chalcedony SI distribution maps for surface waters (top left), upper aquifer (top right), and lower aquifer (bottom left), Piceance Basin, Co. Black dots represent sample locations. Blue regions represent areas that are undersaturated with respect to the mineral and red regions represent areas that are oversaturated. Off-white represents regions in equilibrium with the mineral. Darker colors represent highly over/undersaturation with SI values greater or less than 10 times the weighted SI. Purple and green lines represent faults mapped on the Mahogany Zone and surface, respectfully.

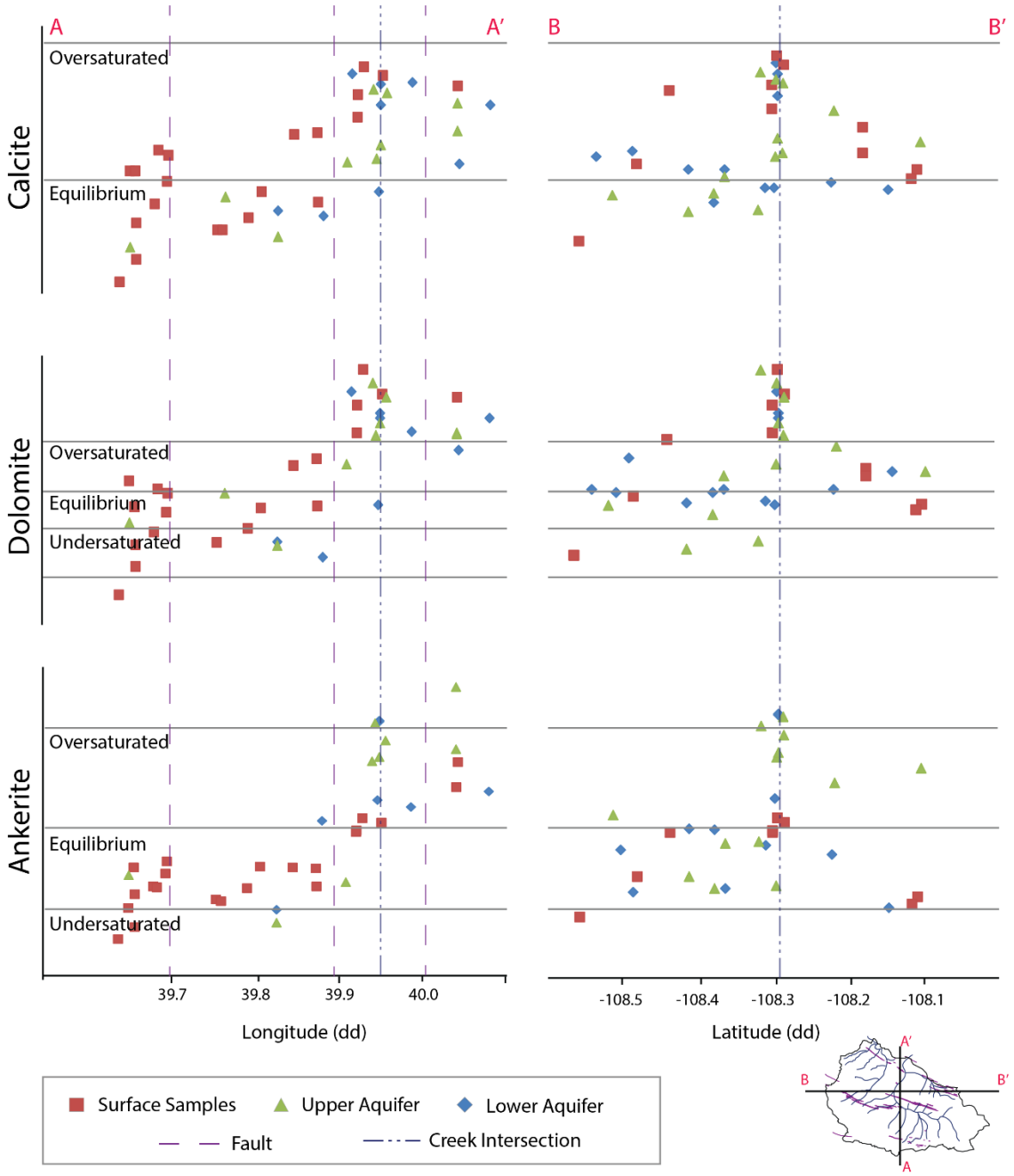

Figure 49. Cross sections for calcite, dolomite, and ankerite for each aquifer unit: surface (red square points), upper aquifer (green triangle points) and lower aquifer (blue diamonds). Two tracks for each mineral are displayed, one going west-east across the basin and the other south-north. Gray lines were included to mark zones of equilibrium and over/undersaturation.

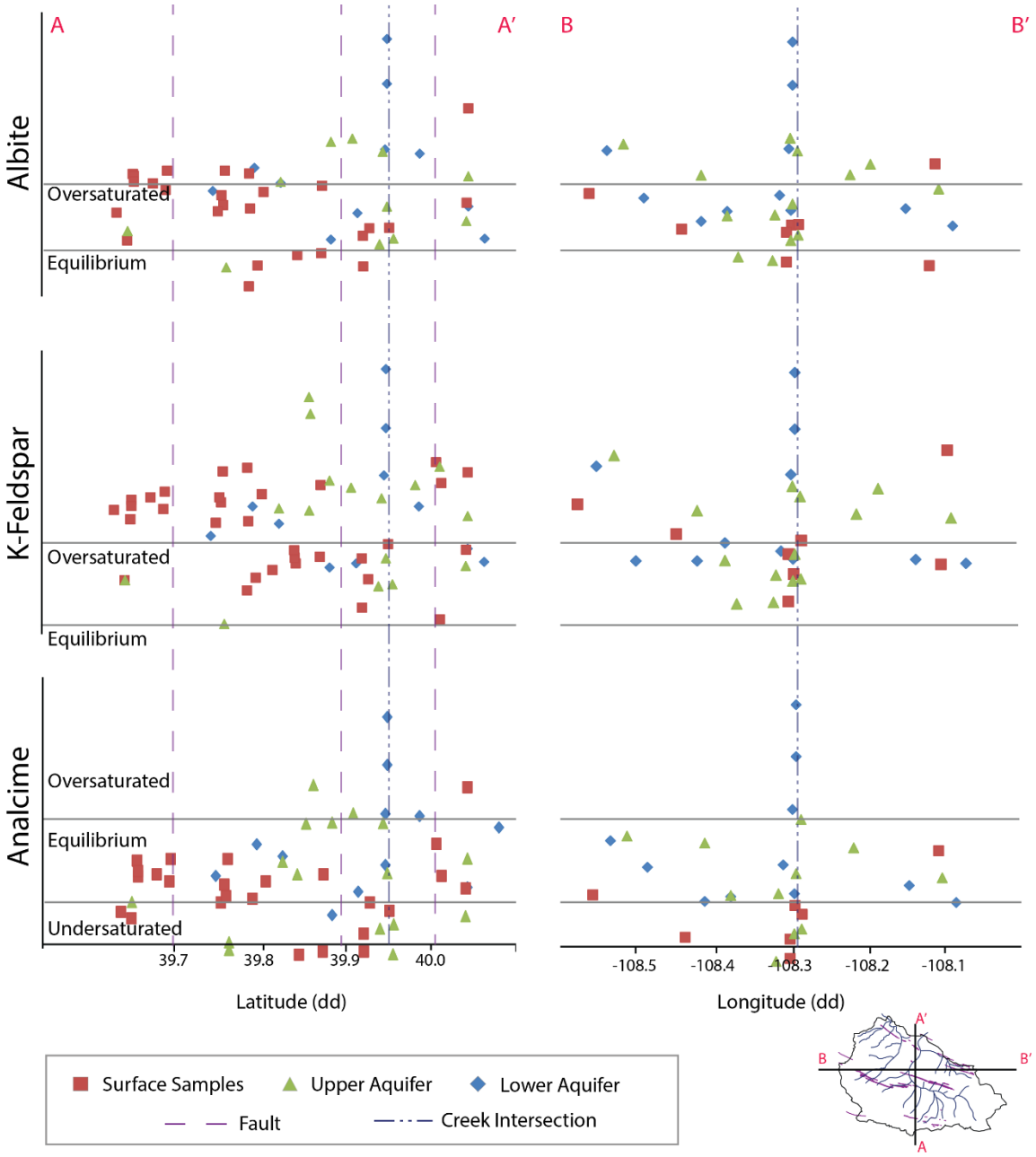

Figure 50. Cross sections for albite, K-feldspar, and analcime for each aquifer unit: surface (red square points), upper aquifer (green triangle points) and lower aquifer (blue diamonds). Two tracks for each mineral are displayed, one going west-east across the basin and the other south-north. Gray lines were included to mark zones of equilibrium and over/undersaturation.

DISCUSSION

Carbonate SI Trends

As groundwater flows from south to north, the SI values for calcite, disordered-dolomite, and ankerite generally increase to oversaturation in all aquifers. Across the basin (east to west) the pattern of saturation is more complex and varies by aquifer. SI values in surface samples generally increase toward the basin center at Piceance Creek and then decrease away from the creek (Figure 49, Transect B). In the lower aquifer, samples are generally in equilibrium (or slightly oversaturated) and then SI values increase quite drastically at the intersection with Piceance Creek, often to high oversaturation. Oversaturation of carbonates is unusual as carbonates are buffers and respond quickly to system changes to maintain equilibrium. Oversaturation in the basin is likely due to mineralogic sequences, presence of organic matter, and groundwater flow paths.

Oversaturation is influenced by the mineralogic sequence that groundwater encounters during transit. In systems where groundwater first equilibrates with calcite and then encounters dolomite, dolomite will continue to dissolve and magnesium concentrations will increase until the water reaches equilibrium. The increase in calcium and carbonate will result in calcite oversaturation (Freeze and Cherry, 1979). This process is observed in the surface samples for calcite and disordered-dolomite following a flow path from southwest to north (Figure 38 and Figure 40). Calcite is in equilibrium along the

western boundary and tends towards oversaturated. The water is initially undersaturated with respect to dolomite but reaches equilibrium after flowing a short distance (Figure 40). Thus, the water appears to equilibrate with calcite prior to equilibrating with dolomite.

The effects of natural organic matter are another way to account for the oversaturation of carbonate minerals in the basin. Organic complexation can inhibit calcium carbonate precipitation (Flaathen et al., 2011; Lin and Singer, 2005; Chave and Suess, 1970). Organic material in the Piceance Basin is sourced from the organic oil shales in the Green River Formation and the richest, most extensive layer of oil shale is the Mahogany Zone aquitard.

Also, the high concentrations of organics in the Green River Formation can result in overestimated carbonate activities. Carbonate activities are calculated solely from the alkalinity and pH measurements, however, organic matter can produce considerable amounts of organic acids which are being grouped into the same calculation. Other acids, such as boric and phosphoric, may also contribute, leading to high oversaturation of carbonate minerals in the basin.

In consideration of the effect of organic matter on carbonate activities, groundwater flow paths can influence the spatial regions in which effects are most prominent. The regions with the highest SI values for carbonates coincides with regions of upward groundwater flow from the lower aquifer. The lower aquifer is in contact with organic material and groundwater must permeate through the organic rich Mahogany Zone to discharge (if not pass through via

fault pathways). The concentration of organic carbon in the groundwater may increase along the flow path and result in highly oversaturated water with respect to carbonate minerals via precipitation inhibitors and/or increased organic acids in the water sample.

Cole and Picard (1978) and Poole (2014) concluded that dolomite was the dominant carbonate mineral in the Green River Formation. Poole (2014) found that calcite and ferroan dolomite increase in the upper zone of the Green River Formation. Cole and Picard (1978) noted that calcite is rare in the basin center and ankerite increases towards the center but is absent along the margins. For the calcite equilibrium reaction:

$$CaCO_{3(s)} \leftrightarrow Ca_{(aq)} + CO_{3\,(aq)}, \tag{3.8}$$

when the water is oversaturated, the reaction proceeds to the left and precipitation occurs. When the water is undersaturated, the reaction proceeds to the right and dissolution follows. Thus, for groundwater in equilibrium and oversaturated with respect to a mineral, it is likely that mineral is present. Based on SI results from the lower aquifer, this study found calcite, dolomite, and ankerite minerals to be present throughout the Green River Formation. The ankerite stoichiometry used to estimate the solubility product is on the boarder of a ferroan dolomite and is in equilibrium in more samples than any other carbonate mineral. This may indicate that the dominant carbonate mineral in the basin based on the water chemistry is a ferroan dolomite (or, loosely “ankerite”) rather than pure dolomite. In the upper aquifer, the saturation results indicate that

dawsonite is present in the eastern portion of the basin and the other carbonate minerals are either absent or rare. On the surface, calcite is the dominant carbonate along the basin margin, but overall, ankerite is the dominant carbonate mineral.

Nahcolite and halite where found to be highly undersaturated in all aquifer units of the basin, with the exception of nahcolite being just undersaturated in the lower aquifer in the northern region. Considering the presence of the saline zone and the sodium bicarbonate dominant water chemistry, it may seem peculiar that water isn't closer to equilibrium or in equilibrium with this mineral. This is likely due to the impermeable nature of the saline zone. Flow lines do not move through this low conductivity zone, leaving the exposed surface area the only region available for dissolution reactions.

Ankerite, dawsonite, and nahcolite are of particular interest as mineral traps for CO_2 sequestration. Mineral trapping has been considered the safest mechanism for long-term storage of CO_2 in underground reservoirs (Pham et al., 2012; Pham et al., 2011) and these minerals have been modeled as optimal candidates (Pham et al., 2012; Pham et al., 2011; Flaathan et al., 2011). Ideal groundwater environments for this mechanism are saturated to oversaturated with respect to these minerals. Carbon dioxide is injected into the subsurface and as the groundwater reacts to establish equilibrium, the CO_2 is incorporated into the secondary formation of the mineral. Dolomite has been considered as a potential mineral trap, however, the high energy of activation for dolomite growth limits the ability for secondary formation to high temperature environments

(Pham et al., 2011). This helps to explain the high oversaturation of ordered dolomite observed in this study. Ankerite and dawsonite are found to be saturated to oversaturated in the groundwater in all hydrologic units, and may be potential contenders for future CO_2 sequestration research. Although nahcolite was undersaturated in the sampled groundwater, the deposit is well documented and poses as another possible mineral trap.

Silicate SI Trends

The cross sections for albite, K-spar, and analcime (Figure 50) are very similar to each other. The trend across the basin (east-west) is similar for each aquifer unit; SI values tend to decrease towards the basin center, where the lower aquifer samples rapidly increase to oversaturation, and the surface samples and upper aquifer samples tend to continue to decrease in the basin center. Almost all values for albite and K-spar are oversaturated while analcime has the greatest number of samples in equilibrium (most prevalent in surface samples). Analcime is a secondary mineral formed from the weathering of volcaniclastics. As volcaniclastics sediments are common in the Uinta Formation, waters in these upper units should be closest to equilibrium with analcime. Along the south-north transect (A-A'), a trend is difficult to discern. However, it should be noted that samples in the lower aquifer are most influenced by the intersection of the Piceance Creek, and demonstrate a rapid increase in SI values. North of the creek, lower aquifer sample analcime SI values decrease. Surface samples

and upper aquifer samples along this transect do not appear to be affected by the faults or creek interaction.

Quartz has a very high energy of activation and tends to be oversaturated in natural waters. In all hydrologic units, quartz is generally oversaturated (Figure 47) with the exception of the lower aquifer. Some points in the lower aquifer are in equilibrium with quartz and in the north, a sample point is undersaturated with respect to this mineral. Quartz and other silica dioxides' solubility are very dependent on temperature (solubility increases with temperature) and pH (once at 8, the solubility increases rapidly with small increases in pH). Based on the determined flow paths, it appears equilibrium for quartz was reached along the longest flow path and had the time, temperature, and pH to reach equilibrium in the north. In the lower aquifer, pH values are generally over 8 and temperatures greater than 16˚C. Groundwater is in equilibrium with chalcedony for most samples in the lower aquifer and some in the upper aquifer, making chalcedony is the dominant silica-oxide phase in the system, except at the deep zone in the north where quartz is the controlling phase.

Cole and Picard (1978) found albite, K-feldspar, and analcime are rare to abundant in the Green River Formation and Poole (2014) found these minerals increase near the upper zone of the Green River Formation. The results from this study agree, with very few samples being undersaturated and an overall increase in saturation for K-spar in the upper aquifer. With the consideration of silica phases other than quartz, the results agree with Poole's and Cole and Picard's findings of common to abundant quartz. In the Uinta Formation, Day et al. (2010)

mentioned the presence of quartz, feldspar, calcite and analcime. Results from this study concur with this finding; groundwater is generally in equilibrium to oversaturated with respect to feldspar, calcite, and analcime minerals.

CHAPTER 4 – CONCLUSION

Conclusions and Conceptual Model

Groundwater chemistry in the Piceance Creek Basin ranges from calcium-magnesium-sulfate to sodium-bicarbonate type water. Shallow surface water in recharge zones are characterized by mixed cations and bicarbonate and sulfate anions. The lower aquifer waters are primarily sodium-bicarbonate type and the upper aquifer represents a mix of water types between the two. Many processes contribute to the geochemical distribution of ions in the basin, i.e. groundwater flow paths and mixing zones, stratified sedimentary units and mineral abundance, cation exchange, and sulfur redox. However, some processes are more influential. Surface water and upper aquifer groundwater starts as bicarbonate dominant and evolves to bicarbonate and sulfate dominant. The source of sulfate is speculative, but may be partly due to the dissolution of sulfate-bearing carbonates. Lower aquifer waters are principally controlled by nahcolite dissolution from the underlying saline zone. Processes such as sulfate reduction and cation exchange contribute to the overall sodium-bicarbonate water type, but the mineral abundance and solubility of nahcolite is most influential.

These processes explain the depth dependence of dominant anion occurrence in the basin as well as observations from the margin to the basin center, but in the northern regions, at the discharge point of Piceance Creek,

upwelling of lower aquifer waters are the most influential factor for water composition. Upward movement of lower aquifer water via permeation through the Mahogany Zone aquitard or through preferential fault pathways, such as Alkali Flats fault, carries the highest concentrations of sodium and bicarbonate in the basin to the upper aquifer and surface. These high concentrations dominate the water composition in the upper aquifer and surface. An illustration of these mechanisms and their geospatial significance can be found in Figure 51.

Minerals in the basin vary significantly geospatially. The spatial trends observed in the mineral SI distribution maps and the cross sections for the lower aquifer are overall in agreement with the observations presented by Poole (2014) and Cole and Picard (1978) except for the hypersaline minerals, nahcolite and halite. Although these mineral deposits are present in the basin center, the water chemistry is highly undersaturated with the largest SI values being -0.47 and -2.82, respectfully. However, this discrepancy is likely due to the lack of permeability of the saline layer and sample depths.

Saturation indicies results for carbonate minerals in the lower aquifer show ankerite as the dominant carbonate mineral. Cole and Picard (1978) concluded it to be dolomite, but as the mole fraction of iron used to estimate the ankerite solubility product in this study is near that of a ferroan dolomite, it may very well be in agreement. Other carbonates in the basin tend to be oversaturated. This is likely due to a combination of kinetics, mineral equilibrium sequences, and presence of organic matter.

The sequence of minerals equilibrated in the groundwater can play an important role that is observed in surface samples. Previous studies have demonstrated that organic complexation can inhibit calcium carbonate precipitation. This may be the case in the lower aquifer and possibly in the lower zones of the upper aquifer leading to oversaturated waters. Organic matter can also affect the carbonate activity calculation which does not differentiate between carbonate alkalinities and organic acids. This can result in overestimated carbonate values and oversaturated waters. High oversaturation of carbonate minerals is common in the basin center. This may be influenced by groundwater permeating through the organic-rich Mahogany Zone and increasing the effects of organic matter on the water saturation. A conceptual diagram displaying general trends in carbonate saturation is shown in Figure 52. Sampling bias and field measurements of pH are also likely contributors to oversaturated carbonate sample results and should be explored further in future work.

Albite, K-feldspar, and analcime are generally in equilibrium to oversaturated in the basin, which concurs with conclusions from Poole (2014), Day et al. (2010), and Cole and Picard (1978) that these minerals are present in varying quantities throughout the basin. Quartz is oversaturated in all hydrologic units except for some regions in the lower aquifer. At these points, the temperature, pH, and residence time of the water are great enough to achieve equilibrium. Other silica dioxide phases reached equilibrium in a greater number of samples. Chalcedony was found to be in equilibrium in regions where the temperature was above 16˚C and pH >8.

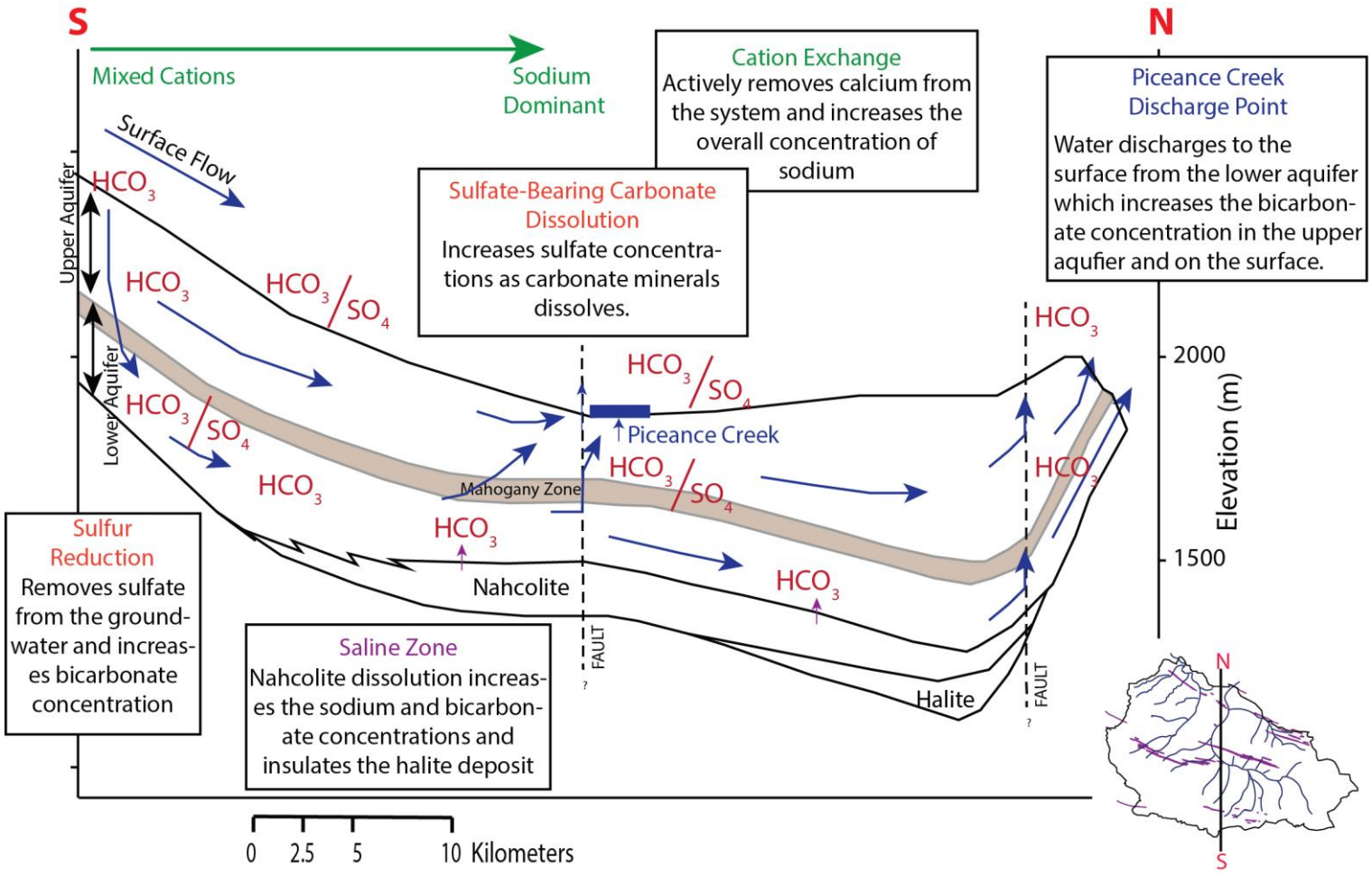

Figure 51. Conceptual cross section of the Piceance Creek Basin illustrating the spatial controls on ion variations. The diagram starts in the south at the basin margin and ends in the north at the discharge point where Piceance Creek meets White River.

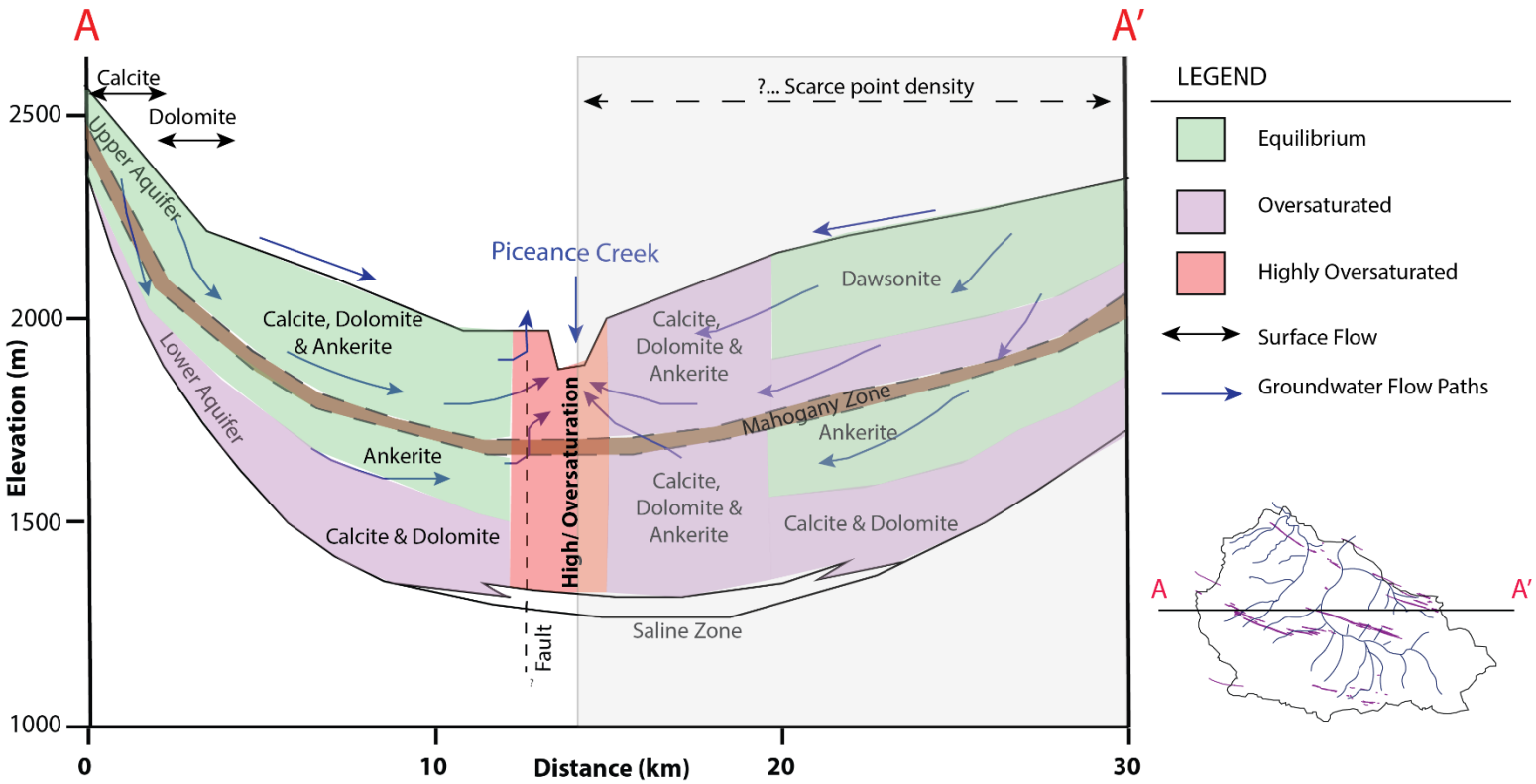

Figure 52. Conceptual cross section of carbonate mineral equilibriums in the Piceance Creek Basin. The cross section goes west to east. Green sections indicate groundwater is in equilibrium with the labeled mineral(s), purple indicates oversaturation, and in the red zone, all carbonate minerals are highly oversaturated. Surface flow is denoted at the top with double-sided arrows showing approximate locations of equilibrium carbonates.

Future Work

There are still many data and unexplored observations that should be addressed in future work. Future work on the project should consider 1) trace element data. Trace element data was largely overlooked in this project and should be further investigated in terms of ion concentration distribution trends, but also its influence on mineral saturation. Particularly arsenic, mercury, selenium, boron, and chromium should be investigated as these elements are regulated and known to have adverse health effects on humans and animals above certain concentrations. Bromine should also be considered as chloride-bromide ratios are useful in reconstructing the origin and movement of groundwater; 2) field sampling to eliminate data gaps. Additional groundwater sampling should be conducted to increase the coverage of data points in the upper and lower aquifer and missing parameters, such as redox potential (pe), accurate pH measurements using flow-cells, and isotope data. Redox potential measurements are key to evaluating redox environments, reactions, and for accurate speciation of redox elements. Accurate pH measurements are essential to SI calculations for carbonate minerals and carbon-14 isotopes could help refine flow paths by age/residence times.

Works Cited

Antweiler, R.C., and Taylor, H.E., 2008, Evaluation of statistical treatments of left-censored environmental data using coincident uncensored data sets: Environmental Science and Technology, v. 42, no. 10, pgs. 3732-3738.

Appelo, C.A.J, Postma, D., 2010, Geochemistry, groundwater and pollution, second edition: CRC press.

Bartos, T.T, and Ogle, K.M., 2002, Water quality and environmental isotopic analyses of ground-water samples collected from the Wasatch and Fort Union Formations in areas of coalbed methane development - implications to recharge and ground-water flow, eastern powder river basin, Wyoming: U.S. Geological Survey Water-Resources Investigations, Report 02-4045.

Birdwell, J.E., Mercier, T.J., Johnson, R.C., and Brownfield, M.E., 2013, In-place oil shale resources examined by grade in the major basins of the Green River Formation, Colorado, Utah, and Wyoming: U.S. Geological Society Fact Sheet 2012-3145, pub. January 2013.

Box, C.E.P., and Cox, D.R., 1964, An Analysis of Transformations: Journal of the Royal Statistical Society, Series B, v. 26, no. 2, pgs. 211-252.

Bradley, W.H., and Eugster, H.P., 1969, Geochemistry and Paleolimnology of the Trona Deposits and Associated Authigenic Minerals of the Green River Formation of Wyoming: U.S. Geological Survey Professional Paper, 496-B.

Brown, J.D., 2009, Choosing the right type of rotation in PCA and EFA: JALT Testing & Evaluation SIG Newsletter, vol. 13(3), p. 20-25.

Chave, K., and Seuss, E., 1970, Calcium carbonate supersaturation in seawater: Effects of dissolved organic matter: Limnol. Oceanography, vol. 15, pgs. 633 - 637.

Chebotarev, I. I., 1955, Metamorphism of natural waters in the crust of weathering: Geochimica et Cosmochimica Acta, v. 8, pgs. 22-48, 137-170, 198-212.

Chia, L., and Navrotsky, A., 1996, Synthesis, characterization, and energetics of solid solution along the dolomite-ankerite join, and implications for the stability of ordered $CaFe(CO_3)_2$: American Mineralogist, v. 81, pgs. 1141-1147.

Childs, C., 2004, Interpolating surfaces in ArcGIS Spatial Analyst: ArcUser Developers Corner, July-September, pgs. 32-35.

Coffin, D.L, Welder, F.A., and Glanzman, R.K., 1971, Geohydrology of the Piceance Creek structural basin between the White and Colorado Rivers, northwestern Colorado: U.S. Geological Survey Hydrologic Investigations Atlas HA-370.

Cole, R.D., and Picard, M.D., 1978, Comparative mineralogy of nearshore and offshore lacustrine lithofacies, Parachute Creek Member of the Green

River Formation, Piceance Creek Basin, Colorado, and eastern Uinta Basin, Utah: Geological Society of America Bulletin, v. 89, p. 1441-1454.
Davidson, P.M., Symmes, G.H., Cohen, B.A.., Reeder, R.J., and Lindsley, D.H., 1993, Synthesis of the new compound $CaFe(CO_3)_2$ and experimental constraints on the $(Ca,Fe)CO_3$ join: Geochimica et Cosmochimica Acta, v. 57, pgs. 5101-5109.
Day, M., Hansen, E., Gulliver, T., and Mckinzie, B., 2010, Northwest Piceance Creek Basin Hydrogeology: 30th Oil Shale Symposium, Colorado School of Mines.
Deng, S., Dong, H., Lv, G., Jiang, H., Yu, B., and Bishop, M.E., 2010, Microbial dolomite precipitation using sulfate reducing and halophilic bacteria: Results from Qinghai Lake, Tibetan Plateau, NW China: Chemical Geology, v. 287, pgs. 151-159.
Desborough, G.A., 1978, A biogenic-chemical stratified lake model for the origin of oil shale of the Green River Formation: An alternative to the playa-lake model: Geological Society of America Bulletin, v. 89, p. 961-971.
Deutsch, W.J., 1997, Groundwater Geochemistry: Fundamentals and Applications to Contamination: Lewis Publishers, New York.
Donnel, J.R., 1961, Tertiary geology and oil-shale resources of the Piceance Creek Basin, between the Colorado and White Rivers, Northwestern Colorado: US Government Printing Office, no. 1082.
Dyni, J.R., 2005, Geology and resources of some world oil-shale deposits: U.S. Geological Survey Scientific Investigations Report 2005-5294.
Dyni, J.R., 2003, Geology and resources of some world oil-shale deposits: U.S. Geological Survey Scientific Investigations Report 2003-5294.
Energy Information Administration, 2013, Technically recoverable shale oil and shale gas resources: An assessment of 137 shale formations and 41 countries outside the United States: U.S. Department of Energy.
Energy Information Administration, 2006, Annual Energy Outlook 2006 with Projections to 2030: Office of Integrated Analysis and Forecasting U.S. Department of Energy.
Environmental Protection Agency, 2015, U.S. EPA national primary drinking water regulations: https://www.gvsu.edu/cms3/assets/6BDDB6FE-EF92-1DFF-13B97ABEB2F2651C/lowgrand_wit/standards.pdf (accessed September 2015)
Environmental Protection Agency, 1977, Trace elements associated with oil shale and its processing: EPA-908/4-78-003.
Eugster, H.P., and Surdam, R.C., 1973, Depositional Environment of the Green River Formation of Wyoming: A Preliminary Report: Geological Society of America Bulletin, v. 84, p. 1115-1120.
Evans, J.D., 1996, Straightforward statistics for the behavioral sciences: Brooks/Cole Publishing, Pacific Grove, CA.
Flaathen, T.K., Oelkers, E.H., Gislason, S.R., and Aagaard, P., 2011, The effect of dissolved sulphate on calcite precipitation kinetics and consequences

for subsurface CO_2 storage: Energy Procedia, vol. 4 (2011), pgs. 5037-5043.
Folk, R.L., and Land, L.S., 1975, Mg/Ca ratio and salinty: two controls over crystallization of dolomite: AAPG bulletin, v. 59(1), pgs. 60-68.
Freeze, R.A., and Cherry, J.A., 1979, Groundwater: Chemical evolution of natural groundwater: Prentice-Hall, Inc. publication [London], p. 237-297.
Giang Luu, T.T., Sthiannopkao, S., and Kim, K.W., 2009, Arsenic and other trace elements contamination in groundwater and a risk assessment study for the residents in the Kandal Province of Cambodia: Environmental International, v. 35, pgs. 455-460.
Giere, R., and Stille, P. (ed), 2004, Energy, waste and the environment: a geochemical perspective: London Geological Society Special Publication, no. 236, pg. 179.
Goldsmith, J.R., Graf, D.L., Witters, J., and Northrop, D.A., 1962, Studies in the system $CaCO_3$-$MgCO_3$-$FeCO_3$: 1. Phase relations; 2. A method from major-element spectrochemical analysis: 3. Compositions of some ferroan dolomites: Journal of Geology, v. 70, pgs. 659-688.
Grubbs, F.E., 1969, Procedures for detecting outlying observations in samples: American Society for Quality, Technometrics, v. 11, no. 1, pgs. 1-21.
Glynn, P.D., and Reardon, E.J., 1990, Solid-solution aqueous-solution equilibria: Thermodynamic theory and representation: American Journal of Science, v. 290, pgs. 164-201.
Jenks, G.F., 1967, The data model concept in statistical mapping: International Yearbook of Cartography, v. 7, pgs. 186-190.
Johnson, R.C., Mercier, T.J., Brownfield, M.E., Pantea, M.P., and Self, J.G., 2010, An Assessment of in-place oil shale resources in the Green River Formation, Piceance Basin, Colorado. Chapter 1 of 7, Oil Shale and Nacholite Resources of the Piceance Basin, Colorado, U.S. Geological Survey Digital Data Series DDS–69–Y.
Johnson, R.L., Homquist, D., Redding, K., and McDaniel, C., 2015, Water Quality with Vernier: Vernier Software and Technology Lab Book, ch. 15-1, 15-2.
Kampschulte, A., and Strauss, H., 2004, The sulfur isotopic evolution of Phanerozoic seawater based on the analysis of structurally substituted sulfate in carbonates: Chemical Geology, v. 204, pgs. 255-286.
Li, J., and Heap, A.D., 2008, A review of spatial interpolation methods for environmental scientists: Geoscience Australia, no. 23, GeoCat no. 68229.
Lin, Y., Singer, P.C., and Aiken, G.R., 2005, Inhibition of calcite precipitation by natural organic material: kinetics, mechanism, and thermodynamics: Environmental Science and Technology, vol. 39, no 17, pgs. 6420 - 6428.
Müller, G., Irion, G.E.O.R.G., and Förstner, U., 1972, Formation and diagenesis of inorganic Ca- Mg carbonates in the lacustrine environment: Naturwissenschaften v. 59(4), pgs. 158-164.

Olivie-Laquet, G., Gruau, G., Dia, A., Riou, C., Jaffrezic, A., and Henin, O., 2000, Release of trace elements in wetlands: role of seasonal variability: Water Resources, v. 35, no. 4, p. 943-952.

Palmer, C.D., 2015, Reservoir temperature estimator (RTEst) user's manual. IN: Mattson, E.D., Smith, R.W., Neupane, G., Palmer, D.D., Fujita, Y., McLing, T.L., Reed, D.W., Cooper, C., and Thompson, V.S., 2015, Improved geothermometry through multivariate reaction-path modeling and evaluation of geomicrobiological influences on geochemical temperature indicators: Idaho National Laboratory, INL/EXT-14-33959.

Palmer, C.D., Mattson, E.D., and Perkins, R.B., 2010, Aqueous and mineralogical changes during hydrous oil shale retorting: 2010 Annual Meeting of The Geological Society of America, Denver.

Palmer, C.D., Mattson, E.D., Perkins, R.B., Plummer, M., and Wood, T., 2009, Spatial distribution of geochemical changes about an oil shale retort: *29th Oil Shale Symposium*, Golden, CO.

Parkhurst, D.L., and Appelo, C.A.J., 2013, Description of input and examples for PHREEQC version 3--A computer program for speciation, batch- reaction, one-dimensional transport, and inverse geochemical calculations: U.S. Geological Survey Techniques and Methods, book 6, chap. A43, pg. 497, http://pubs.usgs.gov/tm/06/a43.

Perkins, R.B., Grathoff, G.H., Palmer, C.D., and Mattson, E.D, 2008, Mineralogical changes in oil shale from hydrous retorting: 18th Annual Goldschmidt Conference, Vancouver, B.C. Oral presentation. *Geochimica et Cosmochimica Acta*, 72, A737.

Pham, V.T.H., Aagard, P., and Hellevang, H., 2012, On the potential for CO_2 mineral storage in continental flood basalts – PHREEQC batch- and 1D diffusion-reaction simulations: Geochemical Transactions, 13:5.

Pham, V.T.H., Lu, P., Aagard, P., Zhu, C., and Hellevang, H., 2011, On the potential of CO_2-water-rock interactions for CO_2 storage using a modified kinetic model: International Journal of Greenhouse Gas Control, 1002-1015.

Pingitore, N.E., Meitzner, G., and Love, K.M., 1995, Identification of sulfate in natural carbonates by x-ray absorption spectroscopy: Geochimica et Cosmochimica Acta, v. 59, pgs. 2477-2483.

Piper, A.M, 1944, A graphic procedure in the geochemical interpretation of water-analyses: EOS, Transactions American Geophysical Union, vol. 25(6), pgs. 914-928.

Poole, S., 2014, Quantitative mineralogy and distributions of minerals of the Green River Formation, Piceance Creek Basin, Western Colorado: Colorado School of Mines, Master of Science thesis.

Robinson, B., Bolan, N., Mahimairaja, S., and Brent, C., 2006, Solubility, mobility and bioaccumulation of trace elements: abiotic processes in the rhizophere: Trace Elements in the Environment, p. 97-110.

Robson, S.G., and Saulnier, G.J., 1981, Hydrogeochemistry and simulated solute transport, Piceance Basin, northwestern Colorado: U.S. Geological Survey Professional Paper 1196.

Sanborn, A.F., 1977, Possible future petroleum of Uinta and Piceance Basin and vicinity northeast Utah and northwest Colorado: Rocky Mountain Association of Geologist, symposium proceedings, p. 151 – 166.

Scott, R.A., Smyth, H.R., Morton, A.C., and Richardson, N. (ed), 2014, Sediment provenance studies in hydrocarbon exploration and production: London Geological Society Special Publication, no. 386, pg. 56.

Smedley, P.L., and Kinniburgh, D.G., 2001, A review of the source, behavior and distribution of arsenic in natural waters: Applied Geochemistry, v. 17 (2002), p. 517-568.

Smith, E.M., Carroll, A.R., and Singer, B.S., 2008, Synoptic reconstruction of a major ancient lake system: Eocene Green River Formation, western United States: Geological Society of America Bulletin, v. 120, p. 54-84.

Stumm, G.W., Laaksuharju, M., Nilsson, A.C., and Wikberg, P., 1992, Redox potentials and redox reactions in deep groundwater systems: Chemical Geology, v. 98, pgs. 131-150.

Tanavsuu-Milkeviciene, K., and Sarg, J.F., 2012, Evolution of an organic-rich lake basin - stratigraphy, climate and tectonics: Piceance Creek basin, Eocene Green River Formation: Journal of the International Association of Sedimentologists, v. 59, p. 1735-1768.

Taylor, J.O., 1987, Oil shale, water resources, and valuable minerals of the Piceance Basin, Colorado: The challenge and choices of development: U.S. Geological Survey Professional Paper, no. 1310.

Thomas, J.C., and McMahon, P.B., 2012, Overview of groundwater quality in the Piceance Basin, Western Colorado: U.S. Geological Survey Scientific Investigations Report 2012-5198.

Thurstone, L.L., 1947, Multiple factor analysis: a development and expansion of vectors of the mind: University of Chicago.

Tuttle, M.L., Dean, W.E., and Parduhn, N.L., 1983, Major and trace elements in the Mahogany Zone oil shale in two cores from the Green River Formation, Piceance Basin, Colorado: Symposium of Geochemistry and chemistry of oil shale presented before The Division of Fuel Chemistry, Geochemistry and Petroleum Chemistry, Inc., American Chemical Society, March 20-25, 1983.

Tuttle, M.L, 1973, Geochemical, biogeochemical, and sedimentological studies of the Green River Formation, Wyoming, Utah, and Colorado: U.S. Geological Survey Bulletin, 1973-A-G.

U.S. Geological Survey, 2015, The National Map, data download and visualization services: http://viewer.nationalmap.gov/launch/ (accessed June 2015).

U.S. Geological Survey, 2009, Piceance Basin Water-Quality Data Repository: http://rmgsc.cr.usgs.gov/cwqdr/Piceance/data.shtml (accessed October 2013).

U.S. Geological Survey, 2000, GW_Chart (Version 1.29.0.0): http://water.usgs.gov/nrp/gwsoftware/GW_Chart/GW_Chart.html (accessed June 2015).

Van Lith, Y., Warthmann, R., Vasconcelos, C., and McKenzie, J.A., 2003, Sulphate-reducing bacteria induce low-temperature Ca-dolomite and high Mg-calcite formation: Geobiology, v. 1, pgs. 71-79.

Weeks, J.B., Leavesley, G.H., Welder, F.A., and Saulnier, G.J., 1974, Simulated Effects of Oil-Shale development on the Hydrology of Piceance Basin, Colorado: U.S. Geological Survey Professional Paper, v. 908, p. 1-24.

Welch, A.H., 2001, Arsenic cycling in ground water – Processess leading to widespread high concentrations: In Arsenic in the Asia Pacific Region, Adelaide, Australia, p. 89-90.

Wenk, H.R., Meisheng, H., Lindsey, T., and Morris, J.W., 1991, Superstructures in ankerite and calcite: Physics and chemistry of minerals, v. 17(6), pgs. 527-539.

Woods, T.L., and Garrels, R.M., 1992, Calculated aqueous-soultion-solid-soultion reactions in the low-temperature system CaO-MgO-FeO-CO_2-H_2O: Geochimica et Cosmochimica Acta, 56(8), pgs. 3031-3043.

APPENDIX A: DATABASE SUPPLEMENTAL TABLES

Summary of the data contributors to the Piceance Basin Data Repository

Agency Name	Sites	Date Range	
Antero Resources	159	7/12/2005	7/16/2009
Colorado Department of Agriculture	43	3/31/1998	10/26/2000
City of Grand Junction	3	6/22/1988	10/28/2008
Wright Water Engineeres, Inc., CO	15	4/26/2002	7/17/2002
Colorado Oil and Gas Conservation Commission	1,048	4/2/1956	10/14/2008
EnCana Oil and Gas (USA) Inc.	496	5/4/2001	4/13/2009
Mine Consultant	24	8/10/1995	12/6/2006
Occidental Petroleum Company	22	6/17/2009	4/30/2009
Town of Palisade (via Western Water and Land)	17	5/21/2007	10/22/2008
U.S. Forest Service	1	9/27/2006	6/27/2007
U.S. Geological Survey	1,456	7/16/1946	4/27/2009
U.S. National Park Service	1	4/18/2001	11/5/2001
William Production RMT Company	12	4/26/2002	7/17/2002

Results for statistical hypothesis tests comparing ion concentrations collected by different agencies.

	USGS/ENCANA		USGS/COGCC		ENCANA/COGCC	
	Test	H	Test	H	Test	H
Temp	TTEST	0				
pH	MW	0	MW	0	MW	0
Calcium	MW	0				
Magnesium	MW	0				
Sodium	TTEST	0				
Potassium	MW	0				
Chloride	MW	0	TTEST	0	MW	1
Sulfate	TTEST	0	MW	1	MW	0

H values calculated with an alpha value = 0.5

Results for statistical hypothesis tests comparing ion concentrations collected during different decades.

	70s/80s		70s/00s		80s/00s	
	Test	H	Test	H	Test	H
Temp	MW	1	MW	0	MW	0
pH	MW	0	MW	0	MW	0
Calcium	MW	1	MW	0	MW	1
Magnesium	TTEST	1	MW	0	MW	0
Sodium	MW	0	MW	0	MW	0
Potassium	MW	0	MW	0	MW	0
Chloride	TTEST	0	MW	1	MW	1
Sulfate	TTEST	1	MW	0	MW	0
Alkalinity	MW	0	MW	1	MW	1

H values calculated with an alpha value = 0.5

Results for statistical hypothesis tests comparing ion concentrations collected during different season.

	Summer/Winter	
	Test	H
Temp	TTEST	1
pH	TTEST	1
Calcium	TTEST	1
Magnesium	TTEST	1
Sodium	TTEST	0
Potassium	TTEST	0
Chloride	TTEST	0
Iron	TTEST	0
Sulfate	TTEST	0
Alkalinity	TTEST	0

H values calculated with an alpha value = 0.5
Summer was defined as samples collected between May and September.
Winter was defined as samples collected between November and March.

Results for statistical hypothesis tests comparing ion concentrations collected during different seasons and by aquifer.

	Surface Summer/Winter		Upper Aquifer Summer/Winter		Lower Aquifer Summer/Winter	
	Test	H	Test	H	Test	H
Temp	MW	1	MW	0	MW	0
pH	MW	1	MW	0	MW	0
Calcium	MW	1	MW	0	MW	0
Magnesium	MW	1	MW	0	MW	0

H values calculated with an alpha value = 0.5
Summer was defined as samples collected between May and September.
Winter was defined as samples collected between November and March.

APPENDIX B: DETAILS OF STATSTICAL METHODS

All statistical analysis was performed in Matlab Version R2011a

```
% Megan Masterson
% PCA & Factor Analysis of AOI major ion data. Outliers
were removed prior to this analysis and mineral
concentrations converted to z-scores.
clc; clear all; close all;

% Load data
load 'elementTable_MajorTrace_NoSpecCond_wAl.mat';

%% Remove unused columns for analysis
original = major
major = major(:, (4:end));
trace = trace(:, (4:end));

%Change to common units of mg/L
for i = 14:size(trace,2)
    trace(:,i) = trace(:,i)*0.001;
end

figure (1)
boxplot(major, 'orientation', 'horizontal', 'labels',
{'Depth', 'Alk' 'Ca'...
    'Cl', 'K', 'Mg', 'Na', 'pH', 'Sulfate', 'Temp'})

%% - PCA - %%
% standardize data
major_std = std(major);
major_sr = major./repmat(major_std, size(major,1), 1);

[COEFF,SCORE, latent, t2] = princomp(major_sr);
% COEFF - known as "loadings" The largest coefficients in
the first column are associated with the position of the
variables.  For example, (1,1) = X while (4,1) = Depth

%SCORE - contains the coordinates of the original data in
the new coordinate system.  A plot of the first two columns
```

```
of scores shows the major data projected onto the first two
principal components:
figure (2)
plot(SCORE(:,1), SCORE(:,2), '+')
xlabel ('1st Principal Component')
ylabel ('2nd Principal Component')

% LATENT - AKA "variances" - a vector containing the
variance explained by the corresponding PC.  Each column of
scores as a sample variance equal to the corresponding
element of variances.  You can easily calculate the percent
of the total variability explained by each PC
cumlat = cumsum(latent)./sum(latent);
percent_explained = 100*latent/sum(latent);
percent_explained

figure (3)
pareto(percent_explained)
xlabel('Prinicipal Component')
ylabel('Variance Explained (%)')
title ('Major Data')

%% - Factor Analaysis - %%
[Loadings, specificVar, T, stats, F]=factoran(major, 3);
Loadings;
specificVar;

% - Factor Rotation - %
[LoadingsPM, specVarPM, TPM, statsPM, FPM] =
factoran(major, 3, 'rotate', 'varimax');
FPM;  %Factor Scores

%% Correlation table
majorcorr = corr(major);
```

Factor Scores from Factor Analysis

SiteID	Factor1	Factor 2	Factor 3	SiteID	Factor1	Factor 2	Factor 3
200253	-0.321	-1.544	-1.043	200749	-0.2841	-1.3253	-0.7378
200285	-0.201	-1.456	-0.353	200753	-0.1665	-0.5128	0.5711
200286	-0.224	-1.102	-0.196	200756	-0.2872	-1.1861	-0.6137
200295	-0.201	-0.843	0.255	200758	-0.1932	-0.5866	0.3755
200321	-0.417	-1.479	-1.524	200763	-0.3002	-0.9601	-0.6254
200336	-0.374	-1.569	-1.293	200769	-0.1989	-0.5687	0.4084
200358	-0.433	-1.361	-1.532	200781	-0.2419	-0.6307	0.0864
200360	-0.449	-1.030	-1.459	200784	-0.2766	-0.6807	0.2884
200369	-0.389	-1.586	-1.415	200786	-0.2184	-0.4905	0.3663
200374	-0.421	-1.403	-1.384	200787	-0.2114	-0.7620	0.2184
200378	-0.151	-1.028	0.237	200790	-0.1653	-0.9206	0.2011
200392	-0.126	-0.931	0.521	200792	-0.1776	-0.8450	0.1726
200399	-0.065	-0.812	0.860	200795	-0.1410	-1.0229	0.2613
200400	-0.065	-0.812	0.860	200806	-0.1547	1.2823	-0.8790
200417	0.085	-0.527	1.710	200808	-0.3431	-1.1615	-0.9614
200420	-0.049	-0.717	1.107	200817	-0.2829	-0.7980	-0.6364
200425	-0.475	1.364	0.167	200818	-0.2829	-0.7980	-0.6364
200436	-0.299	-1.188	-0.622	200820	-0.2924	-0.9866	-0.6895
200437	-0.201	-0.830	0.157	200825	-0.2916	-1.0092	-0.7003
200444	-0.301	1.173	0.746	200826	-0.3084	-1.0985	-0.7023
200445	0.653	1.158	-0.728	200832	-0.4046	-0.8324	-0.9970
200446	1.444	1.110	-0.792	200836	-0.5013	0.2439	-1.0219
200451	-0.338	-1.033	-0.779	200841	-0.3165	-1.0159	-0.7772
200452	-0.583	1.436	-0.779	200851	-0.3562	-0.7648	-0.7516
200453	-0.557	1.434	-0.816	200856	-0.4274	0.4112	-0.3059
200460	0.018	-0.387	1.725	200863	-0.4888	2.3122	-0.3465

Factor Scores from Factor Analysis

SiteID	Factor1	Factor 2	Factor 3	SiteID	Factor1	Factor 2	Factor 3
200465	-0.210	-0.985	0.055	200935	-0.3486	-0.7595	-0.5697
200464	-0.256	-0.896	-0.173	200872	-0.3726	-0.8175	-0.7819
200466	-0.115	-0.013	0.395	200989	-0.4559	-0.9728	-1.3458
200473	-0.150	-1.002	0.208	350101	-0.6594	2.7744	-0.0748
200475	-0.563	2.304	0.051	350601	-0.2343	0.0527	0.3081
200476	-0.429	1.356	-0.835	350602	-0.2324	0.1099	0.2841
200480	-0.187	-0.841	0.260	350603	-0.4332	0.7527	-0.0364
200482	-0.261	-0.509	0.156	350701	-0.2115	0.9807	-0.6244
200484	-0.137	-0.949	0.431	350702	-0.0727	-0.2748	1.2018
200488	-0.243	0.022	0.503	350703	-0.4814	0.7981	-0.4149
200489	-0.527	1.237	-0.451	350704	-0.4969	1.0834	-0.2620
200492	0.283	0.606	3.315	351201	-0.0489	0.8039	-1.0981
200493	0.283	0.606	3.315	351202	0.4100	1.1790	-0.8337
200498	-0.284	-1.061	-0.388	351203	-0.3841	0.9769	0.1233
200500	-0.491	1.647	-0.033	351204	1.9584	1.6654	-0.4423
200501	-0.510	1.835	0.021	351301	-0.4750	1.1793	-0.6767
200502	-0.463	1.555	-0.784	351302	-0.4837	0.9598	-0.6873
200503	0.225	0.268	3.302	351303	-0.4902	1.0785	-0.7177
200504	-0.298	0.767	0.536	351601	-0.1773	2.1543	-0.2818
200511	-0.115	-0.828	0.622	351602	-0.3494	1.5171	-0.7011
200516	-0.352	-1.140	-0.921	351603	-0.4154	1.3777	-0.8010
200518	-0.040	-0.663	1.085	351701	-0.2997	1.7295	-0.5310
200521	-0.086	-0.834	0.779	351702	-0.2210	0.5556	-1.1498
200527	-0.002	-0.724	1.296	351703	-0.1822	1.3957	-0.7875
200529	-0.001	0.656	-1.070	351901	-0.5266	1.2523	-0.4523
200530	-0.196	1.019	-0.967	351902	-0.5386	1.1109	-0.2976
200532	-0.083	-0.981	0.683	351903	-0.5845	1.3359	-0.8436

Factor Scores from Factor Analysis

SiteID	Factor1	Factor 2	Factor 3	SiteID	Factor1	Factor 2	Factor 3
200535	-0.031	-0.633	1.141	352901	0.3367	1.5996	-0.6447
200553	-0.064	-1.074	0.766	353001	-0.4876	0.3641	-1.2793
200552	0.340	0.437	4.161	352902	0.2953	2.1979	-0.3749
200562	-0.011	-0.954	1.107	353002	-0.4385	0.4284	-1.2698
200566	0.125	-0.444	2.272	353003	-0.4774	1.0509	-0.9797
200567	-0.397	0.837	-1.027	353101	2.2041	-0.1673	-0.9568
200568	-0.273	-0.513	-1.186	353102	5.9129	-0.3438	-0.6218
200571	-0.273	-0.513	-1.186	353103	6.3152	0.1902	-0.2871
200573	-0.024	-0.437	1.337	355301	0.0896	2.4447	0.4201
200574	-0.451	-1.500	-1.732	355302	0.1051	1.4836	-0.1997
200580	-0.305	0.692	0.300	355303	-0.3141	1.4905	0.6069
200583	1.998	-0.008	-1.163	355304	-0.1023	0.8942	1.7533
200584	-0.333	-1.295	-0.994	355401	1.1029	1.2583	-0.3780
200585	-0.332	-1.028	-0.915	355402	1.2917	0.8555	-0.7212
200589	-0.340	-1.126	-0.867	355403	-0.4027	0.5454	-0.0943
200590	-0.319	-1.057	-0.730	355404	-0.3929	0.4844	-0.0246
200593	-0.372	-1.191	-1.137	355501	0.1842	2.4106	0.0311
200594	-0.327	-0.922	-0.597	355502	0.3865	2.0384	-0.1039
200599	-0.020	-0.779	1.179	355503	-0.1266	1.2165	0.2889
200601	-0.219	-1.255	-0.336	355504	-0.2778	0.9619	0.9202
200606	-0.204	-1.185	-0.190	355505	-0.3110	1.1680	0.8719
200609	-0.216	-1.004	-0.131	356101	-0.0668	-0.2007	1.2925
200610	-0.209	-1.100	-0.120	356102	-0.0722	-0.3698	1.1618
200612	-0.319	1.332	0.820	356201	-0.0125	0.0662	1.9016
200613	-0.643	3.455	0.450	356202	-0.0278	-0.3885	1.4226
200614	2.462	-0.215	-0.282	356301	0.0240	-0.0486	1.4754
200621	7.969	-1.069	-0.577	356302	-0.2897	-0.6895	-0.3344

Factor Scores from Factor Analysis

SiteID	Factor1	Factor 2	Factor 3	SiteID	Factor1	Factor 2	Factor 3
200629	-0.232	-0.232	0.456	356401	-0.3334	-0.5456	-0.2894
200630	-0.199	-0.930	0.069	356501	-0.2245	-0.2432	0.4999
200641	-0.154	-0.785	0.407	356702	2.0498	-0.6944	-1.4623
200640	0.147	-0.136	1.581	356701	0.8810	0.3806	-1.1692
200650	-0.225	-1.037	-0.460	356801	-0.2211	0.0772	-0.2155
200651	-0.149	-0.775	0.437	356802	-0.1969	0.2155	0.1277
200654	-0.150	-0.594	0.545	356901	-0.2050	-0.1862	0.0790
200656	-0.143	-0.435	0.697	356902	-0.2372	0.0535	0.2457
200658	-0.142	-0.691	0.514	357101	-0.2548	0.4613	0.4137
200669	-0.332	-1.323	-0.955	357201	-0.5537	0.1606	-1.2036
200674	-0.256	-0.350	-0.694	357401	-0.3406	2.3435	-0.3169
200677	-0.182	-0.614	-0.875	357501	0.0813	-0.3025	1.7383
200687	0.738	1.904	-0.386	357901	-0.3330	-0.8762	-0.7211
200690	-0.355	1.210	-0.386	358001	3.9549	0.1724	-0.4497
200692	-0.293	-1.295	-0.752	358301	0.7860	0.1473	0.4480
200702	-0.155	1.014	1.709	358401	0.0690	0.0533	1.5358
200708	-0.127	-0.941	0.515	358601	-0.1620	-0.1130	0.5782
200725	-0.332	-1.346	-1.015	359201	0.2671	0.3671	1.1869
200731	0.059	-0.665	1.680	359301	-0.4453	-0.0294	-0.3753
200734	-0.099	-0.252	1.206	359401	0.1667	1.0413	3.6759
200746	-0.274	-0.801	-0.439	359501	0.2176	0.4210	3.4841

APPENDIX C: ANKERITE IAP CALCULATION

Ankerite IAP calculation performed in Matlab Version R2011a

```
clc;
clear all;

load 'Ank_IAP_Jan2016_wksp.mat'

%% Remove High CBE values outside of +-30
CBError = 5;

Depth = Depth(CBE <=CBError & CBE >=-CBError);
Fe = Fe(CBE <=CBError & CBE >= -CBError);
Ca = Ca(CBE <=CBError & CBE >= -CBError);
Mg = Mg(CBE <=CBError & CBE >= -CBError);
CO3 = CO3(CBE <=CBError & CBE >= -CBError);
Aquifer = Aquifer(CBE <=CBError & CBE >= -CBError);

%% Only GRF samples
Aq = 300;  %300 is for GR aquifer, 200 is Uinta, 100 is
surface
Depth = Depth(Aquifer >= Aq);
Fe = Fe(Aquifer >= Aq);
Ca = Ca(Aquifer >= Aq);
Mg = Mg(Aquifer >= Aq);
CO3 = CO3(Aquifer >= Aq);

%% Establish trials.  X is a stoichometric coefficent for
Ankerite
x = [0:0.1:0.7];

%% calulate the IAP value for each trail of x
for i = 1:length(x)  %8 col
    for j = 1:length(Fe)    %38 row
                iapx(j,i) = (Ca(j) * (Mg(j)^(1-x(i)))*
(Fe(j)^x(i))*(CO3(j)^2));
    end
end

iapx = log10(iapx);
```

```
%% calculate the frequency of each trail for plotting
num = 15;
bins = linspace(min(min(iapx)), max(max(iapx)), num);
freq = zeros(size(bins,2)-1,size(iapx,2));   % 50 x 8

for i = 1:length(bins)-1     % 49
    for j = 1:size(iapx,1)  % 731
        for k = 1:size(iapx,2)  %8
            if iapx(j,k)>= bins(i) & iapx(j,k) < bins(i+1);
                freq(i,k) = freq(i,k)+1;
            end
        end
    end
end

%% plot it up

bplot = bins(1:length(bins)-1);

figure (1)
clf
plot(bplot, freq(:,1), 'k-')
hold on;
plot(bplot, freq(:,2),  'b-')
plot(bplot, freq(:,3),  'g-')
plot(bplot, freq(:,4),  'c-')
plot(bplot, freq(:,5),  'y-')
plot(bplot, freq(:,6),  'r-')
plot(bplot, freq(:,7),  'm-')
plot(bplot, freq(:,8),  'k-o')
xlabel({'log(IAP) Ankerite';...
    'CaMg_{1-x}Fe_{x}CO_{3} + 2H = Ca + (1-x)Mg + (x)Fe +
2HCO_{3}' })
ylabel('Frequency')

histn = 8;
figure (2)
subplot(4,2,1)
histfit(iapx(:,1),histn)
xlabel ('x = 0')
ylabel ('frequency')
subplot(4,2,2)
histfit(iapx(:,2),histn)
xlabel ('x = 0.1')
```

```
ylabel ('frequency')
subplot(4,2,3)
histfit(iapx(:,3),histn)
xlabel ('x = 0.2')
ylabel ('frequency')
subplot(4,2,4)
histfit(iapx(:,4),histn)
xlabel ('x = 0.3')
ylabel ('frequency')
subplot(4,2,5)
histfit(iapx(:,5),histn)
xlabel ('x = 0.4')
ylabel ('frequency')
subplot(4,2,6)
histfit(iapx(:,6),histn)
xlabel ('x = 0.5')
ylabel ('frequency')
subplot(4,2,7)
histfit(iapx(:,7),histn)
xlabel ('x = 0.6')
ylabel ('frequency')
subplot(4,2,8)
histfit(iapx(:,8),histn)
xlabel ('x = 0.7')
ylabel ('frequency')

figure (3)
boxplot(iapx)
ylabel({'log(IAP) Ankerite'; 'CaMg_{1-x}Fe_{x}CO_{3} + 2H =
Ca + (1-x)Mg + (x)Fe + 2HCO_{3}'})
xlabel ('x index')

figure (4)
histfit(iapx(:,6), histn)
xlabel({'log(IAP) Ankerite';
'CaMg_{0.5}Fe_{0.5}(CO_{3})_{2} = 1.00Ca + (0.50)Mg +
(0.50)Fe + 2.00CO_{3}'})
ylabel('frequency')

%% Stats
stats = zeros(k, 5);
for i = 1:length(stats) %8 rows
    for j = 1:5     %5 cols
        if j == 1
    stats(i,j) = x(i);
```

```
        else if j == 2
    stats(i, j) = std(iapx(:,i));
        else if j == 3
    stats(i, j) = mean(iapx(:,i));
            else if j == 4
    stats(i, j) = mode(iapx(:,i));
                else if j == 5
    stats(i, j) = median(iapx(:,i));
                    end
                    end
                end
            end
        end
    end
end

%% Boxcox Transformation
nonneg = 10.^(iapx(:,6));
[transdat, lambda] = boxcox(nonneg);

meantrans = mean(transdat); % mean value of the boxcox
translated data
meandata = (meantrans*lambda + 1)^(1/lambda);
% return mean to regular data value
meandata = log10(meandata);  % return to a log value

figure (5)
histfit(transdat, histn)
xlabel({'log(IAP) Ankerite';
'CaMg_{0.5}Fe_{0.5}(CO_{3})_{2} = 1.00Ca + (0.50)Mg +
(0.50)Fe + 2.00CO_{3}'})
ylabel('frequency')
% at stoichiometry of 0.5 IAP = -17.9653
```

APPENDIX D: MINERAL EQUILIBRIUM WEIGHTING SCHEME

Coefficients of Variation used to calculate mineral weight

Basis Species	Coefficient of Variation
H2O	0.00
Al+++	0.15
Ba++	0.05
Ca++	0.05
Cl-	0.05
Fe++	0.05
Fe+++	0.05
H+	0.23
HCO3-	0.10
K+	0.05
Mg++	0.05
Na+	0.05
O2(aq)	0.10
SO42-	0.05
SiO2(aq)	0.05

Mineral weight and weighted saturation index

Mineral	Formula	Weight	WSI	3 x WSI	10 x WSI
Albite	NaAlSi3O8	4.66	0.21	0.64	2.15
Analcime	Na.96Al.96Si2.04O6:H2O	4.77	0.21	0.63	2.09
Ankerite	CaMg0.5Fe0.5(CO3)2	6.36	0.16	0.47	1.57
Barite	BaSO4	32.56	0.03	0.09	0.31
Calcite	CaCO3	9.00	0.11	0.33	1.11
Dawsonite	NaAlCO3(OH)2	5.23	0.19	0.57	1.91
Dolomite	CaMg(CO3)2	6.36	0.16	0.47	1.57
Gypsum	CaSO4:2H2O	32.56	0.03	0.09	0.31
K-Feldspar	KAlSi3O8	4.66	0.21	0.64	2.15
Nahcolite	NaHCO3	20.59	0.05	0.15	0.49
Quartz	SiO2	46.05	0.02	0.07	0.22
Halite	NaCl	32.56	0.03	0.09	0.31

APPENDIX E: pH CORRECTED MINERAL SAUTRATION RESULTS

Corrected pH assuming calcite equilibrium

SiteId	Aquifer	Calculated pH	Measured pH	Calculated CBE	Measured CBE
200554	Lower	13.43	8.41	-89.82	-91.45
200446	Lower	7.58	8.00	-11.87	-11.87
351302	Upper	8.07	8.40	-11.31	-11.34
358902	Upper	7.28	8.00	-4.63	-4.62
200560	Surface	7.05	8.06	-4.37	-4.41
200564	Lower	13.60	7.93	-4	-4.93
351701	Lower	7.40	8.40	-3.69	-3.71
200559	Upper	12.01	7.81	-3.34	-3.26
352902	Lower	7.67	8.20	-2.97	-2.98
356801	Upper	7.35	9.20	-2.83	-3.03
200540	Lower	12.34	8.02	-2.79	-2.84
200476	Upper	7.67	7.90	-2.72	-2.72
200399	Surface	7.10	7.80	-2.71	-2.72
200400	Surface	7.10	7.80	-2.71	-2.72
200536	Upper	12.37	8.86	-2.68	-2.74
359401	Upper	7.22	8.20	-2.67	-2.85
200584	Surface	7.23	7.30	-2.66	-2.66
200285	Surface	7.14	7.10	-2.64	-2.64
200601	Surface	7.17	7.20	-2.56	-2.56
200795	Surface	7.10	7.30	-2.42	-2.42
200590	Surface	7.24	7.70	-2.42	-2.43
357101	Upper	7.56	7.60	-2.41	-2.41
200790	Surface	7.10	7.50	-2.38	-2.38
200589	Surface	7.29	7.60	-2.34	-2.35
200621	Surface	7.20	8.20	-2.28	-2.28
200498	Surface	7.29	7.50	-2.28	-2.28
200758	Surface	7.24	7.80	-2.27	-2.28
200841	Surface	7.26	7.40	-2.24	-2.24
200464	Surface	7.20	7.40	-2.23	-2.23
356201	Upper	7.05	7.90	-2.22	-2.23
358401	Upper	6.92	7.50	-2.19	-2.19
200532	Surface	7.06	7.40	-2.18	-2.18
353101	Lower	7.43	7.80	-2.17	-2.17
200593	Surface	7.32	7.50	-2.07	-2.07
200465	Surface	7.28	7.60	-2.03	-2.03

Corrected pH assuming calcite equilibrium

SiteId	Aquifer	Calculated pH	Measured pH	Calculated CBE	Measured CBE
200527	Surface	7.03	7.20	-2.01	-2.01
200460	Surface	7.15	7.50	-1.99	-2
200392	Surface	7.14	7.30	-1.94	-1.94
200690	Upper	7.41	8.10	-1.93	-1.94
357401	Lower	7.37	8.20	-1.88	-1.89
200505	Lower	7.79	9.00	-1.87	-1.89
356701	Upper	7.90	8.40	-1.83	-1.83
200749	Surface	7.19	7.50	-1.78	-1.78
200609	Surface	7.15	7.60	-1.77	-1.78
200480	Surface	12.25	7.30	-1.75	-1.53
200378	Surface	7.12	7.40	-1.71	-1.72
350703	Lower	7.99	7.90	-1.68	-1.68
200437	Surface	7.22	7.30	-1.68	-1.68
200692	Surface	7.28	7.20	-1.68	-1.68
356501	Upper	7.19	8.10	-1.63	-1.67
200781	Surface	7.28	7.70	-1.6	-1.61
200565	Lower	13.66	7.89	-1.59	-2.01
200436	Surface	7.24	7.10	-1.57	-1.57
200482	Surface	7.28	7.30	-1.55	-1.55
357501	Upper	6.91	7.10	-1.53	-1.53
350101	Lower	8.23	8.50	-1.5	-1.51
200452	Upper	8.56	8.70	-1.49	-1.49
200613	Lower	8.04	8.90	-1.48	-1.49
200489	Lower	7.85	8.10	-1.48	-1.48
200504	Upper	7.45	7.80	-1.42	-1.42
200806	Lower	7.92	8.10	-1.39	-1.39
200784	Surface	7.16	7.70	-1.39	-1.4
200580	Upper	7.48	7.90	-1.3	-1.3
200599	Surface	7.11	7.60	-1.29	-1.29
200725	Surface	7.24	7.30	-1.24	-1.24
355505	Lower	7.53	8.20	-1.23	-1.25
200708	Surface	7.17	7.30	-1.22	-1.22
200640	Surface	7.09	7.50	-1.18	-1.18
200473	Surface	12.32	7.30	-1.17	-1.04
200551	Surface	6.84	7.67	-1.15	-1.16
351301	Lower	7.83	8.20	-1.06	-1.06
200253	Surface	12.31	7.30	-1.05	-0.92
200500	Lower	8.22	8.20	-1.01	-1.01

Corrected pH assuming calcite equilibrium

SiteId	Aquifer	Calculated pH	Measured pH	Calculated CBE	Measured CBE
358201	Lower	7.14	7.90	-0.96	-0.97
200818	Surface	7.19	7.80	-0.96	-0.96
200731	Surface	6.98	7.90	-0.96	-0.97
200825	Surface	12.34	7.30	-0.94	-0.85
200588	Surface	6.83	7.77	-0.93	-0.94
200817	Surface	7.19	7.80	-0.91	-0.92
200568	Surface	7.03	7.40	-0.9	-0.9
200571	Surface	7.03	7.40	-0.9	-0.9
351601	Lower	7.45	8.40	-0.89	-0.89
200587	Upper	12.07	7.81	-0.85	-0.82
200529	Upper	7.72	7.70	-0.85	-0.85
200792	Surface	7.16	7.70	-0.84	-0.85
200535	Surface	12.30	7.30	-0.81	-0.72
200286	Surface	7.19	7.40	-0.74	-0.74
200501	Lower	8.27	8.50	-0.73	-0.74
352001	Lower	7.68	8.20	-0.71	-0.71
200445	Lower	7.30	8.50	-0.7	-0.7
200585	Surface	7.14	7.00	-0.66	-0.66
351901	Lower	7.55	8.20	-0.65	-0.65
200573	Surface	7.10	7.70	-0.62	-0.62
200453	Lower	7.83	8.20	-0.59	-0.59
200567	Upper	7.97	7.90	-0.55	-0.55
200734	Surface	7.07	7.50	-0.55	-0.55
357201	Upper	7.96	8.10	-0.51	-0.51
350601	Lower	7.08	7.50	-0.5	-0.61
355401	Lower	7.31	8.30	-0.49	-0.49
200360	Surface	7.49	7.50	-0.45	-0.45
200503	Surface	7.04	7.80	-0.44	-0.44
200511	Surface	7.11	7.40	-0.39	-0.39
200563	Upper	13.26	7.83	-0.34	-0.39
200756	Surface	7.23	7.50	-0.33	-0.33
200820	Surface	7.21	7.40	-0.32	-0.32
200444	Lower	7.47	8.60	-0.14	-0.14
200574	Surface	7.47	7.20	-0.14	-0.14
200321	Surface	7.42	7.10	-0.13	-0.13
200518	Surface	7.09	7.40	-0.1	-0.1
200763	Surface	7.25	7.40	0.02	0.02
350701	Lower	7.67	7.70	0.03	0.02

Corrected pH assuming calcite equilibrium

SiteId	Aquifer	Calculated pH	Measured pH	Calculated CBE	Measured CBE
355301	Lower	7.28	8.10	0.07	0.07
200989	Surface	7.59	7.80	0.12	0.12
200562	Surface	12.30	7.30	0.13	0.11
200836	Upper	7.78	8.30	0.18	0.18
200832	Surface	7.44	7.80	0.19	0.19
353003	Lower	7.56	7.70	0.21	0.21
200417	Surface	7.01	7.70	0.21	0.21
200420	Surface	7.16	7.40	0.21	0.21
200566	Surface	7.01	7.20	0.23	0.24
200581	Upper	7.37	8.30	0.27	0.26
353001	Upper	7.81	7.80	0.27	0.27
200569	Surface	6.93	7.30	0.28	0.28
200863	Lower	7.66	8.20	0.32	0.32
200521	Surface	7.06	7.40	0.32	0.32
200808	Surface	7.30	7.50	0.32	0.32
200872	Surface	7.36	7.70	0.33	0.34
359201	Upper	7.37	7.70	0.34	0.27
200669	Surface	7.33	7.50	0.38	0.38
200492	Surface	7.29	7.60	0.52	0.52
200530	Upper	7.86	7.90	0.53	0.53
200630	Surface	7.19	7.60	0.53	0.53
200935	Surface	7.30	8.40	0.57	0.58
358301	Lower	7.39	8.40	0.58	0.59
200358	Surface	7.45	7.50	0.62	0.61
200451	Surface	7.30	7.60	0.66	0.66
200295	Surface	7.26	7.40	0.7	0.7
358601	Upper	7.04	7.70	0.72	0.61
200475	Lower	7.92	8.10	0.76	0.76
200687	Lower	7.40	7.70	0.84	0.84
200488	Upper	7.50	8.70	0.94	0.97
200583	Upper	7.95	8.50	0.95	0.95
200553	Surface	7.10	7.20	0.99	0.99
200369	Surface	7.26	7.20	1.17	1.17
356101	Upper	7.10	7.00	1.18	1.18
357901	Upper	7.21	7.60	1.18	1.17
200466	Surface	7.34	7.70	1.19	1.19
200484	Surface	7.17	7.40	1.2	1.2
200851	Surface	7.30	7.60	1.27	1.27

Corrected pH assuming calcite equilibrium

SiteId	Aquifer	Calculated pH	Measured pH	Calculated CBE	Measured CBE
200606	Surface	7.17	7.20	1.31	1.31
200826	Surface	7.29	7.50	1.39	1.39
200552	Surface	7.11	7.80	1.41	1.42
200610	Surface	12.26	7.30	1.57	1.4
200425	Lower	7.71	7.70	1.67	1.67
200653	Surface	7.09	7.97	2.03	2.05
200650	Surface	7.19	7.50	2.03	2.03
200856	Lower	7.24	8.20	2.15	2.18
200786	Surface	7.33	7.90	2.36	2.37
200612	Upper	7.55	8.90	2.52	2.62
351202	Lower	7.68	8.70	2.58	2.57
200746	Surface	7.20	7.60	2.71	2.71
350702	Upper	7.09	7.30	2.89	2.69
200614	Surface	7.00	7.90	2.95	2.95
200336	Surface	7.22	7.10	3.04	3.04
200702	Upper	7.12	8.80	3.26	3.43
356301	Upper	7.09	8.10	3.42	3.45
356901	Upper	7.30	8.30	3.43	3.42
200516	Surface	7.36	7.60	3.5	3.51
200533	Upper	6.64	6.77	3.64	3.64
356401	Upper	7.39	7.90	3.99	2.58
200374	Surface	7.40	7.20	7.4	7.4
200558	Lower	7.49	7.78	9.55	9.54
359501	Upper	11.95	7.70	10.13	8.75
359301	Upper	8.21	7.80	17.57	17.52